Inhibitory Interneuron Dysfunction in *SCN8A* Developmental and Epileptic Encephalopathy

Raquel Maurer Miralles

B.S. College of William & Mary, 2019

A Dissertation presented to the Graduate Faculty

of the University of Virginia in Candidacy for the Degree of Doctor in Philosophy

Neuroscience Graduate Program

University of Virginia

October 30, 2024

Manoj K. Patel, PhD (Dissertation Advisor) _____

Sarah C. Kucenas, PhD (Executive Committee Member) _____

Jaideep Kapur, MBBS, PhD _____

Howard P. Goodkin, MD, PhD _____

Mark P. Beenhakker, PhD _____

Table of Contents

Summary

SCN8A developmental and epileptic encephalopathy (DEE) is a severe epilepsy syndrome caused by *de novo* mutations in the gene *SCN8A*, which encodes the voltage-gated sodium channel isoform $Na_v1.6$. Patients with *SCN8A* DEE experience drug-resistant seizures and are at a higher risk of sudden unexpected death in epilepsy (SUDEP), along with many notable comorbidities such as cognitive and motor dysfunction. Typically, mutations leading to *SCN8A* DEE are gain-of-function, with loss-of-function mutations most often leading to intellectual disability, developmental delay, or absence seizures. Efficient treatments are limited for patients with *SCN8A* DEE, although gene therapies targeting the root cause of the disorder are currently in development. Presently, literature in the field of *SCN8A* DEE suggests that excitatory neuron dysfunction is the primary driver of the disease phenotype. To identify potential new therapeutics, we must further clarify the physiology of this devastating disease. Importantly, key subtypes of inhibitory interneurons have yet to be studied in the context of *SCN8A* DEE.

In this dissertation thesis, I examine two key subtypes of inhibitory interneurons, parvalbumin-positive (PV) and vasoactive intestinal peptide-positive (VIP) interneurons, and their physiological changes in *SCN8A* DEE. Using two mouse models with patient-derived *SCN8A* mutations, I show that *SCN8A* mutations augment key sodium currents in both PV and VIP interneurons, resulting in changes in their excitability. To uncover a deeper understanding of the *SCN8A* DEE network, I examined synaptic connections between *Scn8a* mutant PV interneurons and excitatory pyramidal cells (PCs), indicating that there is an impairment of inhibitory synaptic transmission in *SCN8A* DEE. Using a

Cre-dependent system, I selectively expressed the R1872W *SCN8A* mutation in both PV and VIP interneurons and show that while this *SCN8A* mutation selectively in VIP interneurons does not result in seizure susceptibility, it conveys susceptibility to spontaneous seizures when selectively expressed in PV interneurons, a highly unexpected finding. Ultimately, the results presented here provide key contributions to the mechanistic understanding of *SCN8A* DEE and inhibitory dysfunction in gain-of-function sodium channelopathies.

Publications

Wengert, E., **Miralles, R.**, Wedgwood, K., Wagley, P., Strohm, S., Panchal, P., Majidi, A., Wenker, I., Gaykema, R., Patel, M.K. Somatostatin-positive Interneurons Contribute to Seizures in SCN8A Epileptic Encephalopathy. Journal of Neuroscience 41(44):9257-9273. Nov 2021.

Miralles, R., Patel, M. K. It Takes Two to Tango: Channel Interplay Leads to Paradoxical Hyperexcitability in a Loss-of-Function Epilepsy Variant. Epilepsy Currents 22(1):69-71. Feb 2022.

Thompson, J., **Miralles, R.**, Wengert, E., Wagley, P., Yu, W., Wenker, I., Patel, M.K. Astrocyte Reactivity in a Mouse Model of SCN8A Epileptic Encephalopathy. Epilepsia Open 7(2): 280-292. June 2022.

Wenker, I. C., Boscia, A. R., Lewis, C., Tariq, A., **Miralles, R.**, Hanflink, J. C., Saraf, P., Patel, M. K. Forebrain epileptiform activity is not required for seizure-induced apnea in a mouse model of Scn8a epilepsy. Frontiers in Neural Circuits 16: 1002013. September 2022.

Miralles, R., Patel, M. K. That's a wrap: could controlling activity-regulated myelination prevent absence seizures?. Epilepsy Currents 22(6). November 2022.

Miralles, R., Patel, M. K. Unspooling the thread: VIP interneurons linked with autism spectrum disorder behaviors but not seizures in Dravet Syndrome. Epilepsy Currents 24(1):62-64. December 2023.

Wengert, E., **Miralles, R.**, Patel, M. K. Voltage-Gated Sodium Channels as Drug Targets in Epilepsy-Related Sodium Channelopathies. Ion Channels as Targets in Drug Discovery. Textbook chapter at Springer Nature, April 2024.

Miralles, R., Boscia, A. R., Kittur, S., Wengert, E. R., Vundela, S. R., Patel, M. K. Parvalbumin Interneuron Impairment Leads to Synaptic Transmission Deficits and Seizures in SCN8A Epileptic Encephalopathy. Accepted at JCI Insight, August 2024.

Fellowships/Academic Awards

NIH National Research Service Award Predoctoral Fellowship *April 2024 - Present*

NIH Diversity Supplement *June 2022 - April 2024*

Virginia Brain Institute Fellowship *July 2021 – June 2022*

Acknowledgements

My journey to receiving a PhD would not have been possible (or enjoyable) without the support of my colleagues and my community. First, I am so incredibly grateful to both of my parents, who raised me to be ambitious, inquisitive, and independent. I can't express how much they mean to me, and I strive to make them proud every day.

I would like to thank my thesis advisor, Dr. Manoj Patel, for being a wonderful mentor throughout my graduate school career. Without his guidance, I would not have grown into the scientist I am today. He is an incredibly caring and attentive mentor, and I could not think of a better person to advise me on the road to my PhD.

I am also grateful to all the members of the Patel Lab, past and present. Without Eric, who taught me nearly everything I know about patch clamp electrophysiology, my success may not have been possible. Even after his graduation, his continued guidance has been extremely valuable. To the other members of the lab, Alexis, Caeley, Tyler, Irene, Matt: thank you for all your help. I truly couldn't have done it without you. I would also like to highlight my undergraduate students: Jessica, Shreya, and Shrinidhi. Thank you for your patience with me as I learned how to be a mentor. In particular, Shrinidhi has been absolutely invaluable as a sort of "mini-me" when it comes to patch clamping, and I am truly fortunate that I had the opportunity to mentor her.

The Neuroscience Graduate Program at UVA has been a special place to learn and grow as a scientist. My thesis committee, Drs. Sarah Kucenas, Jaideep Kapur, Mark Beenhakker, and Howard Goodkin, have continually been both supportive and constructive with their comments in and out of committee meetings, and I thoroughly

appreciate their guidance. I have also made many friends through the NGP: to Jenny, Addison, Debbie, Stephanie, Dana, Sarah, AnnaLin, and everyone else, thank you for your support both scientifically and personally. I would also like to thank Kim Knotts, who has been subject to my many unscheduled pop-ins to her office, which have been invaluable when I needed help with an administrative question or otherwise.

Outside of UVA, it has been critical for me to ground myself outside of the research sphere. To my good friend Eliza, I am so glad we met and know that spending time with you always fills my bucket. Also, thank you to my pottery studio, City Clay, which helped me find my footing in Charlottesville and has since served as an incredible outlet. My ceramics students have been a constant source of joy, and I can't imagine the last few years without them.

The last year of my PhD improved significantly when I discovered the Charlottesville board games group. To all the friends I have met there, and to my wonderful boyfriend, Mark, thank you for being a much-needed beacon in this final stretch of graduate school.

Last but not least, I would like to thank my long-time friends, Lani, Lydia, Conrad, Rebecca, and Sarah. As you all know by now, grad school is a rollercoaster, and you all have been there for me the whole ride.

List of Abbreviations

VGSC—Voltage-gated sodium channel

$Na_v1.6$ —Voltage-gated sodium channel isoform encoded by the *SCN8A* gene

SUDEP — Sudden Unexpected Death in Epilepsy

AP — Action Potential

AIS — Axon Initial Segment

PV — Parvalbumin

SST— Somatostatin

VIP — Vasoactive Intestinal Peptide

I_{NaP} – Persistent sodium current

I_{NaR} – Resurgent sodium current

DEE — Developmental and Epileptic Encephalopathy

$V_{1/2}$ – Half-maximal voltage

LOF – Loss-of-function

GOF – Gain-of-function

EEG—Electroencephalogram

Chapter I. Introduction

Seizures are paroxysmal bursts of electrical activity in the brain caused by hyperexcitable and/or hypersynchronous neuronal activity. Epilepsy is a neurological disorder characterized by recurrent, unprovoked seizures.[1] It is one of the most common neurological disorders with approximately 7.6 per 1,000 persons lifetime prevalence.[1,2] An estimated 30% of all epilepsies are genetic in origin, with many resulting from mutations in ion channel genes.[3,4] *SCN8A* developmental and epileptic encephalopathy (DEE) is a severe genetic epilepsy caused by *de novo* mutations in the *SCN8A* gene,[5] which encodes the sodium channel $Na_V1.6$.[6] *SCN8A* DEE is characterized by treatment-resistant seizures, developmental delay, cognitive dysfunction, and an increased incidence of sudden unexpected death in epilepsy (SUDEP).[7–10] $Na_V1.6$ is expressed widely in the central nervous system, and is prominent at the axon initial segment (AIS) of both excitatory and inhibitory neurons.[11–13]

Previous studies primarily focus on how *SCN8A* mutations impact excitatory neurons, with limited studies on the importance of inhibitory interneurons. Despite advances in understanding the physiological mechanisms of *SCN8A* DEE, current treatments are often unable to control seizures and reduce the risk of SUDEP, highlighting the need to further understand the underlying network mechanisms of this disorder. In this introduction, I describe the structure and function of voltage gated sodium channels, and then discuss epilepsy-related sodium channelopathies with a focus on *SCN8A* DEE.

Voltage Gated Sodium Channels

Function

The first sodium currents were recorded by Hodgkin & Huxley in squid giant axons. Their papers provide a basis for modern neurophysiology, identifying electrical signals initiated by voltage-dependent inward sodium current[14–17]. In response to positive charge, sodium channels open, causing an influx of sodium and a depolarization of the cell. Then, within 1-2ms, the sodium current is inactivated and becomes unresponsive to depolarization, decreasing sodium conductance. During this period, voltage-gated potassium channels are activated, and the potassium conductance increases. The potassium current leads to an outflux of intracellular potassium and repolarization of the cell, with an overshoot causing hyperpolarization. As the cell is hyperpolarized, inactivated sodium channels recover and once again become sensitive to depolarization. This process describes basic sodium channel activity and the general action potential (AP) waveform. As VGSC function is heavily tied to the AP waveform, any modification to VGSC function could lead to a disruption in the AP waveform, and as such, a disruption in cells throughout the nervous system.

Structure

VGSCs in the human brain are comprised of an α subunit and one to two beta subunits (β1 and β2), where the α subunit and β2 subunit are linked by a disulfide bond[18]. VGSC α subunits have four homologous domains (DI-IV) containing six α-helical transmembrane segments[19,20], whereas each of the β subunits contains a single transmembrane segment along with a large extracellular domain and small intracellular domain,[21,22] shown in Figure 1. Two additional β subunits were found later, β3, which is closely related to β1[23] and β4, which is more closely related to β2.[24] Expression of mRNA for only the α subunit is sufficient for expression of a somewhat functional VGSC, able to produce sodium currents without either β subunit.[25] A recent report suggests that the α subunits of VGSCs interact with each other to assemble into a dimer, resulting in coupled gating properties.[26] However, the β subunits of VGSCs are essential for typical function, as they have important roles in the voltage dependence and kinetics of sodium channel gating.[21,22,24]

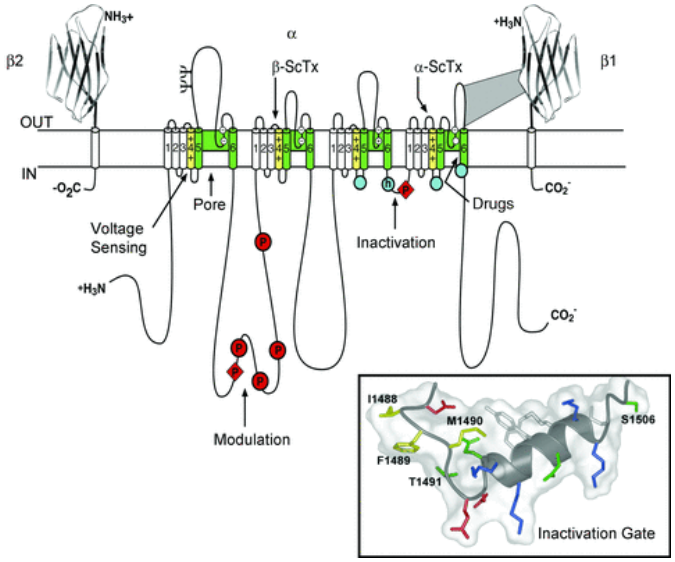

Figure 1.1: VGSC Structure *(From Catterall, 2012)*

Annotated structure of a VGSC showing DI-IV and S1-6 in each domain. Pore-lining segments in green, voltage-sensing segments in yellow, with drug interaction sites shown and the inactivation gate highlighted.

The crystal structure of a bacterial VGSC was discovered in 2011, allowing for insights into the structural basis of VGSC gating and selectivity.[27] S4 is the voltage

sensing transmembrane segment of the VGSC and S5-6 form the pore region.[20,27–29] S4 contains highly conserved arginine residues that serve as gating charges.[20,29] In response to depolarization, these positively charged residues move outwards and exchange ion pair partners to be neutralized by negative charges in the surrounding segments, in accordance with the *sliding helix* model of gating.[30,31] In S5-6, the selectivity filter in the VGSC pore is made up of the side chains of four glutamate residues and is significantly larger than its counterpart present in voltage-gated potassium channels due to the fact that sodium ions actually pass through the filter in a hydrated form.[27] This allows high selectivity for sodium ions. Fast inactivation of the sodium channel is mediated by a short intracellular loop between DIII and DIV of the α subunit (indicated in Figure 1.1), which blocks the sodium channel pore during inactivation by folding into the channel structure.[32] This inactivation gate possesses a motif with three hydrophobic amino acids that serves as somewhat of a latch to maintain closure.[33]

Diversity

Ten genes encode the different sodium channel α subunits, which are expressed in various tissues. They include $Na_v1.1$ numerically through $Na_v1.9$ as well as Na_x, a non-voltage-gated sodium channel involved in salt sensing.[28] These different isoforms have slight yet important differences in structure, channel properties, expression patterns, developmental time course of expression, and overall contribution to the physiological behavior of individual neurons and neural circuits. The ten sodium channel α subunits are enumerated in the table below, adapted from Catterall, 2012:

Sodium Channel	Gene	Primary Tissues
$Na_v1.1$	*SCN1A*	CNS
$Na_v1.2$	*SCN2A*	CNS
$Na_v1.3$	*SCN3A*	CNS
$Na_v1.4$	*SCN4A*	Skeletal muscle
$Na_v1.5$	*SCN5A*	Heart, un-innervated skeletal muscle
$Na_v1.6$	*SCN8A*	CNS
$Na_v1.7$	*SCN9A*	PNS
$Na_v1.8$	*SCN10A*	PNS
$Na_v1.9$	*SCN11A*	PNS
Na_x	*SCN6A, SCN7A*	Uterus, astrocytes, hypothalamus

Epilepsy-related sodium channelopathies

As noted in the table above, $Na_v1.1$, $Na_v1.2$, $Na_v1.3$, and $Na_v1.6$ are the voltage-gated sodium channels primarily present in the central nervous system. Variants in each of these sodium channel genes have been associated with DEE syndromes, which are severe and treatment-resistant epilepsy syndromes, typically with substantial comorbidities. These variants are generally classified as gain-of-function (GOF), where there is an increase in sodium channel activity, or loss-of-function (LOF), where there is a decrease in sodium channel activity. Generally, GOF or LOF variants associated with DEE lead to increased excitability in excitatory neurons or decreased function of

inhibitory interneurons, respectively, resulting in an excitation/inhibition imbalance and a seizure phenotype (Figure 1.2). However, we now know there are multiple deviations from this: LOF mutations can result in excitatory hyperexcitability,[34] and GOF mutations can result in reduced inhibitory drive,[35,36] which I discuss further in this thesis. The remainder of this introduction focuses on each of the primary sodium channels in the central nervous system and their associated epilepsy-related channelopathies, with some discussion on novel therapeutics.

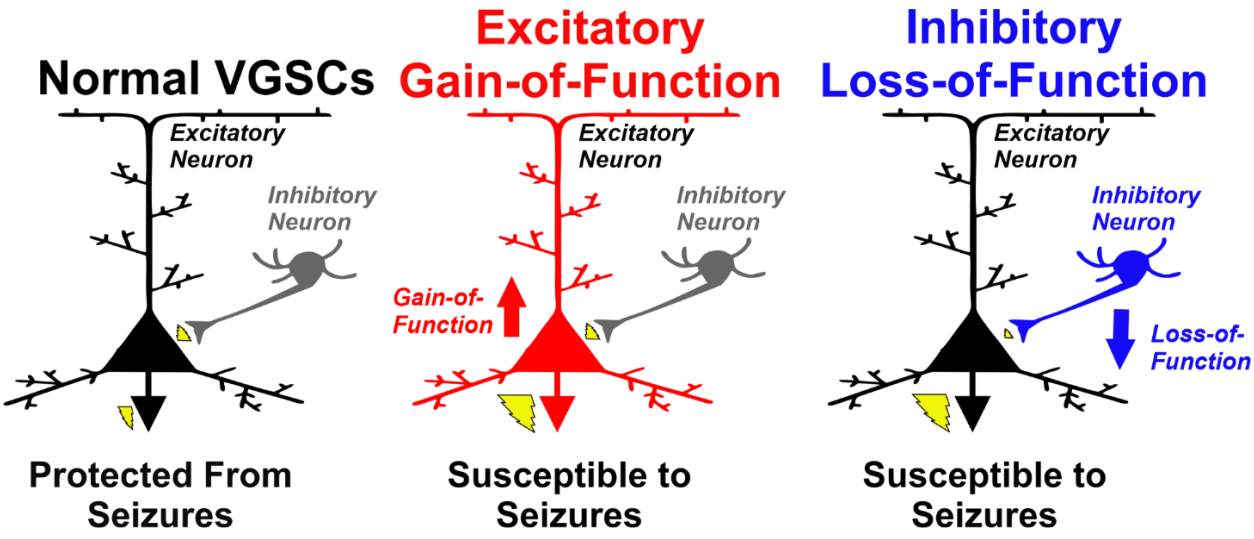

Figure 1.2. Network mechanisms of epilepsy caused by GOF or LOF mutations in sodium channels. Sodium channels in the CNS are expressed in excitatory and inhibitory neurons. The figure shows a simplified view of the effects of gain- or loss-of-function mutations expressed in either excitatory or inhibitory neurons. This indicates the mechanisms of overall network excitability and susceptibility to seizures.

SCN1A

$Na_v1.1$, encoded by the gene *SCN1A*, is expressed throughout the central nervous system (CNS), with expression beginning between the first and second postnatal weeks and remaining through adulthood.[37] Expression of $Na_v1.1$ is low in excitatory pyramidal cells,[12,38] however, expression is high in inhibitory interneurons,

both somatostatin-positive (SST) and parvalbumin-positive (PV). Specifically, in PV cells, it may play a role in the maintenance of high frequency firing.[38,39] $Na_v1.1$ is found primarily in the proximal portion of the AIS of these inhibitory interneurons, in which the isoform $Na_v1.6$ occupies the distal AIS.[12,13,38,40] Mutations in the *SCN1A* gene often lead to a LOF in $Na_v1.1$ channels via haploinsufficiency and this leads to a DEE phenotype known as Dravet Syndrome (DS).[41] Clinically, seizures occur within the first year of life and are generally drug-resistant. Patients with DS are at a high risk of SUDEP, with about 20% experiencing premature mortality due to SUDEP.[42] Many non-seizure symptoms are also associated with DS, particularly behavioral abnormalities along with intellectual and developmental impairment.[43]

As seizures in DS are usually drug-resistant, treatment via anti-seizure medications (ASMs) is generally difficult and often requires individualized treatment plans with multiple ASMs.[44] Valproate and clobazam are both often used in the treatment of DS, along with other ASMs such as levetiracetam, and more recently, stiripentol, cannabidiol, and fenfluramine.[45,46] Some ASMs lead to adverse effects in DS patients, particularly sodium channel blockers, as patients with DS already typically suffer from a loss-of-function in the $Na_v1.1$ sodium channel.[47]

Physiologically, haploinsufficiency of $Na_v1.1$ channels leads to hypoexcitability of PV and SST interneurons in mouse models of DS.[48] Interestingly, in mouse models of DS, this hypoexcitability is only seen in a transient developmental time window, P18-21,[49] whereas a distinct synaptic impairment is present both in that developmental window and in adulthood.[50] Additionally, $Na_v1.1$ expression has been found in disinhibitory interneurons, namely vasoactive intestinal peptide (VIP) interneurons. A

subset of these VIP interneurons are hypoexcitable in *Scn1a*$^{+/-}$ mice,[51] potentially contributing to overall circuit dysfunction.

Precision therapies are beginning to emerge to directly target the genetic origins of DS. In recent studies, gene activation of the wild-type allele of *Scn1a* has shown a rescue of inhibitory interneuron firing and a significant reduction of seizures.[52] Furthermore, an antisense oligonucleotide (ASO) developed by Stoke Therapeutics is currently in clinical trials as a therapy for DS patients with *SCN1A* mutations. This ASO was developed using Targeted Augmentation of Nuclear Gene Output (TANGO) therapy and aims to use alternative splicing to upregulate expression of the wild-type allele and create productive $Na_V1.1$, with the goal to combat the haploinsufficiency seen in DS.[53,54] In a mouse model of Dravet Syndrome, TANGO-mediated upregulation of functional *Scn1a* was able to increase levels of $Na_V1.1$, reduce seizure frequency, and increase survival.[53,55] At the cellular level, TANGO-ASO is able to rescue hypoexcitability in PV interneurons.[55] The basic mechanism of TANGO-ASO is shown in Figure 1.3.

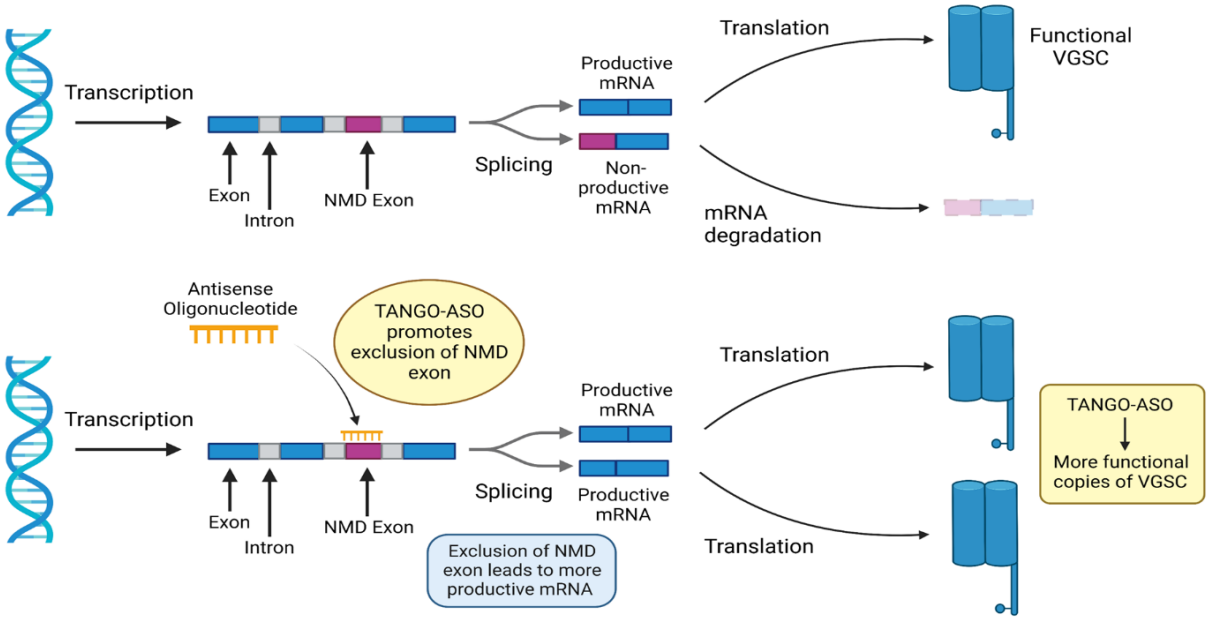

Figure 1.3: TANGO-ASO. Mechanism of TANGO-ASO for use in epilepsy-related sodium channelopathies. An antisense oligonucleotide promotes the exclusion of the nonsense-mediated decay exon, which typically makes one copy of mRNA a target for degradation. With this exclusion, splicing leads to two productive copies of mRNA, allowing the production of more productive protein (i.e. sodium channels).

Less commonly, GOF $Na_v1.1$ mutations lead to an epileptic encephalopathy phenotype. Previous studies have suggested characteristics (i.e. elevated persistent sodium current and non-inactivating sodium channels) similar to those seen in patients with gain-of-function sodium channel mutations.[56–59] In cultured cells, GOF $Na_v1.1$ mutations lead to enhanced channel opening and accelerated inactivation,[35] and cultured PV interneurons entered a state of action potential failure known as depolarization block, a cessation of firing in neurons due to sustained sodium current.[60,61]

SCN2A

The *SCN2A* gene encodes $Na_v1.2$, which is localized in the proximal AIS of neurons and plays an important role in action potential backpropagation into the soma.[62] $Na_v1.2$ is expressed primarily in pyramidal cells,[63] but interestingly, it is also present in some SST-positive interneurons and highly expressed in disinhibitory interneurons.[13,39] $Na_v1.2$ is expressed throughout the brain and spinal cord, with expression beginning early in development.[37] In the first two weeks of mouse postnatal life, the entire AIS is dominated by $Na_v1.2$, and between the second and third weeks of postnatal life, there is a distinct developmental switch where $Na_v1.6$ instead becomes expressed at the distal AIS.[64]

Mutations in *SCN2A* are associated with autism spectrum disorder (ASD),[65] benign familial neonatal-infantile seizures,[66] and developmental and epileptic encephalopathy.[67,68] Both GOF and LOF mutations in *SCN2A* are associated with epilepsy, with gain-of-function $Na_v1.2$ variants usually associated with an earlier seizure onset and more severe phenotype than loss-of-function variants.[67,69] Although loss-of-function mutations are sometimes associated with seizures, they more commonly lead to ASD.[70] Delayed inactivation and increased persistent current (I_{NaP}) have been shown in multiple studies assessing various GOF $Na_v1.2$ variants[71–73]; these mutations likely lead to pyramidal cell hyperexcitability which in turn fosters the network hyperexcitability and seizure phenotype. Although $Na_v1.2$ is present primarily in excitatory neurons, LOF $Na_v1.2$ variants may lead to seizures via compensatory mechanisms of potassium (K) channels.[34]

SCN3A

$Na_v1.3$, encoded by the gene *SCN3A*, is very highly expressed during development but has low levels of expression after birth in mice.[37] Mutations in *SCN3A* may have elucidated some specific developmental functions of $Na_v1.3$, particularly in neural folding and gyrification.[74] *SCN3A*-related epilepsy is primarily due to GOF mutations,[75] and patients with *SCN3A* mutations often develop brain malformations, including polymicrogyria, a condition associated with abnormal cortical folding, not typically found in patients with other sodium channelopathies.[74,76] Physiologically, transfected HEK cells revealed increased I_{NaP}, hyperpolarized channel activation, and slowed inactivation in channels with GOF $Na_v1.3$ mutations.[76]

SCN8A

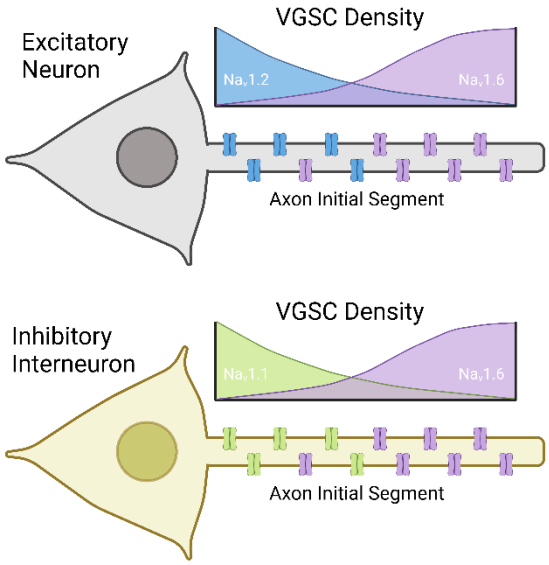

Figure 1.4. VGSC expression pattern in neuronal subtypes. $Na_v1.6$ is present at the distal AIS of both excitatory neurons and inhibitory interneurons. In excitatory neurons, $Na_v1.2$ is present at the proximal AIS, and in inhibitory interneurons, $Na_v1.1$ is present at the distal AIS.

The voltage gated sodium channel $Na_v1.6$ is integral in neuronal excitability as it is concentrated at the axon initial segment, nodes of Ranvier, and synapses within the CNS. It is crucial in the generation of action potentials.[11,12] In adults, while $Na_v1.2$ is present at the proximal AIS, $Na_v1.6$ is localized to the distal AIS.[62] As mentioned previously, there is a distinct developmental switch between $Na_v1.2$ and $Na_v1.6$ at the distal AIS and nodes of Ranvier after the first two weeks of

postnatal life in mice. Following this developmental switch, $Na_v1.6$ is widely present throughout the brain.[12,62] $Na_v1.6$ is highly expressed in excitatory pyramidal cells[12], and although more prevalent in pyramidal cells, $Na_v1.6$ is also present in inhibitory interneurons and is involved in their action potential initiation.[13] A simplified cartoon indicating the relative expression levels of $Na_v1.6$, $Na_v1.2$, and $Na_v1.1$ in excitatory and inhibitory neurons is shown in Figure 1.4.

SCN8A DEE was first identified in 2012 after whole genome sequencing of a family identified a *de novo* variant in the *SCN8A* gene of a proband. The *de novo* mutation identified in the *SCN8A* gene resulted in an asparagine (N) to aspartic acid (D) substitution that occurred at amino acid residue 1768 (N1768D).[5] Following the identification of this proband, many more *SCN8A* mutations and cases of *SCN8A* DEE were identified, now amassing to approximately 550 patients (*SCN8A* website). Within a study from a single country in 2021, there was an incidence of 1 *SCN8A* mutation per roughly 56,247 live births in the population.[77] Seizure onset in *SCN8A* DEE patients generally occurs at about 4 months of age and patients are characterized by drug resistant seizures and increased risk of SUDEP, along with intellectual and developmental deficits. Interestingly, although febrile seizures are somewhat common within patients with other epilepsy-related sodium channelopathies, they are rarely reported in *SCN8A* DEE patients[9,78,79].

SCN8A mutations that result in developmental and epileptic encephalopathy are primarily gain-of-function.[79] Loss-of-function mutations in *SCN8A* have been identified, but they are often less severe, resulting in developmental and cognitive deficits sometimes without seizures.[80,81] Many patients with LOF mutations do experience

seizures, however, with a median seizure onset of around 40 months, but few LOF mutations result in an epileptic encephalopathy phenotype,[79] and the physiological mechanisms behind LOF *SCN8A* DEE are poorly understood. Many of the recurrent mutations in *SCN8A* leading to DEE are shown in Figure 1.5, with red representing primarily GOF mutations and blue representing primarily LOF mutations. Importantly, many mutations are not simply gain- or loss-of-function but share characteristics of both (i.e. R223G, which decreases current density but causes a hyperpolarizing shift in the activation curve).[77,82,83]

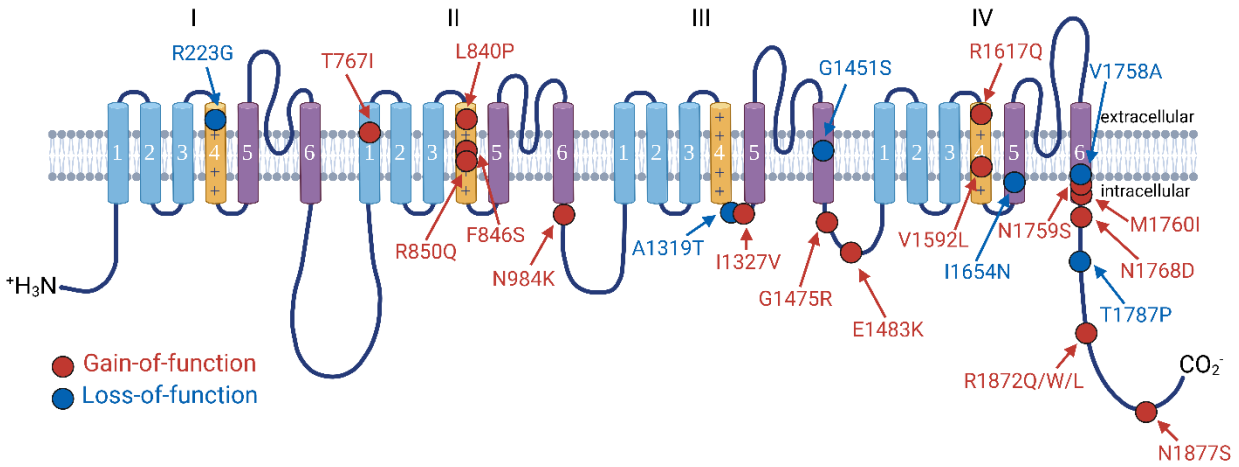

Figure 1.5: Structure and mutations of $Na_V1.6$. Annotated structure of $Na_V1.6$ including several physiologically characterized *SCN8A* mutations that lead to an *SCN8A*-related epilepsy phenotype. Structure shows Na channel domains DI-IV and S1-6 in each domain, with pore-lining segments in purple and voltage-sensing segments in yellow. Gain-of-function mutations are in red, with loss-of-function mutations noted in blue.

Precision therapies are currently being developed for *SCN8A* DEE. A selective inhibitor of $Na_V1.6$, NBI-921352, has been developed to treat *SCN8A* DEE, with potential broad applications to other types of epilepsy.[84] *In vitro*, NBI-921352 reduced the magnitude of I_{NaP} and I_{NaR}, and reduced the excitability of excitatory neurons.[84] *In vivo*, NBI-921352 was more successful in inhibiting electrically-induced seizures in

rodent models than non-selective sodium channel blockers,[84] indicating the potential therapeutic use of this novel drug that is currently in clinical trials. Additionally, there is an ASO developed to reduce the expression of *Scn8a* and thus, decrease the levels of $Na_v1.6$. In doing so, the *Scn8a* ASO successfully reduces seizures and increases life expectancy of mice with GOF $Na_v1.6$ variants.[85] Using this same *Scn8a* ASO also reduced the seizure frequency and phenotype severity in mouse models of DS,[85] potentially providing an interesting way to approach sodium channelopathies in the future.

Mouse Models

In 2014, a mouse model was created with a knock-in of the N1768D *SCN8A* mutation identified in the first described patient of *SCN8A* DEE (*Scn8a*$^{D/+}$).[86] These mice exhibit spontaneous seizures and an increased incidence of SUDEP, similar to the phenotype of the original patient.[87] Interestingly, sex differences have been shown in this mouse model of SCN8A DEE, with reduced mortality in female mice.[88] After the creation of this mouse model, another mouse model was generated with a Cre-dependent conditional knock-in of the recurrent *SCN8A* mutation Arg1872Trp (R1872W; *Scn8a*$^{W/+}$).[89] This mutation is known

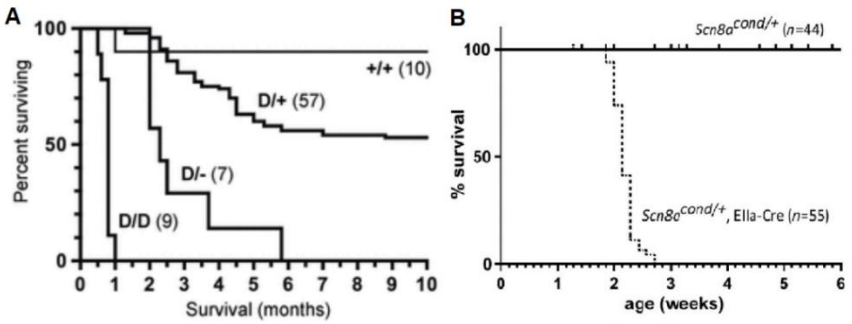

Figure 1.6: Survival of *Scn8a*$^{D/+}$ and *Scn8a*$^{W/+}$ mouse models *(Adapted from Wagnon et al, 2015 and Bunton-Stasyshn et al, 2019)* **(A)** shows the survival curves for the mouse model harboring the patient-derived *Scn8a* mutation N1768D. **(B)** shows the survival curve for the conditional knock-in mouse model harboring the patient-derived *SCN8A* mutation R1872W. *Scn8a*$^{cond/}$, EIIa-Cre represents the mouse harboring this mutation in all cells.

to be severe in patients and this mouse model was created in order to encapsulate the phenotype of more severe *SCN8A* mutations. In these mice, the R1872W mutation led to SUDEP within three postnatal weeks when expressed ubiquitously and within sixteen weeks when expressed only in forebrain excitatory neurons.[89] Figure 1.6 represents the survival of both *Scn8a*$^{D/+}$ and *Scn8a*$^{W/+}$ mice, where *Scn8a*$^{cond/+}$, EIIa-Cre possesses a global Cre-dependent knock-in of the R1872W mutation. To further study the broad phenotypic spectrum of *SCN8A* DEE, a third mouse model was created harboring the *de novo SCN8A* mutation R1620L. The mouse model exhibits behavioral deficits consistent with *SCN8A* DEE patients along with spontaneous seizures and an increased susceptibility to induced seizures.[90]

Gain-of-Function Physiology

As mentioned previously, the *SCN8A* mutations most often leading to a DEE phenotype encode a GOF $Na_v1.6$ variant. The initial report discussing the first identified *SCN8A* mutation characterized the biophysical properties of a GOF $Na_v1.6$ variant in transfected cells. These channels show significantly increased I_{NaP} and a depolarizing shift in the inactivation curve, indicating impaired channel inactivation as a mechanism of *SCN8A* DEE.[5]

$Na_v1.6$ is known to be highly expressed in the AIS of pyramidal cells,[12] and as we may anticipate with a GOF channel variant, pyramidal cells in *Scn8a*$^{D/+}$ mice are hyperexcitable, with distinct early after-depolarization (EAD) events in specific regions.[91,92] Generally, excitability in these mice appears to differ throughout brain regions, with increased EADs in the CA1 region of the hippocampus and heightened spontaneity in the CA1 and CA3 regions.[92] Expression of the R1872W mutation

exclusively in mouse excitatory forebrain neurons (*Scn8a*$^{W/+}$; EMX-Cre) led to SUDEP prior to four months of age, indicating the importance of excitatory cells in the pathology of *SCN8A* DEE.[89]

Considering the contribution of inhibitory interneurons to DS, it is essential to consider inhibitory interneurons in the context of *SCN8A* DEE, as $Na_v1.6$ is present in inhibitory interneurons and is involved in their action potential initiation.[13] In 2017, it was shown that knockout of *Scn8a* in thalamic interneurons lead to absence seizures in mice,[93] indicating that inhibitory interneurons likely do play a role in the broad field of *SCN8A* epilepsy. However, a study from 2019 suggests that the involvement of inhibitory interneurons is limited in *SCN8A* DEE: no seizures or seizure-induced death was observed with the expression of the R1872W *SCN8A* mutation exclusively in inhibitory interneurons via Gad2-Cre.[89] In contrast to this, we showed previously that SST interneurons may play a role in the seizure phenotypes of the D/+ (N1768D) and W/+ (R1872W) mouse models of *SCN8A* DEE, as SST interneurons from these mice enter depolarization block more readily than SST interneurons from wildtype animals[36], similar to prior research seen with gain-of-function *SCN1A* mutations.[35] Further, animals expressing the R1872W mutation exclusively in SST interneurons are susceptible to audiogenic seizures, and interestingly, chemogenetic activation of SST interneurons prolonged seizures,[36] indicating the potential importance of inhibitory interneurons to *SCN8A* DEE. However, SST interneurons only make up ~30% of all inhibitory interneurons,[94] leaving a large portion of critical inhibitory cells, notably PV and VIP interneurons, the other two largest classes of inhibitory interneurons, unstudied. The central hypothesis examined in this thesis is as follows:

Gain-of-function mutations in SCN8A lead to alterations in the physiology of inhibitory interneurons and ultimately, contribute to the severe phenotype of SCN8A developmental and epileptic encephalopathy.

In this thesis, I examine PV and VIP inhibitory interneurons and their potential contributions to the *SCN8A* DEE phenotype. As models, I will use both the *Scn8a*$^{D/+}$ and *Scn8a*$^{W/+}$ models of *SCN8A* DEE, which express the N1768D *SCN8A* mutation globally and the R1872W *SCN8A* mutation conditionally (Cre-dependent), respectively. This will allow me to examine the physiological consequences of *SCN8A* mutations on inhibitory interneuron subtypes individually and as a component of the *SCN8A* DEE network. I will also primarily use whole-cell patch clamp electrophysiology as a technique to elucidate the physiology of PV and VIP interneurons. In Chapter II, I will show that a GOF *Scn8a* mutation exclusively expressed in PV interneurons is sufficient to generate seizures and demonstrate that inhibitory dysfunction likely plays an important role in seizure generation in *SCN8A* DEE. In Chapter III, I will show that VIP interneurons do express $Na_v1.6$ and are impacted by *SCN8A* mutations, but they may instead be involved in another aspect of the *SCN8A* DEE phenotype. In total, this dissertation will indicate the contribution of two major inhibitory neuron subtypes to *SCN8A* DEE and discuss the implications of this on the field of sodium channelopathies and epilepsy more generally.

Chapter II: Parvalbumin Inhibitory Interneurons Lead to Synaptic Transmission Deficits and Seizures in *SCN8A* Developmental and Epileptic Encephalopathy

Rationale

The balance of excitation and inhibition in the brain is critical in seizure generation. Inhibitory interneurons suppress the activity of their target excitatory neurons in an effort to control network dynamics and prevent any excessive excitation that may lead to seizures,[94–97] Inhibitory interneurons are incredibly diverse; a recent study has identified 28 subtypes based on morphological, electrophysiological, and transcriptomic data.[98] Due to their diversity, classifications of cortical inhibitory interneurons are often changing, but currently there are five major identified subclasses: parvalbumin (PV), somatostatin (SST), vasoactive intestinal peptide (VIP), Lamp5, and Sncg interneurons.[94,97–100] The most numerous subtype is PV interneurons, which make up about 40% of inhibitory interneurons and provide feed-forward and feed-back inhibition to networks through reliable, high-frequency firing.[94,97] PV interneurons are known to express relatively high levels of $Na_v1.6$ compared to other inhibitory interneurons,[101] and yet have been previously unstudied in the context of *SCN8A* DEE, significantly limiting our understanding of the seizure network in this disorder. As previously mentioned, inhibitory interneuron dysfunction has been heavily implicated in Dravet Syndrome; previous studies of DS indicate that PV interneurons are hypoexcitable during a critical developmental time window.[48,49] In adult mice, PV interneurons show deficits in synaptic transmission and synchronization that likely

contribute to the chronic phenotype of Dravet Syndrome.[50,102] Additionally, PV interneurons have also been implicated in temporal lobe epilepsy (TLE). In mouse models of TLE, previous studies show a reduction in parvalbumin staining, indicating a potential loss of PV interneurons,[103,104] and others suggest a role for PV interneurons in abnormal synapse formation.[105,106]

Introduction

In this chapter, we used two mouse models of *SCN8A* DEE harboring the N1768D (*Scn8a*$^{D/+}$) and R1872W (*Scn8a*$^{W/+}$) patient-derived *SCN8A* variants. These models recapitulate key features of the disease through spontaneous seizures and increased risk of seizure-induced death.[86,87,89] *Scn8a*$^{D/+}$ mice express a germline knock-in of the N1768D variant,[86,87] whereas *Scn8a*$^{W/+}$ mice harbor a Cre-dependent knock-in of the R1872W variant.[89] Additionally, our previous studies show that both models are susceptible to audiogenic seizures,[36,107] enabling rapid assessment of seizure susceptibility.

Here, we used both the global *Scn8a*$^{D/+}$ model and the conditional *Scn8a*$^{W/+}$ model of *SCN8A* DEE to assess the phenotype of mutant PV interneurons individually and as a component of the *SCN8A* DEE network. We report that selective expression of the R1872W *SCN8A* variant in PV interneurons (*Scn8a*$^{W/+}$-PV) is sufficient to induce spontaneous and audiogenic seizures and premature seizure-induced death, indicating the importance of this inhibitory subtype to *SCN8A* DEE as a whole. Whole-cell patch clamp electrophysiology recordings of PV interneurons demonstrated an increased susceptibility to action potential failure via depolarization block. Consequently, we also observed a decrease in spontaneous inhibition received by pyramidal cells in *Scn8a*

mutant mice. Recordings of voltage-gated sodium currents showed an elevation of the I_{NaP} in both models and an elevation of resurgent sodium current (I_{NaR}) in the *Scn8a*$^{W/+}$-PV model, potentially contributing to the depolarization block phenotype. A decrease in miniature inhibitory postsynaptic currents (mIPSCs) generated in *Scn8a*$^{W/+}$-PV pyramidal cells (PCs) was also observed, suggesting a possible synaptic deficit between PV interneuron and pyramidal cells (PV:PC pairs), and dual recordings of synaptically connected cells revealed an increase in PV:PC synaptic transmission failure as well as a prolonged synaptic latency. In summary, these data reveal a significant and previously unappreciated impairment of PV interneurons and their synaptic connections to excitatory pyramidal cells in *SCN8A* DEE. Selective expression of a *SCN8A* variant in PV interneurons shows that these impairments are sufficient to cause seizures and SUDEP in mice, indicating the importance of this critical interneuron subtype to seizure generation and redefining our understanding of the cortical microcircuit function in this disease.

Materials and methods

Mouse husbandry and genotyping

Scn8a$^{D/+}$ and *Scn8a*$^{W/+}$ mice were generated as previously described and maintained through crosses with C57BL/6J mice (Jax, #000664) to keep all experimental mice on a C57BL/6J genetic background.[87,89] Cell type-specific expression of R1872W was achieved using males heterozygous for the R1872W allele and C57BL/6J females homozygous for PV-Cre (Jax, #017320) to generate mutant mice (*Scn8a*$^{W/+}$-PV). [89] Homozygous PV-IRES-Cre females were used for breeding to ensure minimal germline recombination due to Cre, as shown previously.[108,109] Because certain

transgenic mice entail the insertion of Cre directly into the coding sequence and due to the need for a fluorescent reporter to reliably identify PV interneurons in-slice, for all experiments we used WT controls that contained the same Cre allele but lacked the allele encoding the *Scn8a* variant. Fluorescent labeling of PV interneurons was achieved by first crossing *Scn8a*$^{D/+}$ or *Scn8a*$^{W/+}$ mice with C57BL/6J mice homozygous for a Cre-dependent tdTomato reporter (Jax, #007909) to generate *Scn8a*$^{D/+}$;tdTomato or *Scn8a*$^{W/+}$;tdTomato mice. Then, male *Scn8a*$^{D/+}$;tdTomato or *Scn8a*$^{W/+}$;tdTomato mice were crossed with female mice homozygous for PV-Cre. Experimental groups used ≥3 randomly selected mice to achieve statistical power and roughly equal numbers of male and female mice. All genotyping was conducted through Transnetyx automated genotyping PCR services.

In vivo seizure monitoring

Custom electroencephalogram (EEG) headsets (PlasticsOne) were implanted in 5-week-old *Scn8a*$^{W/+}$-PV mice and 6-8-week-old *Scn8a*$^{D/+}$ mice using standard surgical techniques as previously described.[110] Anesthesia was induced with 5% and maintained with 0.5%-3% isoflurane. Adequacy of anesthesia was assessed by lack of toe-pinch reflex. A midline skin incision was made over the skull and connective tissue was removed. Burr holes were made at the lateral/anterior end of the left and right parietal bones to place EEG leads, and at the interparietal bone for ground electrodes. EEG leads were placed bilaterally in the cortex or unilaterally placed in the cortex and superior colliculus using a twist. A headset was attached to the skull with dental acrylic (Jet Acrylic; Lang Dental). Mice received postoperative analgesia with ketoprofen (5

mg/kg, i.p.) and 0.9% saline (0.5 mL i.p.) and were allowed to recover a minimum of 2-5d before seizure-monitoring experiments.

Mice were then individually housed in custom-fabricated chambers and monitored for the duration of the experiment. The headsets were attached to a custom low-torque swivel cable, allowing mice to move freely in the chamber. EEG signals were amplified at 2000× and bandpass filtered between 0.3 and 100 Hz, with an analog amplifier (Neurodata model 12, Grass Instruments). Biosignals were digitized with a Powerlab 16/35 and recorded using LabChart 7 software at 1 kS/s. Video acquisition was performed by multiplexing four miniature night vision-enabled cameras and then digitizing the video feed with a Dazzle Video Capture Device and recording at 30 fps with LabChart 7 software in tandem with biosignals.

Audiogenic seizure assessment

Audiogenic seizure susceptibility was determined using standard protocols, similar to those previously described.[107] To test for audiogenic seizures, mice were taken from their home cage and transferred to a clean test cage where they were allowed to acclimate for ~20 seconds before the onset of a 15 kHz acoustic stimulus. The stimulus duration lasted for 50 seconds or until the animal had a behavioral seizure. Audiogenic seizures were recorded using a laptop webcam.

Immunohistochemistry

Brain tissue for immunohistochemistry was processed as previously described.[36,111] Mice were anesthetized and transcardially perfused with 10 mL PBS followed by 10 mL 4% PFA. Brains were immersed in 4% PFA overnight at 4°C and

stored in PBS. 30 µm coronal brain sections were obtained using a cryostat. Sections were incubated with primary antibodies diluted in 2% goat serum (Jackson ImmunoResearch Laboratories) with 0.1% Triton X (Sigma-Aldrich) at a concentration of 1:500 in KPBS. The following primary antibodies were used: mouse anti-PV (Millipore; 1:200), rabbit anti-$Na_v1.6$ (Alomone; 1:200), mouse anti-AnkG (NeuroMab;1:100). The secondary antibodies, goat anti-mouse AlexaFluor-488 (Invitrogen) and goat anti-rabbit Alexa-Fluor 633 (Invitrogen), was diluted 1:1000 in goat serum (2%) and Triton-X (0.1%) in KPBS. Sections were stained free-floating in primary antibody on a shaker at 4°C overnight and with secondary antibody for 1 h at room temperature the following day. Tissues were counterstained with NucBlue Fixed Cell ReadyProbes Reagent (DAPI) (ThermoFisher Scientific, catalog #R37606) included in the secondary antibody solution. Tissues were mounted on slides using AquaMount (Polysciences).

Imaging was performed on a Zeiss LSM 700 confocal microscope using a 20x, 40x, or 63x objective. We used 2 slices per mouse to assess the respective immunoreactivity. Cell counting and quantification of staining intensity were performed using ImageJ. The same threshold was applied for all mouse genotypes.

Brain Slice Preparation

Preparation of acute brain slices for patch-clamp electrophysiology experiments was modified from standard protocols previously described.[36,89,91] Mice were anesthetized with isoflurane and decapitated. The brains were rapidly removed and kept in chilled ACSF (0°C) containing (in mM): 125 NaCl, 2.5 KCl, 1.25 NaH_2PO_4, 2 $CaCl_2$, 1 $MgCl_2$, 0.5 L-ascorbic acid, 10 glucose, 25 $NaHCO_3$, and 2 Na-pyruvate. For dual-cell patch-clamp experiments, the slicing solution was modified to contain (in mM): 93 N-

Methyl-D-glucamine (NMDG), 2.5 KCl, 1.25 NaH_2PO_4, 20 HEPES, 5 L-ascorbic acid (sodium salt), 2 thiourea, 3 sodium pyruvate, 0.5 $CaCl_2$, 10 $MgSO_4$, 25 D-glucose, 12 N-acetyl-L-cysteine, 30 $NaHCO_3$; pH adjusted to 7.2-7.4 using HCl (osmolarity 310 mOsm). Slices were continuously oxygenated with 95% O_2 and 5% CO_2 throughout the preparation. 300 µm coronal or horizontal brain sections were prepared using a Leica Microsystems VT1200 vibratome. Slices were collected and placed in ACSF warmed to 37°C for ~30 min and then kept at room temperature for up to 6 h.

Electrophysiology Recordings

Brain slices were placed in a chamber superfused (~2 ml/min) with continuously oxygenated recording solution warmed to 32 ± 1°C. In either *Scn8a*$^{D/+}$;tdTomato;PV-Cre, *Scn8a*$^{W/+}$;tdTomato;PV-Cre, or WT;tdTomato;PV-Cre mice, cortical layer IV/V PV interneurons were identified as red fluorescent cells, and pyramidal neurons were identified based on morphology and absence of fluorescence via video microscopy using a Carl Zeiss Axioscope microscope. Whole-cell recordings were performed using a Multiclamp 700B amplifier with signals digitized by a Digidata 1322A digitizer. Currents were amplified, lowpass filtered at 2 kHz, and sampled at 100 kHz. Borosilicate electrodes were fabricated using a Brown-Flaming puller (model P1000, Sutter Instruments) to have pipette resistances between 1.5 and 3.5 mΩ. All patch-clamp electrophysiology data were analyzed using custom MATLAB scripts and/or ClampFit 10.7.

Intrinsic Excitability Recordings

Current-clamp recordings of neuronal excitability were collected in ACSF solution identical to that used for preparation of brain slices. The internal solution contained the

following (in mM): 120 K-gluconate, 10 NaCl, 2 $MgCl_2$, 0.5 K_2EGTA, 10 HEPES, 4 Na_2ATP, 0.3 NaGTP, pH 7.2 (osmolarity 290 mOsm). Intrinsic excitability was assessed using methods adapted from those previously described.[36,91] Briefly, resting membrane potential was manually recorded from the neuron at rest. Current ramps from 0 to 400 pA over 4 s were used to calculate passive membrane and AP properties, including threshold, upstroke and downstroke velocity, which are the maximum and minimum slopes on the AP, respectively; amplitude, which was defined as the voltage range between AP peak and threshold; APD_{50}, which is the duration of the AP at the midpoint between threshold and peak; input resistance, which was calculated using a −20 pA pulse in current-clamp recordings; and rheobase, which was defined as the maximum amount of depolarizing current that could be injected into neurons before eliciting an AP. AP frequency–current relationships were determined using 1 s current injections from −140 to 1200 pA. Spikes were only counted if AP overshoot was >0 mV and amplitude was >20 mV. The threshold for depolarization block was operationally defined as the current injection step that elicited the maximum number of APs (i.e., subsequent current injection steps of greater magnitude resulted in fewer APs because of entry into depolarization block).

Sodium Current Recordings

Persistent (I_{NaP}) and resurgent (I_{NaR}) sodium currents were recorded in the whole-cell patch clamp configuration in-slice, whereas transient sodium current was recorded in the outside-out configuration. The internal solution for all voltage-gated sodium channel recordings contained the following (in mM): 140 CsF, 2 $MgCl_2$, 1 EGTA, 10 HEPES, 4 Na_2ATP, and 0.3 NaGTP with the pH adjusted to 7.3 and osmolality to 300

mOsm. The external solution for recording persistent and resurgent sodium currents has been previously described[112,113] and contained (in mM): 100 NaCl, 40 TEACl, 10 HEPES, 3.5 KCl, 2 $CaCl_2$, 2 $MgCl_2$, 0.2 $CdCl_2$, 4 4-aminopyridine (4-AP), 25 D-glucose. Outside-out recordings of transient sodium current were collected in ACSF as the external solution. Steady-state I_{NaP} was elicited using a voltage ramp (20 mV/s) from −80 to −20 mV. To record I_{NaR}, PV interneurons were held at −100 mV, depolarized to 30 mV for 20 ms, then stepped to voltages between −100 mV and 0 mV for 40 ms. After collecting recordings at baseline, protocols were repeated in the presence of 500 nM tetrodotoxin (TTX; Alomone Labs) to completely block I_{NaP} and I_{NaR} currents. Traces obtained in the presence of TTX were subtracted from those obtained in its absence. The half-maximal voltage for activation of I_{NaP} was calculated as previously described [113]. Patch-clamp recordings in the outside-out configuration were collected using a protocol modified from an approach previously described.[36,91] Voltage-dependent activation and steady-state inactivation parameters were recorded using voltage protocols previously described.[36] For all sodium current recordings, we waited 2 minutes after achieving whole-cell configuration to account for initial shifts in the voltage-dependence of activation.

Inhibitory Postsynaptic Current Recordings

Patch-clamp recordings of inhibitory postsynaptic currents generated in pyramidal cells were performed using the same ACSF external solution and an internal solution containing (in mM): 70 K-Gluconate, 70 KCl, 10 HEPES, 1 EGTA, 2 $MgCl_2$, 4 MgATP, and 0.3 Na_3GTP, with the pH adjusted to 7.2-7.4 and osmolarity to 290 mOsm. Pyramidal cells were held at -70 mV and a 1-min gap-free recording was performed in

the voltage-clamp configuration to assess spontaneous IPSC frequencies before bath application of 500 nM TTX to record miniature IPSCs. After recording spontaneous and miniature IPSCs, 1 µM gabazine was bath applied to block currents and ensure that only inhibitory events were recorded.

Dual-Cell Synaptic Connection Recordings

Unitary IPSCs (uIPSCs) were obtained via two simultaneous patch-clamp recordings from synaptically-connected neurons located within 50 µm of one another in the somatosensory cortex of a horizontal slice. A 2 ms pulse at 1000 pA elicited action potentials in the presynaptic neuron at 1, 5, 10, 20, 40, 80, and 120 Hz. The internal solution was modified to contain (in mM): 65 K-gluconate, 65 KCl, 2 $MgCl_2$, 10 HEPES, 0.5 EGTA, 10 Phosphocreatine-$Tris_2$, 4 MgATP, 0.3 NaGTP; pH adjusted to 7.2-7.4 using KOH (osmolarity 290 mOsm) [50]. Paired pulse ratio (PPR) was calculated as the amplitude of the second IPSC divided by the amplitude of the first IPSC. PPR was not calculated for trials in which the first and/or second IPSC event was a failure. uIPSC failures were identified by the absence of a transient current greater than 5 pA occurring within 5 ms of the presynaptic AP. Synaptically connected pairs were not used for analysis if resting membrane potential shifted >10 mV during recording.

Statistical Analysis

Analysis of electrophysiological data was performed in a blinded manner. All statistical comparisons were made using the appropriate test in GraphPad Prism 9. Categorical data were analyzed using the Fisher's exact test. For membrane and AP properties, spontaneous firing frequency, depolarization block threshold, peak sodium currents, half-maximal voltages, IPSC frequency and amplitude, and synaptic uIPSC

properties, mouse genotypes were compared by one-way ANOVA followed by Dunnett's multiple comparisons test when the data were normally distributed with equal variances, by Brown-Forsythe ANOVA with Dunnett's multiple comparisons test when the data were normally distributed with unequal variances, and by the nonparametric Kruskal–Wallis test followed by Dunn's multiple comparisons test when the data were not normally distributed. Data were assessed for normality using the Shapiro-Wilk test. Bartlett's test with p=0.05 was used to assess equal variance. Data were tested for outliers using the ROUT or Grubbs' method to identify outliers, and statistical outliers were not included in data analysis. A two-way ANOVA followed by Tukey's test for multiple comparisons was used to compare groups in experiments in which repetitive measures were made from a single cell over various voltage commands or current injections. Cumulative distribution (survival) plots were analyzed by the Log-rank Mantel-Cox test. Data are presented as individual data points and/or mean ± SEM. Exact n and p-values are reported in figure legends.

Results

Spontaneous seizures and seizure-induced death in mice with selective expression of mutant $Na_v1.6$ in PV interneurons

We first sought to determine if expression of a GOF *SCN8A* variant selectively in PV interneurons would be sufficient for the development of spontaneous seizures. We used the conditional knock-in *Scn8a*$^{W/+}$ mouse model and crossed homozygous PV-Cre mice with *Scn8a*$^{W/+}$.tdT mice to generate *Scn8a*$^{W/+}$-PV mice, where the R1872W *SCN8A* variant is expressed exclusively in PV interneurons (Figure 2.1A). *Scn8a*$^{W/+}$-PV

mice were implanted with EEG recording electrodes and monitored for 10 weeks. To better conceptualize the phenotype of *Scn8a*$^{W/+}$-PV mice with reference to another *SCN8A* DEE model, we also implanted EEG recording electrodes in *Scn8a*$^{D/+}$ mice, which express the N1768D *SCN8A* variant globally, and monitored for 6-8 weeks. Spontaneous seizures were observed in all recorded *Scn8a*$^{W/+}$-PV mice (*n*=8; Figure 2.1B, D) and *Scn8a*$^{D/+}$ mice (*n*=14, Figure 2.1C, E). Median seizure onset in *Scn8a*$^{W/+}$-PV mice was approximately 10 weeks of age. In *Scn8a*$^{W/+}$-PV mice, seizures typically consisted of a wild running phase, which was immediately followed by a tonic-clonic phase in approximately 26% of seizures (23/89). Analysis of EEG signals from both *Scn8a*$^{D/+}$ and *Scn8a*$^{W/+}$-PV mice revealed spike-wave discharges, a distinct aspect of electrographic seizures (Figure 2.1B, C), highlighting similarities between a global mutation model and a model harboring a *SCN8A* variant exclusively in PV interneurons. *Scn8a*$^{W/+}$-PV mice also died prematurely compared to WT littermates, with a median survival of 16.6 weeks (Figure 2.1F). Electrographic and video recordings confirmed

Scn8a$^{W/+}$-PV mice that died during monitoring succumbed to seizure-induced death (*n*=3; Videos 1 & 2). Interestingly, all fatal seizures exhibited a tonic phase prior to death, consistent with our previous findings in *SCN8A* EE mice [114]. In agreement with

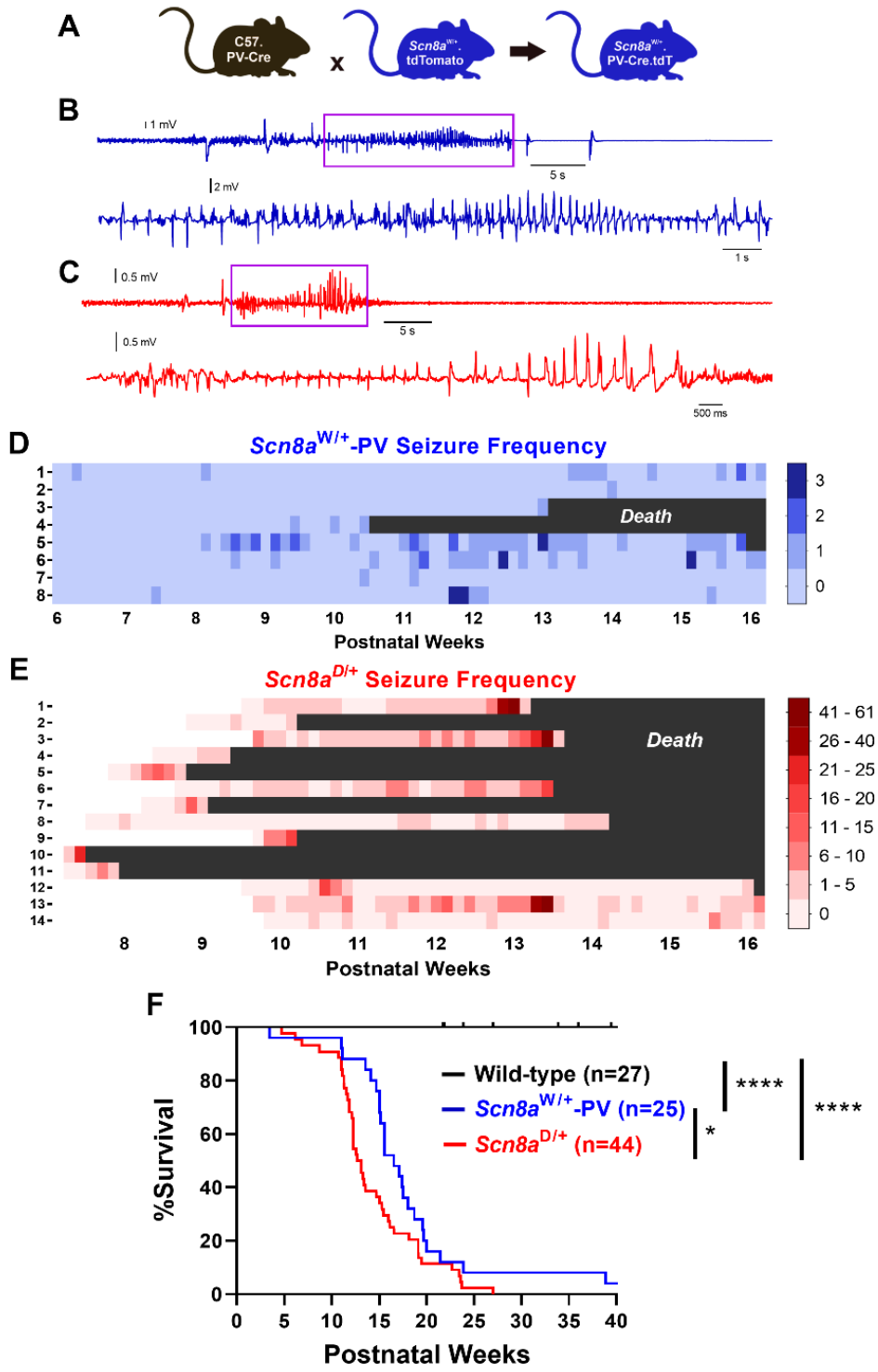

Figure 2.1: Mice expressing the patient-derived *SCN8A* variant R1872W exclusively in PV interneurons exhibit spontaneous seizures and seizure-induced death. (**A**) Breeding strategy used to produce *Scn8a*$^{W/+}$.tdT.PV-Cre mice (*Scn8a*$^{W/+}$-PV mice, used for both *in vivo* and whole-cell patch clamp experiments) and age-matched littermate controls on a C57 background. These mice express the R1872W *SCN8A* mutation exclusively in PV interneurons, which are fluorescently labeled with tdTomato. (**B**) Example EEG recording of a spontaneous seizure (blue) from an adult *Scn8a*$^{W/+}$-PV mouse. Spontaneous seizure shown here resulted in seizure-induced death (supplementary video 1 & 2). Purple box highlights spike wave discharges, expanded below. (**C**) Example EEG recording of a spontaneous seizure (red) from an adult *Scn8a*$^{D/+}$ mouse, which expresses the N1768D *SCN8A* variant globally. Purple box highlights spike wave discharges, expanded below. (**D**) Seizure heatmap of (*n*=8) *Scn8a*$^{W/+}$-PV mice over a period of 10 weeks. (**E**) Seizure heatmap of (*n*=14) *Scn8a*$^{D/+}$ mice over a period of about 8 weeks. Monitoring began at slightly varying ages, indicated by white in heatmap. (**F**) Survival of *Scn8a*$^{W/+}$-PV mice (*n*=25) and *Scn8a*$^{D/+}$ mice (n=44) are significantly reduced when compared with WT (*n*=27; $p<0.0001$; Log-rank Mantel-Cox test). Survival of *Scn8a*$^{D/+}$ mice is decreased compared to *Scn8a*$^{W/+}$-PV mice ($p<0.05$, Log-rank Mantel-Cox test).

previous studies [87], *Scn8a*$^{D/+}$ mice also died prematurely as a result of seizure-induced death (Figure 2.1F; Video 3), which was significantly accelerated compared to *Scn8a*$^{W/+}$-PV mice ($p=0.024$). Overall, these findings show that a gain-of-function variant exclusively expressed in PV interneurons can lead to seizures and seizure-induced death, and this supports a previously unappreciated role for PV interneurons in seizure induction and seizure-induced death in a mouse model of *SCN8A* DEE.

Imaging of parvalbumin interneuron morphology

For all experiments in this chapter, we used WT;tdT;PV-Cre, *Scn8a*$^{D/+}$;tdT;PV-Cre, and *Scn8a*$^{W/+}$;tdT;PV-Cre mice, referred to as WT, *Scn8a*$^{D/+}$, and *Scn8a*$^{W/+}$-PV mice for simplicity, that expressed a Cre-inducible tdTomato fluorescent reporter driven by PV-Cre. All PV-positive cells in these mice should theoretically be fluorescently labeled. To verify that fluorescently labeled cells were indeed parvalbumin-positive, we used immunohistochemistry to stain for parvalbumin in WT, *Scn8a*$^{D/+}$, and *Scn8a*$^{W/+}$-PV mice crossed with tdTomato. We found that >95% of cells in the somatosensory cortex

were both parvalbumin and tdTomato positive (Figure 2.2), indicating the effective expression of our fluorescent reporter.

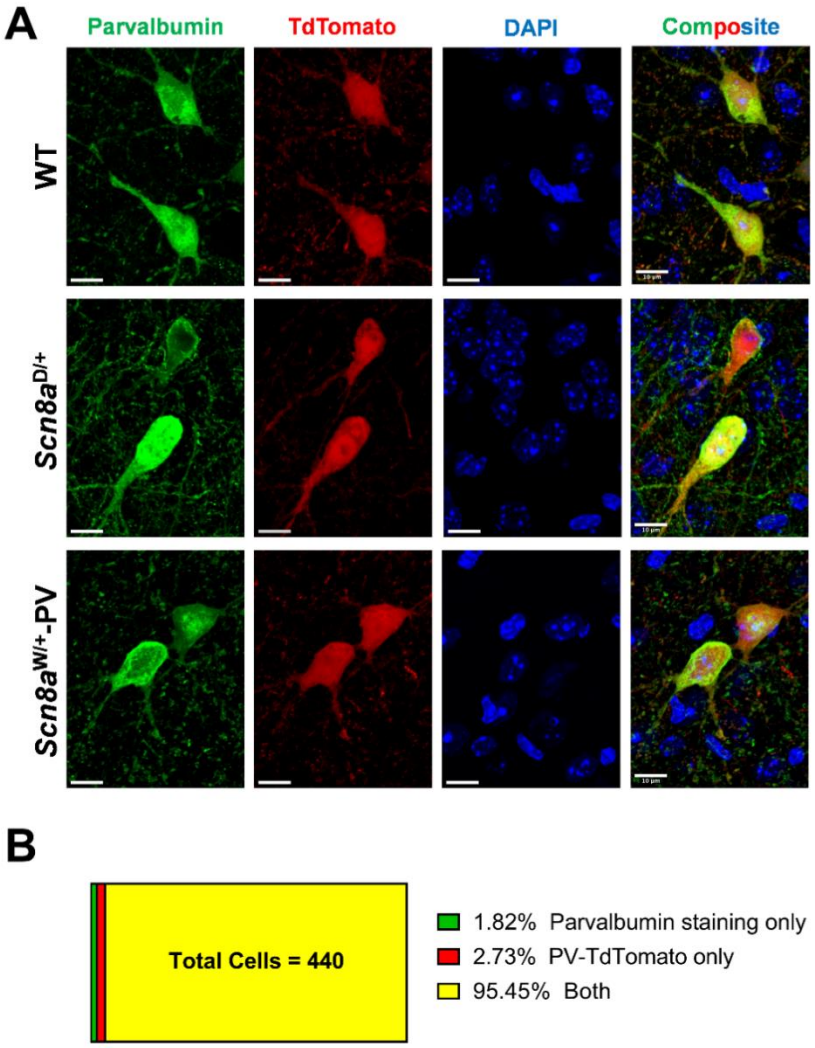

Figure 2.2: Colocalization of parvalbumin and TdTomato in WT, *Scn8a*$^{D/+}$, and *Scn8a*$^{W/+}$-PV mice. (**A**) Example immunohistochemistry images showing colocalization of parvalbumin (green) and tdTomato (red) immunofluorescence in adult WT, *Scn8a*$^{D/+}$, and *Scn8a*$^{W/+}$-PV mice. Scale bar 10 µM. Images were collected from layer IV/V of the somatosensory cortex in n=3 mice from each genotype. (**B**) Cell counting shows that >95% of cells expressed both parvalbumin and tdTomato.

Additionally, it is well known that $Na_v1.6$ is expressed at the distal AIS.[62] Changes in the structural composition of $Na_v1.6$ such as a GOF mutation could lead to changes in sodium channel expression in the axon. To assess potential axonal structural differences, we used immunohistochemistry to stain for $Na_v1.6$ at the AIS. We observed no significant differences in apparent AIS length or $Na_v1.6$ staining intensity

between WT, *Scn8a*$^{D/+}$, and *Scn8a*$^{W/+}$-PV interneurons (Figure 2.3). This may suggest limited structural compensation for increased $Na_v1.6$ activity in PV interneurons.

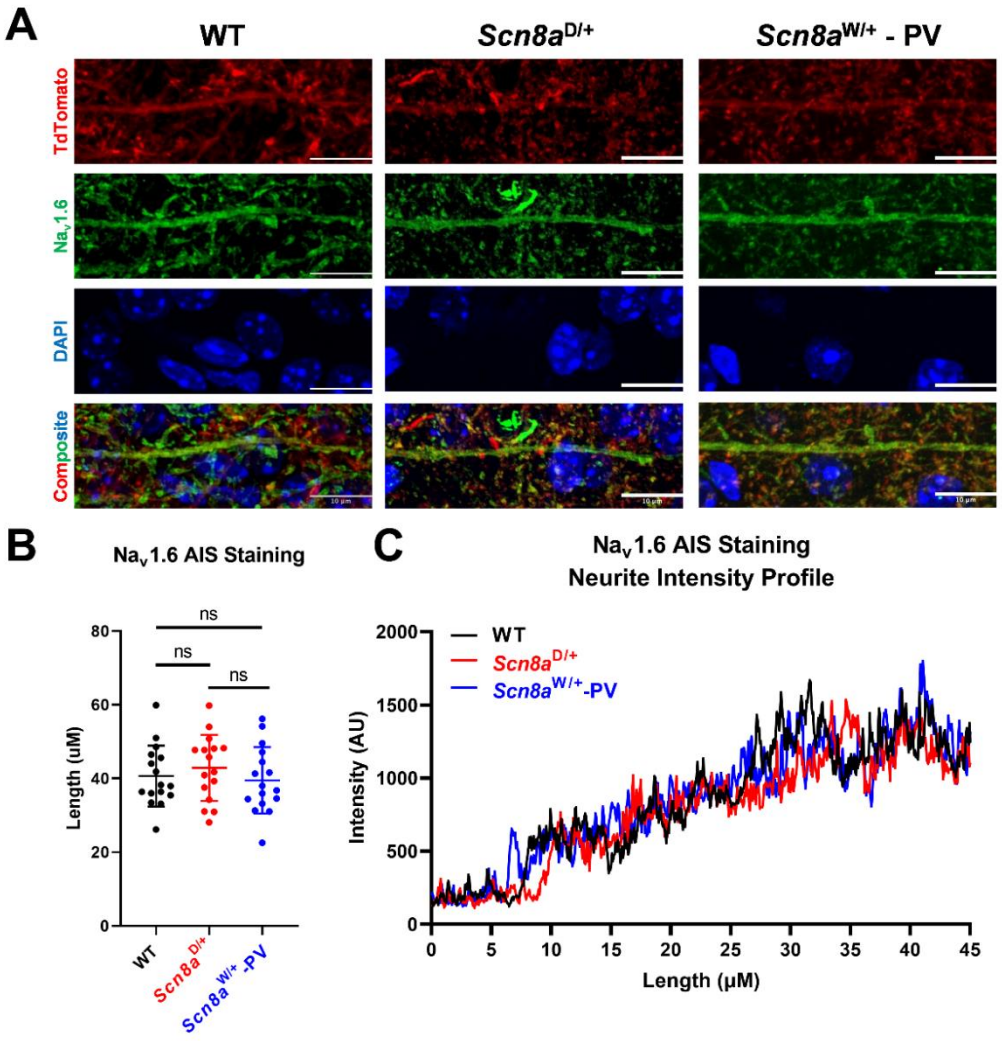

Figure 2.3: $Na_v1.6$ expression patterns in WT, *Scn8a*$^{D/+}$, and *Scn8a*$^{W/+}$-PV mice. (**A**) Example immunohistochemistry images showing tdTomato (expressed via PV-Cre), $Na_v1.6$, and DAPI in adult WT, *Scn8a*$^{D/+}$, and *Scn8a*$^{W/+}$-PV mice. Scale bar 10 µM. (**B, C**) Image quantification from *n*=16 cells of each genotype from *n*=3 mice. There is no difference in $Na_v1.6$ staining length or intensity at the AIS (one-way ANOVA with Dunnett's multiple comparison test).

Depolarization block in *Scn8a* mutant PV interneurons

To assess the intrinsic physiological function of *Scn8a* mutant PV interneurons, we performed electrophysiological recordings of fluorescently labeled PV interneurons in layer IV/V of the somatosensory cortex of adult (5 to 8 weeks) *Scn8a*$^{D/+}$, *Scn8a*$^{W/+}$-PV, and age-matched WT littermates (Figure 2.4 A). WT littermates from both *Scn8a*$^{D/+}$ and *Scn8a*$^{W/+}$-PV genotypes did not exhibit any differences in firing frequencies (p=0.656) and were pooled. Analysis of membrane and action potential (AP) properties revealed that *Scn8a*$^{D/+}$ PV interneurons had decreased downstroke velocity as well as increased AP width when compared to WT (Table 2.1). Using a series of depolarizing current injection steps to assess intrinsic excitability, we observed a difference in excitability (p=0.028) between WT, *Scn8a*$^{D/+}$, and *Scn8a*$^{W/+}$ PV interneurons. Initially, PV interneurons expressing either *Scn8a* variant were hyperexcitable compared to WT littermates at lower current injection steps (<100 pA in *Scn8a*$^{D/+}$ mice, p=0.045 and <360 pA in *Scn8a*$^{W/+}$-PV mice, p=0.030). However, at higher current injection steps, both *Scn8a*$^{D/+}$ and *Scn8a*$^{W/+}$ PV interneurons exhibited progressive action potential failure as a result of depolarization block (>640 pA in *Scn8a*$^{D/+}$ mice, p=0.042; >840 pA in *Scn8a*$^{W/+}$-PV mice, p=0.041; Figure 2.4 B-F). Both *Scn8a*$^{D/+}$ and *Scn8a*$^{W/+}$ PV interneurons were more prone to depolarization block than their WT counterparts over the range of current injection magnitudes (p<0.0001 and p=0.016 respectively; Figure 2.4 F). Depolarization block of inhibitory interneurons has been previously implicated in seizure-like activity both *in vitro* and *in vivo*, and has been proposed as a biophysical mechanism underlying approach of seizure threshold.[35,115–119] Here, the early onset of depolarization block in *Scn8a* mutant PV interneurons indicates a PV hypo-excitability

phenotype, similar to the phenotypes observed in PV interneurons in gain-of-function *SCN1A* DEE and in SST interneurons in *SCN8A* DEE.[35,36]

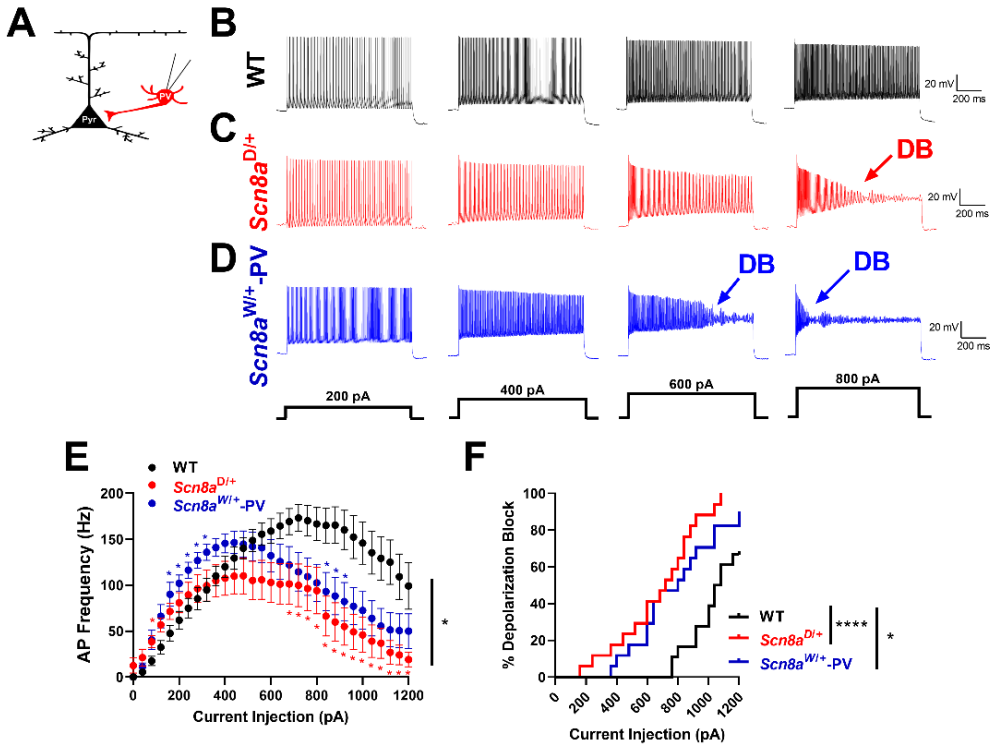

Figure 2.4: Altered excitability and depolarization block in *Scn8a*$^{D/+}$ and *Scn8a*$^{W/+}$-PV interneurons. (**A**) Whole-cell recordings were collected from WT, *Scn8a*$^{D/+}$, and *Scn8a*$^{W/+}$-PV interneurons in layer IV/V of the somatosensory cortex in adult, 5-8 week old mice. (**B-D**) Example traces of WT (**B**, black), *Scn8a*$^{D/+}$ (**C**, red), and *Scn8a*$^{W/+}$ (**D**, blue) PV interneuron firing at 200, 400, 600, and 800 pA current injections. Depolarization block is noted with arrows (DB). (**E**) *Scn8a*$^{D/+}$ (n=17, 6 mice) and *Scn8a*$^{W/+}$ PV (n=17, 5 mice) interneurons experience a decrease in firing via depolarization block (*, p<0.05, two-way ANOVA with Tukey's multiple comparisons test) when compared to WT PV interneurons (n=18, 8 mice). Red or blue stars indicate individual points of significance for either *Scn8a*$^{D/+}$ or *Scn8a*$^{W/+}$-PV, respectively, by multiple comparisons test. (**F**) Cumulative distribution of PV interneuron entry into depolarization block relative to current injection magnitude for WT, *Scn8a*$^{D/+}$, and *Scn8a*$^{W/+}$-PV mice (****, p<0.0001, *, p<0.05, Log-rank Mantel-Cox test).

	Vm (mV)	AP threshold (mV)	Rheobase (pA)	Upstroke Velocity (mV/ms)	Downstroke Velocity (mV/ms)	Amplitude (mV)	APD_{50} (ms)	Input Resistance (MΩ)
Wild-type (n=18, 8)	-65.2 ± 1.6	-40.9 ± 1.5	93.3 ± 15.8	272.1 ± 14.7	-158.4 ± 10.3	59.0 ± 2.5	0.47 ± 0.03	161.0 ± 8.1
Scn8a$^{D/+}$ (n=17, 6)	-62.1 ± 1.7	-43.2 ± 1.8	60.0 ± 10.3	241.4 ± 22.5	*-111.4 ± 10.1* **	62.9 ± 2.7	*0.71 ± 0.05* ***	193.8 ± 12.8
Scn8a$^{W/+}$-PV (n=17, 5)	-62.4 ± 1.6	-39.4 ± 1.2	75.3 ± 8.1	271.6 ± 18.9	-155.5 ± 11.4	63.1 ± 2.7	0.55 ± 0.03	186.3± 12.0

Table 2.1: Membrane and Action Potential Properties of Adult Layer IV/V PV Interneurons. Recordings were carried out in multiple cells from each animal (n=cells, animals). Data are presented as mean ± SEM.

Excitatory neurons in *Scn8a*$^{W/+}$-PV mice

Previous studies have shown that excitatory pyramidal neurons in global knock-in *Scn8a*$^{D/+}$ mice are hyperexcitable compared to WT, suggesting that a global change in neuronal activity of both inhibitory and excitatory neurons likely contributes to the seizure phenotype.[91] To determine if firing is affected in excitatory neurons from *Scn8a*$^{W/+}$-PV mice, which selectively express a *Scn8a* variant in PV interneurons, we recorded the intrinsic excitability of pyramidal neurons from cortical layers IV/V in adult mice (Figure 2.5). Interestingly, we did not observe any differences in the intrinsic excitability of pyramidal neurons between the WT and *Scn8a*$^{W/+}$-PV genotypes (Figure 2.5). This suggests that alterations in the physiology of PV interneurons may be sufficient in facilitating seizures in *SCN8A* DEE. Analysis of action potential parameters revealed an increase in input resistance and a decrease in rheobase (Figure 2.5 E, F; Table 2.2), suggestive of some compensatory changes in excitatory pyramidal cells.

	Vm (mV)	AP threshold (mV)	Rheobase (pA)	Upstroke Velocity (mV/ms)	Downstroke Velocity (mV/ms)	Amplitude (mV)	APD_{50} (ms)	Input Resistance (MΩ)
Wild-type (*n*=14, 5)	-64.4 ± 1.3	-39.9 ± 0.9	104.6 ± 10.7	274.1 ± 18.1	-71.0 ± 8.4	84.2 ± 2.5	1.36 ± 0.14	113.8 ± 9.3
Scn8a$^{W/+}$-PV (*n*=15, 3)	-67.6 ± 1.4	-42.1 ± 1.0	*62.7 ± 7.5* **	267.3 ± 21.6	-63.7 ± 6.5	85.6 ± 3.0	1.49 ± 0.16	*167.7 ± 13.4* **

Table 2.2: Membrane and Action Potential Properties of Adult Layer IV/V Pyramidal Neurons. Recordings were carried out in multiple cells from each animal (n=cells, animals). Data are presented as mean ± SEM.

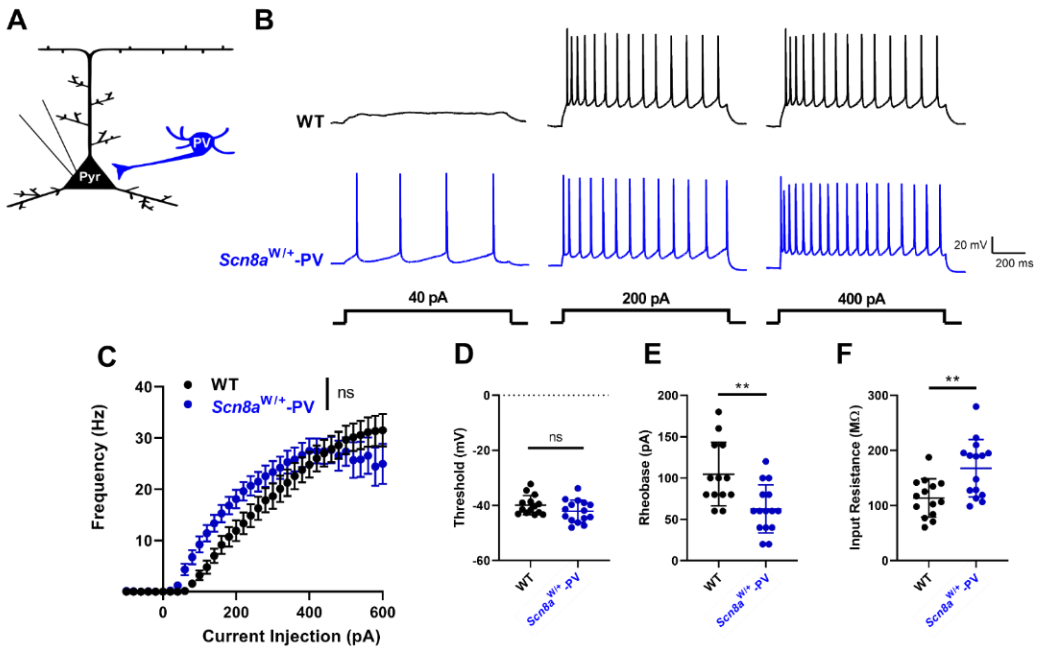

Figure 2.5: Intrinsic excitability of pyramidal cells in *Scn8a*$^{W/+}$-PV mice. (**A**) Whole-cell recordings were collected from pyramidal cells in layer IV/V somatosensory cortex in adult, 5-8 week old WT and *Scn8a*$^{W/+}$-PV mice. (**B**) Example traces of WT (black) and *Scn8a*$^{W/+}$-PV(blue) pyramidal cell firing at 40, 200, and 400 pA current injections. (**C**) Pyramidal cell firing does not significantly differ between WT (n=14, 5 mice) and *Scn8a*$^{W/+}$-PV mice (n=15, 3 mice, p>0.05, 2-way ANOVA). (**D**) There is no significant difference in pyramidal cell AP threshold in WT and *Scn8a*$^{W/+}$-PV mice (p<0.05, unpaired t-test). (**E**) Rheobase in *Scn8a*$^{W/+}$-PV pyramidal cells is significantly lower than WT (**, p<0.01, unpaired t-test). (**F**) Pyramidal cell input resistance is significantly increased in *Scn8a*$^{W/+}$-PV mice (**, p<0.01, unpaired t-test).

Development of parvalbumin interneuron dysfunction in *Scn8a* mutant mice

Additionally, the role of development is an important consideration in understanding the pathophysiology of *SCN8A* DEE. In Dravet Syndrome, differences in PV interneuron intrinsic excitability are only observed during a critical developmental time window (P18-21).[49] To determine if the same was true for PV interneurons in *SCN8A* DEE, we measured intrinsic excitability at the critical P18-21 time window (Figure 2.6). Although no differences in intrinsic excitability were observed (Figure 2.6B), there were significant differences in AP waveform between WT, *Scn8a*$^{D/+}$, and

Scn8a$^{W/+}$-PV interneurons at P18-21. APs in P18-21 *Scn8a* mutant mice were significantly wider with slower upstroke and downstroke velocities than their WT counterparts (Figure 2.6 C-F, Table 2.3). These findings indicate early alterations in PV interneuron AP parameters prior to the onset of spontaneous seizures and may suggest a progression of PV interneuron physiology into adulthood.

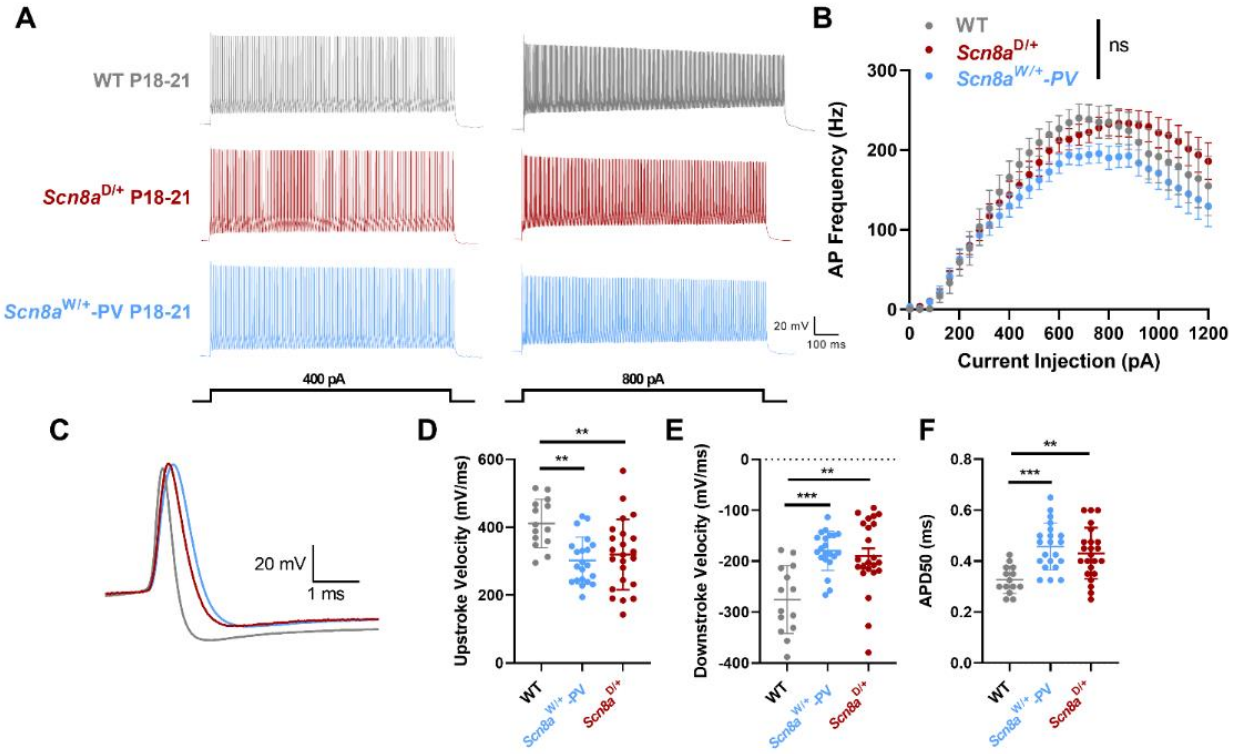

Figure 2.6: Intrinsic excitability of PV interneurons in P18-21 WT, *Scn8a*$^{D/+}$, and *Scn8a*$^{W/+}$-PV mice. (**A**) Example traces of P18-21 PV interneuron firing in WT (gray), *Scn8a*$^{D/+}$ (red), and *Scn8a*$^{W/+}$-PV (blue) mice at 400 and 800 pA current injections. (**B**) PV interneuron firing does not significantly differ between WT (n=14, 3 mice), *Scn8a*$^{D/+}$ (n=21, 4 mice), and *Scn8a*$^{W/+}$-PV mice (n=23, 4 mice, p>0.05, 2-way ANOVA) at P18-21. (**C**) Example of a single AP from WT, *Scn8a*$^{D/+}$, and *Scn8a*$^{W/+}$-PV interneuron. (**D**) Upstroke velocity is significantly decreased in *Scn8a*$^{D/+}$ (**, p<0.01) and *Scn8a*$^{W/+}$-PV (**, p<0.01) interneurons compared to WT (one-way ANOVA with Tukey's multiple comparison test). (**E**) Downstroke velocity is significantly decreased in *Scn8a*$^{D/+}$ (**, p<0.01) and *Scn8a*$^{W/+}$-PV (***, p<0.001) interneurons compared to WT (Kruskal-Wallis test with Dunn's multiple comparison test). (**F**) *Scn8a*$^{D/+}$ (**, p<0.01) and *Scn8a*$^{W/+}$-PV (***, p<0.001) interneurons have wider APs than their WT counterparts (one-way ANOVA with Tukey's multiple comparison test).

	Vm (mV)	AP threshold (mV)	Rheobase (pA)	Upstroke Velocity (mV/ms)	Downstroke Velocity (mV/ms)	Amplitude (mV)	APD_{50} (ms)	Input Resistance (MΩ)
Wild-type (*n*=14, 3)	-66.4 ± 1.1	-37.3 ± 1.1	208.6 ± 20.4	411.5 ± 19.0	-275.4 ± 17.8	66.3 ± 2.0	0.33 ± 0.01	104.0 ± 7.8
Scn8a$^{D/+}$ (*n*=21, 4)	-65.2 ± 1.3	-39.6 ± 1.2	149.5 ± 15.1	*319.6 ± 21.7* **	*-189.7 ± 15.0* **	61.2 ± 2.6	*0.43 ± 0.02* **	106.9 ± 6.2
Scn8a$^{W/+}$-PV (*n*=23, 3)	-64.8 ± 0.8	-36.9 ± 0.9	203.8 ± 24.0	*302.0 ± 15.0* **	*-179.5 ± 8.4* ***	62.1 ± 2.6	*0.46 ± 0.02* ***	116.2 ± 7.9

Table 2.3: Membrane and Action Potential Properties of P18-21 Layer IV/V PV Interneurons. Recordings were carried out in multiple cells from each animal (n=cells, animals). Data are presented as mean ± SEM.

Further, we sought to examine seizure susceptibility throughout adolescent development *in vivo.* Our previous studies have demonstrated the susceptibility of both *Scn8a*$^{D/+}$ and *Scn8a*$^{W/+}$-SST-Cre mice, which harbor the R1872W mutation exclusively in SST inhibitory interneurons, to audiogenic seizures *in vivo*.[36,107] This allowed us to rapidly assess susceptibility to behavioral seizures in *Scn8a*$^{W/+}$-PV mice. To this end, we examined the susceptibility of *Scn8a*$^{W/+}$-PV mice to audiogenic seizures at multiple developmental time points *in vivo*. We observed that at P21, only 2 of 7 *Scn8a*$^{W/+}$-PV mice exhibited audiogenic seizures, whereas at P42, all mice exhibited audiogenic seizures (Figure 2.7). We also observed one seizure-induced death at P28. This data suggests a progressive onset of seizures in adolescent *Scn8a*$^{W/+}$-PV mice.

Figure 2.7: *Scn8a*$^{W/+}$-PV mice develop audiogenic seizures between P21-42. Seizure progression in *Scn8a*$^{W/+}$-PV mice begins with a wild running phase followed by a clonic phase before recovery. Audiogenic seizure testing was performed on n=7 *Scn8a*$^{W/+}$-PV mice at P21, P28. P35. and P42, resulting in a progressive increase in the number of mice seizing in response to the audiogenic stimulus. * At P28, n=1 audiogenic seizure resulted in death.

Gain-of-function $Na_v1.6$ mutations impact sodium channel currents in PV interneurons

Depolarization block in *Scn8a*$^{D/+}$ and *Scn8a*$^{W/+}$ PV interneurons likely arises from abnormal sodium channel activity as a result of the gain-of-function variant, contributing to changes in membrane depolarization levels and subsequent sodium channel availability for AP initiation. Increases in the I_{NaP} have been identified as a major factor in many epileptic encephalopathy-causing variants, including both the N1768D and R1872W variants in *SCN8A* DEE.[5,57,89,91] Further, I_{NaP} is a known determinant of depolarization block threshold.[36] In view of this, we recorded I_{NaP} in PV interneurons in the whole-cell patch clamp configuration (Figure 2.8 A). I_{NaP} was increased in both *Scn8a*$^{D/+}$ (-293.1 ± 38.0 pA; p=0.032) and *Scn8a*$^{W/+}$ (-347.1 ± 49.0 pA; p=0.004) PV interneurons when compared to WT (-166.6 ± 29.7 pA; Figure 2.8 B-E). Half-maximal voltage of activation ($V_{1/2}$) did not differ from WT (-62.0 ± 1.0 mV) in either *Scn8a*$^{D/+}$ (-59.9 ± 1.1 mV; p=0.329) or *Scn8a*$^{W/+}$-PV (-63.9 ± 1.2 mV; p=0.592) mice (Figure 2.8 F). Another component of the sodium current that may affect excitability particularly in fast spiking cells is the resurgent sodium current (I_{NaR}).[120,121] I_{NaR} is a slow inactivating depolarizing current that can contribute to increased AP frequency by providing additional depolarization during the falling phase of an AP.[120–122] I_{NaR} has been previously implicated in temporal lobe epilepsy as well as in sodium channelopathies.[123,124] I_{NaR} was significantly increased in *Scn8a*$^{W/+}$-PV interneurons (-1136.0 ± 178.5 pA; p=0.037), and while we observed an increasing trend, I_{NaR} was not significantly increased in *Scn8a*$^{D/+}$ PV interneurons (-952.8 ± 172.9 pA; p=0.219), when compared to WT (-595.9 ± 84.8 pA) PV interneurons (Figure 2.8 G-J). Current-voltage

relationship of I_{NaR} was not different between WT, *Scn8a*$^{D/+}$, and *Scn8a*$^{W/+}$-PV mice (*p*=0.631; Figure 2.8 K). These results demonstrate an increase in two components of the overall sodium current in PV interneurons, which possibly contributes to their initial hyperexcitability and increased susceptibility to depolarization block. Increases in both I_{NaP} and I_{NaR} likely provide a sustained level of depolarization, resulting in the accumulation of inactivated sodium channels and increased susceptibility to depolarization block.[35,36,125]

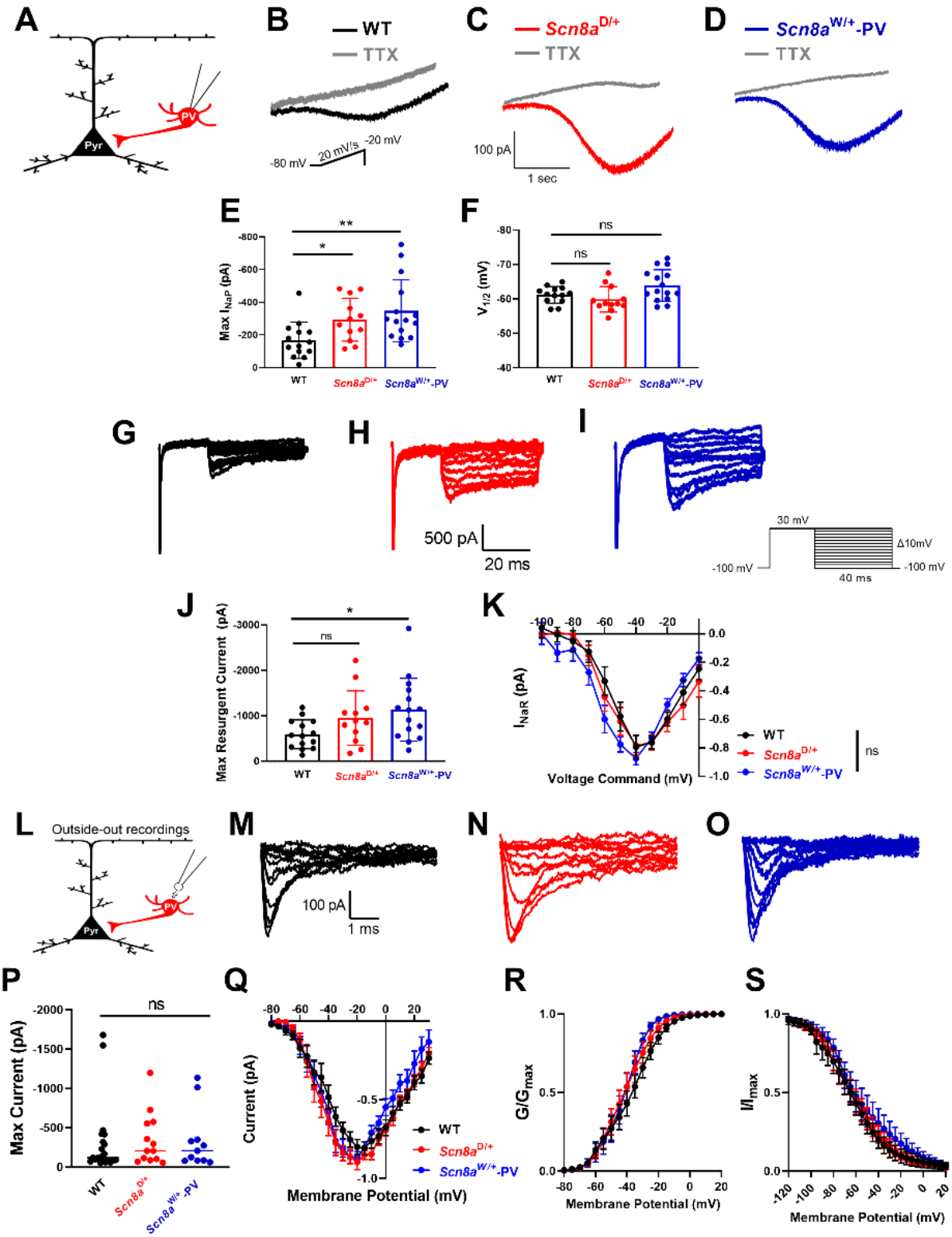
A
PV
Pyr
B
WT
TTX
-80 mV
20 mV/s
-20 mV
C
Scn8aD/+
TTX
100 pA
1 sec
D
Scn8aW/+-PV
TTX
E
Max INaP (pA)
WT
Scn8aD/+
Scn8aW/+-PV
F
V1/2 (mV)
ns
G
H
500 pA
20 ms
I
30 mV
Δ10mV
-100 mV
-100 mV
40 ms
J
Max Resurgent Current (pA)
K
INaR (pA)
Voltage Command (mV)
L
Outside-out recordings
M
100 pA
1 ms
N
O
P
Max Current (pA)
Q
Current (pA)
Membrane Potential (mV)
R
G/Gmax
Membrane Potential (mV)
S
I/Imax
Membrane Potential (mV)

Figure 2.8: Voltage-gated sodium currents in WT, *Scn8a*$^{D/+}$, and *Scn8a*$^{W/+}$ PV interneurons. (**A**) I_{NaP} and I_{NaR} were recorded via whole-cell patch clamp onto PV interneurons in layer IV/V of the somatosensory cortex in adult, 5-8-week-old WT (*n*=14, 5 mice), *Scn8a*$^{D/+}$ (*n*=12, 4 mice), and *Scn8a*$^{W/+}$-PV mice (*n*=15, 5 mice). (**B, C, D**) Example traces of steady state I_{NaP} evoked by slow voltage ramps from WT (**B**, black), *Scn8a*$^{D/+}$ (**C**, red), and *Scn8a*$^{W/+}$ (**D**, blue) PV interneurons. Traces in gray show slow voltage ramp in the presence of 500 nM TTX. (**E**) Elevated maximum I_{NaP} in *Scn8a*$^{D/+}$ (*, p<0.05) and *Scn8a*$^{W/+}$-PV (**, p<0.01) interneurons compared with WT PV interneurons (Kruskal-Wallis test with Dunn's multiple comparison test). (**F**) $V_{1/2}$ values were not different between WT, *Scn8a*$^{D/+}$, and *Scn8a*$^{W/+}$-PV mice (p>0.05, one-way ANOVA with Dunnett's multiple comparison test). (**G-I**) Example traces of TTX-subtracted I_{NaR} for WT (**G**, black), *Scn8a*$^{D/+}$ (**H**, red), and *Scn8a*$^{W/+}$ (**I**, blue). (**J**) Maximum I_{NaR} magnitude was increased between WT and *Scn8a*$^{W/+}$-PV interneurons (*, p<0.05), whereas I_{NaR} magnitude between WT and *Scn8a*$^{D/+}$ PV interneurons was not significantly different (p>0.05, Brown-Forsythe ANOVA with Dunnett's multiple comparison test). (**K**) Current-voltage relationship for I_{NaR} is not significantly different between WT, *Scn8a*$^{D/+}$, and *Scn8a*$^{W/+}$-PV mice (p>0.05, 2-way ANOVA). (**L**) Transient sodium current was assessed in PV interneurons using patch-clamp recordings in the outside out configuration. (**M-O**) Example traces for family of sodium currents recorded from WT (**M**, black), *Scn8a*$^{D/+}$ (**N**, red), and *Scn8a*$^{W/+}$ (**O**, blue) PV interneurons. (**P**) Maximum transient sodium current was not significantly different between WT (*n*=20, 8 mice), *Scn8a*$^{D/+}$ (*n*=12, 4 mice), and *Scn8a*$^{W/+}$ (*n*=12, 4 mice) PV interneurons (p>0.05, Kruskal-Wallis test with Dunn's multiple comparison test). (**Q**) Current-voltage relationship does not differ between WT, *Scn8a*$^{D/+}$, and *Scn8a*$^{W/+}$-PV interneurons (p>0.05, 2-way ANOVA). (**R**) Voltage-dependent conductance curve does not differ significantly between WT, *Scn8a*$^{D/+}$, and *Scn8a*$^{W/+}$ PV interneurons (p>0.05, 2-way ANOVA). (**S**) Steady-state inactivation does not differ significantly between WT (*n*=12, 4 mice), *Scn8a*$^{D/+}$ (*n*=11, 4 mice), and *Scn8a*$^{W/+}$ (*n*=10, 4 mice) PV interneurons (p>0.05, 2-way ANOVA). Boltzmann curves shown are the average of individual curves generated from fits to data points.

Alterations of both activation and steady-state inactivation parameters of the transient sodium channel current have been previously reported in cells expressing GOF *SCN8A* mutations.[5,82,126,127] To examine PV interneuron sodium channel currents, we performed excised somatic patches in the outside-out configuration from PV interneurons (Figure 2.8 L). Sodium current density, voltage-dependent activation, or steady-state inactivation were not different between WT, *Scn8a*$^{D/+}$, and *Scn8a*$^{W/+}$-PV mice (Figure 2.8 M-S; Table 2.4).

	$V_{1/2}$ (activation, mV)	K (activation)	$V_{1/2}$ (inactivation, mV)	K (inactivation)	I_{NaP} at 50ms (pA)
Wild-type (*n*=20, 8; *n*=12, 4)	-38.0 ± 3.0	-6.1 ± 0.5	-63.5 ± 6.0	15.9 ± 3.6	21.9 ± 8.8
Scn8a$^{D/+}$ (*n*=12, 4; *n*=11, 4)	-41.2 ± 3.0	-6.4 ± 0.5	-61.9 ± 4.7	12.9 ± 1.3	33.9 ± 21.5
Scn8a$^{W/+}$-PV (*n*=12, 4; *n*=10, 4)	-42.3 ± 2.7	-5.2 ± 0.4	-51.5 ± 6.9	16.2 ± 2.3	17.7 ± 35.9

Table 2.4: Channel Properties of Layer IV/V PV interneurons. Outside-out recordings were carried out in multiple cells from each animal (n=cells, animals) and in multiple experiments as shown here: genotype (activation n; inactivation n). Data from individual recordings were fit to a Boltzmann function to generate V1/2 and k values. Data are presented as mean ± SEM.

Decreased inhibitory input onto excitatory neurons in *Scn8a* mutant mice

Impaired excitability in *Scn8a* mutant PV interneurons may lead to decreased inhibition onto excitatory pyramidal cells, as PV interneurons are known to directly inhibit pyramidal cells at the soma or AIS.[94,97] To examine how alterations in PV interneuron excitability affect the cortical network, we recorded spontaneous and miniature inhibitory post-synaptic currents (sIPSCs and mIPSCs) from pyramidal cells (Figure 2.9 A) as a functional indicator of PV interneuron activity and connectivity. We found that pyramidal cells generate significantly fewer sIPSCs in both *Scn8a*$^{D/+}$ (4.22 ± 0.64 Hz; p=0.035) and *Scn8a*$^{W/+}$-PV (4.07 ± 1.14 Hz; p=0.003) mice than their WT counterparts (7.97 ± 0.88 Hz; Figure 2.9 B-C), suggesting a decrease in inhibitory input onto pyramidal cells. sIPSC frequencies between *Scn8a*$^{D/+}$ and *Scn8a*$^{W/+}$-PV pyramidal cells were not different (p>0.99), which may imply that PV interneurons are largely responsible for the decrease in somatic inhibitory input in the global *Scn8a*$^{D/+}$ model. sIPSC amplitude was not different between WT (-62.7 ± 4.3 pA), *Scn8a*$^{D/+}$ (-54.7 ± 5.8 pA), and *Scn8a*$^{W/+}$-PV mice (-53.3 ± 8.4 pA; p=0.09, Figure 2.9 D). Additionally, we calculated the total charge transfer from sIPSCs in WT, *Scn8a*$^{D/+}$, and *Scn8a*$^{W/+}$-PV pyramidal cells, and found that the total spontaneous charge transfer onto pyramidal cells was significantly decreased in *Scn8a*$^{W/+}$-PV mice (-15346 ± 3706 pA*s; p=0.008) compared to WT (-41468 ± 7641 pA*s, Figure 2.9 E). Although it was not statistically significant, we also observed a decreasing trend in spontaneous inhibitory charge

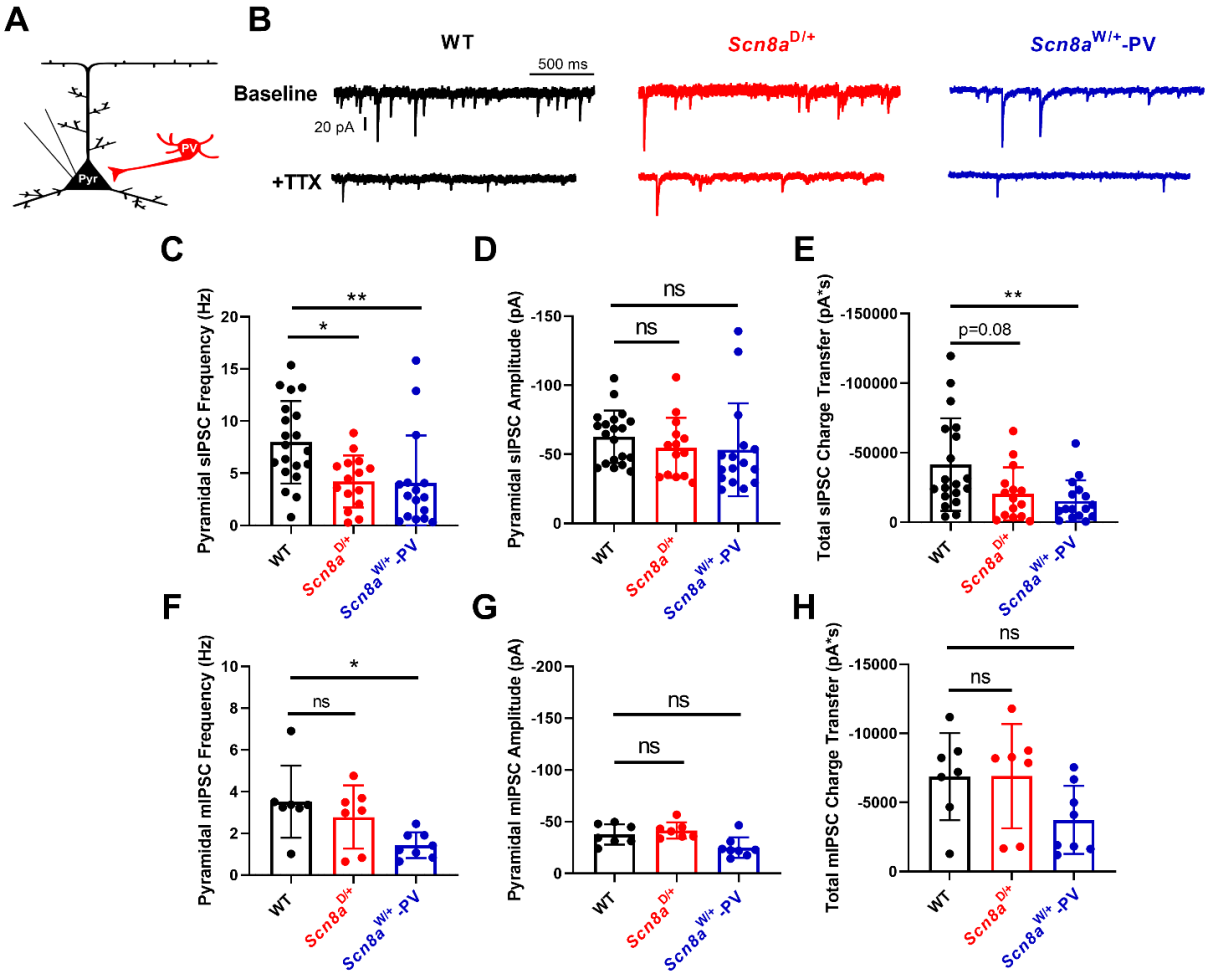

Figure 2.9: Inhibitory post-synaptic currents (IPSCs) generated in pyramidal cells from WT, *Scn8a*$^{D/+}$, and *Scn8a*$^{W/+}$-PV mice. (**A**) Whole-cell recordings of IPSCs were collected from cortical layer V pyramidal cells in adult, 5-8-week-old WT, *Scn8a*$^{D/+}$, and *Scn8a*$^{W/+}$-PV mice. (**B**) Example traces of IPSCs generated in pyramidal cells from WT (black), *Scn8a*$^{D/+}$ (red), and *Scn8a*$^{W/+}$-PV (blue) mice. (**C**) Frequency of sIPSCs generated in pyramidal cells is decreased in *Scn8a*$^{D/+}$ (n=15, 4 mice, *, p<0.05) and *Scn8a*$^{W/+}$-PV (n=16, 5 mice, **, p<0.01) mice when compared to WT (n=20, 6 mice, Kruskal-Wallis test with Dunn's multiple comparison test). (**D**) Amplitude of sIPSCs generated in pyramidal cells is not significantly different between groups (p>0.05, Kruskal-Wallis test with Dunn's multiple comparison test). (**E**) Total sIPSC charge transfer onto pyramidal cells was significantly decreased in *Scn8a*$^{W/+}$-PV mice (p<0.05), whereas total sIPSC charge transfer in *Scn8a*$^{D/+}$ mice was not significantly different (p>0.05, Kruskal-Wallis test with Dunn's multiple comparison test). (**F**) Frequency of mIPSCs recorded from pyramidal cells is decreased in *Scn8a*$^{W/+}$-PV (n=8, 3 mice) mice when compared to WT (n=7, 3 mice, *, p<0.05), whereas frequency of mIPSCs recorded from pyramidal cells in *Scn8a*$^{D/+}$ (n=7, 3 mice) mice did not significantly differ from WT (p>0.05, one-way ANOVA with Dunnett's multiple comparison test). (**G**) Amplitude of mIPSCs recorded from pyramidal cells is not significantly different between WT, *Scn8a*$^{D/+}$, and *Scn8a*$^{W/+}$-PV mice (p>0.05, Brown-Forsythe ANOVA with Dunnett's multiple comparison test). (**H**) Total mIPSC charge transfer onto pyramidal cells did not significantly differ between WT, *Scn8a*$^{D/+}$, and *Scn8a*$^{W/+}$-PV mice (p>0.05, Kruskal-Wallis test with Dunn's multiple comparison test).

include both AP-induced synaptic transients as well as mIPSCs, which occur due to spontaneous vesicle fusion in the absence of an AP.[128,129] To isolate AP-independent events, we performed recordings in the presence of TTX (500 nM). Relative to WT controls (3.52 ± 0.65 Hz), we found no significant difference in pyramidal cell mIPSC frequency in *Scn8a*$^{D/+}$ mice (2.78 ± 0.57 Hz; p=0.821), but we did observe a significant reduction of mIPSC frequency in *Scn8a*$^{W/+}$-PV mice (1.43 ± 0.22 Hz; p=0.027; Figure 2.9 F), which could underlie impaired synaptic transmission in *Scn8a*$^{W/+}$-PV mice. mIPSC amplitude did not differ between WT (-37.7 ± 3.7 pA), *Scn8a*$^{D/+}$ (-41.6 ± 3.0 pA; p=0.667), and *Scn8a*$^{W/+}$-PV mice (-25.1 ± 3.5 pA; p=0.055, Figure 2.9 G), although we did observe a decreasing trend in the mIPSC amplitude for *Scn8a*$^{W/+}$-PV mice. Interestingly, we did not observe any significant differences in mIPSC total charge transfer between WT (-6874 ± 1194 pA*s), *Scn8a*$^{D/+}$ (-6907 ± 1426 pA*s; p=0.984), and *Scn8a*$^{W/+}$-PV mice (-3734 ± 872.6 pA*s; p=0.133, Figure 2.9 H).

PV interneuron synaptic transmission is impaired in *Scn8a* mutant mice

Impairment of synaptic transmission has been suggested as a disease mechanism in multiple epilepsy syndromes, notably Dravet Syndrome,[50,130,131] and proper synaptic signaling is tightly linked to sodium channel function.[132] To assess how $Na_V1.6$ function influences PV interneuron-mediated inhibitory synaptic transmission, we performed dual whole-cell patch clamp recordings of PV interneurons and nearby pyramidal cells (PCs) to find synaptically-connected pairs of cells (Figure 2.10 A). Synaptically-connected pairs were identified using a current ramp in the presynaptic PV interneuron to elicit inhibitory postsynaptic potentials (IPSPs) in the postsynaptic PC corresponding to each AP in the PV interneuron (Figure 2.10 B). The number of

synaptically-connected PV:PC pairs relative to the total number of pairs was not significantly different between WT, *Scn8a*$^{D/+}$, and *Scn8a*$^{W/+}$-PV mice (p=0.634, Figure 2.10 C). In PV:PC connected pairs, we measured the properties of unitary inhibitory postsynaptic currents (uIPSCs) in PCs evoked by stimulation of PV interneurons. To accurately detect uIPSCs, a high chloride internal solution was used to allow recording of uIPSCs as large inward currents and IPSPs as large membrane depolarizations, overall minimizing the possibility of inaccurately reporting a synaptic failure.

Previous studies indicate that the PV:PC synapse is extremely reliable since PV interneurons have multiple synaptic boutons and a high release probability, indicative of a highly stable synapse.[133] PV interneurons are also known to fire reliably at high frequencies.[97] We found that stimulation of PV interneurons at a 1 Hz frequency reliably initiated single action potentials in WT mice. Although we detected some failures in *Scn8a*$^{D/+}$ and *Scn8a*$^{W/+}$-PV mice, there was no significant difference in synaptic failure at a frequency of 1Hz (p=0.160; Table 2.5) between the groups, suggesting no deficit in synaptic transmission at low stimulation frequencies. The amplitudes of the uIPSCs also did not differ between genotypes (Table 2.5, p=0.427). Additionally, to identify any deficits in short-term synaptic plasticity, we used the first two IPSCs (IPSC1 and IPSC2) elicited by a presynaptic action potential to quantify the paired-pulse ratio (PPR). The PV:PC synapse is known to experience short-term plasticity through synaptic depression.[134,135] We observed synaptic depression in WT, *Scn8a*$^{D/+}$, and *Scn8a*$^{W/+}$-PV

connected pairs, with no significant difference in PPR between WT and *Scn8a* mutant pairs (p=0.340 and p=0.189 respectively; Table 2.5).

				Failure Rate													
				1 Hz	5 Hz		10 Hz		20 Hz		40 Hz		80 Hz		120 Hz	
	uIPSC Amplitude (pA)	Latency (ms)	PPR (uIPSC2/ uIPSC1)	Overall	Overall	Last uIPSC	Overall	Last uIPSC	Overall	Last uIPSC	Overall	Last uIPSC	Overall	Last uIPSC	Overall	Last uIPSC
Wild-type (n=4, 3)	-115.0 ± 46.0	0.84 ± 0.07	0.78 ± 0.11	0.04 ± 0.02	0.04 ± 0.03	0.05 ± 0.05	0.05 ± 0.03	0.08 ± 0.08	0.04 ± 0.02	0.05 ± 0.03	0.07 ± 0.05	0.13 ± 0.09	0.10 ± 0.04	0.08 ± 0.08	0.12 ± 0.04	0.2 ± 0.08
Scn8a$^{D/+}$ (n=7, 6)	-71.5 ± 19.0	*1.06 ± 0.04* **	0.61 ± 0.07	0.07 ± 0.04	0.09 ± 0.04	0.13 ± 0.06	0.11 ± 0.04	0.17 ± 0.10	0.13 ± 0.05	0.16 ± 0.11	0.13 ± 0.05	0.17 ± 0.06	*0.32 ± 0.06* *	*0.44 ± 0.10**	*0.38 ± 0.05* *	*0.47 ± 0.05* *
Scn8a$^{W/+}$-PV (n=6, 5)	-44.4 ± 12.2	*1.05 ± 0.03* *	1.02 ± 0.10	0.23 ± 0.08	*0.28 ± 0.06* *	0.25 ± 0.07	*0.25 ± 0.06* *	0.22 ± 0.07	*0.31 ± 0.08* *	0.43 ± 0.10	0.27 ± 0.07	0.35 ± 0.13	*0.39 ± 0.05* **	*0.45 ± 0.03* *	*0.41 ± 0.07* **	*0.50 ± 0.09* *

Table 2.5: Properties of Postsynaptic uIPSCs in Synaptically Connected PV:PC Pairs. Recordings were carried out in multiple synaptically connected pairs of cells from each animal (n=pairs, animals). Data are presented as mean ± SEM.

To analyze activity-dependent synaptic failure, we then used stimulation trains to elicit multiple action potentials at increasing frequencies (5, 10, 20, 40, 80, and 120 Hz; Figure 2.10 D-F; Table 2.5). At each frequency, we measured the failure rate of the first and last uIPSC as well as the overall failure rate. Failure rate of the first uIPSC remained low and consistent between WT, *Scn8a*$^{D/+}$, and *Scn8a*$^{W/+}$-PV mice. At lower frequencies (≤40 Hz), there were no differences in overall failure rate or last uIPSC failure rate between WT and *Scn8a*$^{D/+}$mice, however, failure rates were significantly increased in *Scn8a*$^{W/+}$-PV mice at 5, 10, and 20 Hz (Figure 2.10 G-1-3), with an increasing trend at a 40 Hz stimulation frequency (Figure 2.10 G-4). At 80Hz, the overall failure rate in a 20-pulse train was increased in both *Scn8a*$^{D/+}$ (0.316 ± 0.062; p=0.039) and *Scn8a*$^{W/+}$-PV (0.390 ± 0.048; p=0.009) mice compared to WT (0.101 ± 0.040; Figure 2.10 G-5), with failures occurring approximately three times as frequently in *Scn8a*$^{W/+}$ mutant mice when compared to WT. Similarly, at 120 Hz stimulation frequency with a 30-pulse train, failure rates observed in *Scn8a*$^{D/+}$ and *Scn8a*$^{W/+}$-PV pairs were greater (0.382 ± 0.048 and 0.412 ± 0.068 respectively; p=0.016 and p=0.009) than those observed in their WT counterparts (0.123 ± 0.087; Fig. 2.10 G-6). The progression of total activity-dependent synaptic failure through increasing

presynaptic stimulation frequencies is shown in Figure 2.10 G. Additionally, synaptic failure of the last uIPSC in a stimulation train occurred in >40% of trials on average with a stimulation frequency of 80 or 120 Hz. We observed that this increase in synaptic failure is significant for the last uIPSC in a 80 Hz train in *Scn8a*$^{D/+}$ (p=0.023) and *Scn8a*$^{W/+}$-PV (p=0.025; Table 2.5) as well as in a 120 Hz train (p=0.043 and p=0.030 respectively), supporting a greater degree of activity-dependent failure. Analysis of synaptic latency times, measured from the peak of the presynaptic action potential to the onset of the postsynaptic uIPSC, revealed an increase in synaptic latency in *Scn8a*$^{D/+}$ (p=0.009) and *Scn8a*$^{W/+}$-PV (p=0.012) mice when compared to WT mice (Figure 2.10 H; Table 2.5). Prolonged synaptic latency would suggest an impairment in conduction velocity or GABA release probability, potentially with a longer time lag to vesicle release.[136–139] Efficient synaptic transmission and vesicle release is critical for overall network inhibition.[140]

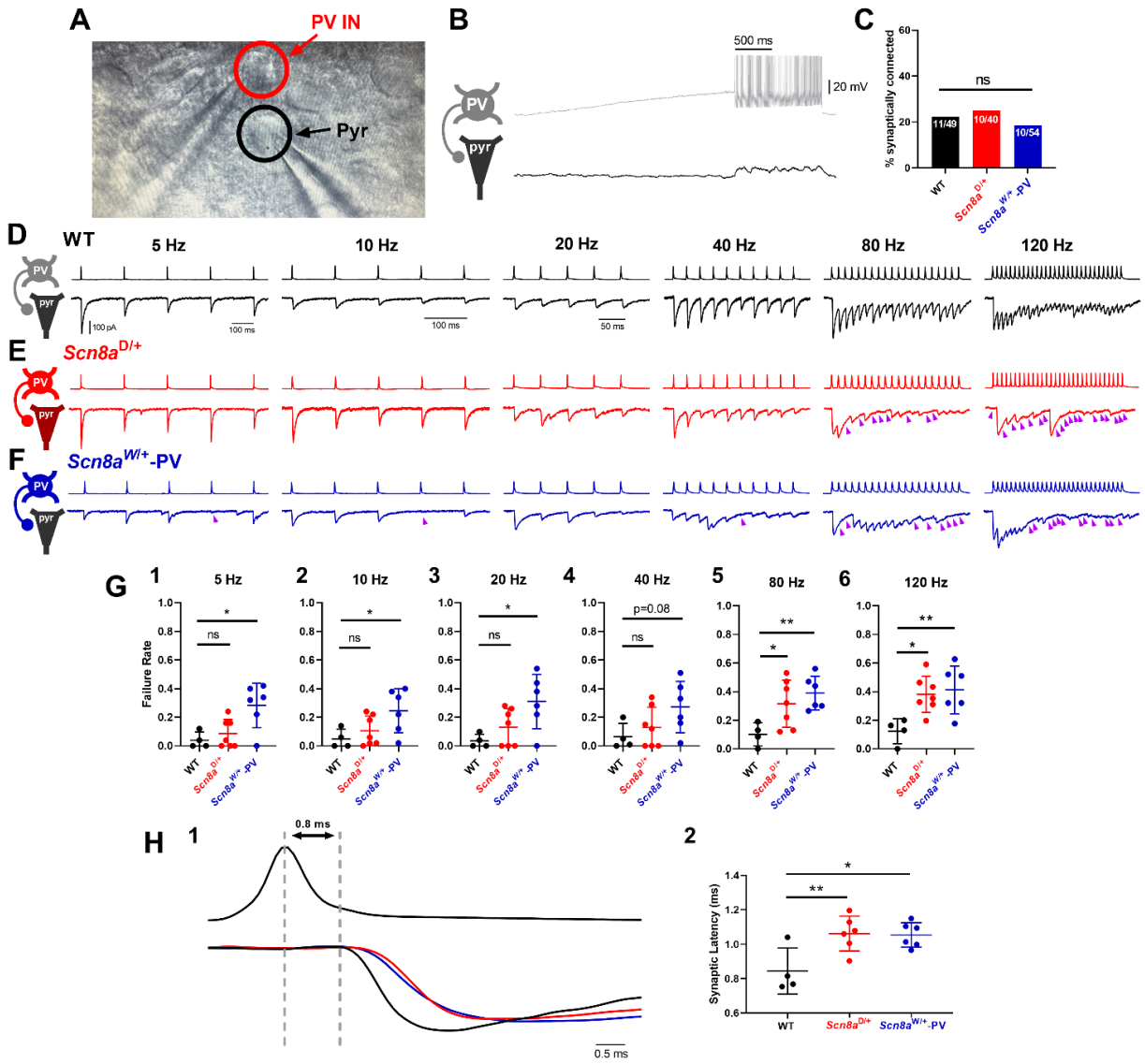

Figure 2.9: Increased synaptic transmission failure and synaptic latency in *Scn8a* mutant mice. (**A**) Image of dual whole-cell recording of a synaptically connected PV interneuron and pyramidal cell pair. (**B**) Example traces from a PV interneuron (grey) and synaptically coupled pyramidal cell (black). (**C**) Proportion of successfully patched PV:PC pairs that were synaptically connected did not differ between WT (49 pairs from 13 mice), *Scn8a*$^{D/+}$ (40 pairs from 8 mice), and *Scn8a*$^{W/+}$-PV (54 pairs from 9 mice) in adult mice. (**D-F**) Example of presynaptic firing and evoked uIPSCs in WT (**D; black**), *Scn8a*$^{D/+}$ (**E; red**), and *Scn8a*$^{W/+}$-PV (**F; blue**) connected pairs at 5 Hz, 10Hz, 20 Hz, 40 Hz, 80 Hz, and 120 Hz. Purple arrows denote uIPSC failures in the postsynaptic neuron. (**G**) Summary data for failure rates of evoked uIPSCs at various frequencies. In *Scn8a*$^{D/+}$ connected pairs (n=7, 5 mice), uIPSC failure rate is not significantly different from WT (n=4, 3 mice) at 5, 10, 20, or 40 Hz (p>0.05, **G1-G4**), but is significantly higher at PV interneuron firing frequencies of 80 and 120Hz (*, p<0.05, **G5-6**). uIPSC failure rate in *Scn8a*$^{W/+}$-PV pairs (n=6, 5 mice) is significantly higher than WT at 5, 10, 20, 80, and 120Hz (*, p<0.05, **G1-3**, **5-6**), but did not significantly differ at 40Hz (p<0.05, **G4**, one-way ANOVA with Dunnett's multiple comparison test). **(H)** Example traces illustrating synaptic latency in WT, *Scn8a*$^{D/+}$, and *Scn8a*$^{W/+}$-PV, measured from the peak of the presynaptic AP to the onset of the evoked uIPSC (**H1**). Grey dotted lines indicate this latency in WT. Latency is increased in *Scn8a*$^{D/+}$ and *Scn8a*$^{W/+}$-PV mice (**H2**, one-way ANOVA with Dunnett's multiple comparison test, *, p<0.05, **, p<0.01).

Discussion

Parvalbumin interneurons prominently express $Na_v1.6$[12,13] and are known to play a major role in various epilepsies.[48,50,103–106,141] However, their role in the pathophysiology of *SCN8A* developmental and epileptic encephalopathy is unknown. Here, we show that: (1) expression of the patient-derived R1872W *SCN8A* GOF variant selectively in PV interneurons conveys susceptibility to spontaneous seizures and premature seizure-induced death; (2) GOF *SCN8A* mutations in PV interneurons lead to initial hyperexcitability and subsequent action potential failure via increased susceptibility to depolarization block; (3) PV interneurons in both GOF *SCN8A* mouse models exhibit epileptiform increases in I_{NaP} currents that would facilitate increased susceptibility to depolarization block; (4) inhibitory input onto excitatory pyramidal cells is significantly reduced in *Scn8a* mutant mice; and (5) there is a progressive, activity-dependent increase in synaptic transmission failure from PV inhibitory interneurons onto excitatory neurons. Our findings highlight a newfound role for PV interneurons in the pathophysiology of seizures and seizure-induced death in mouse models of *SCN8A* DEE.

Expression of R1872W *SCN8A* mutation in PV interneurons is sufficient to cause seizures and premature death

PV interneurons are known to be the main drivers for seizure activity in Dravet Syndrome, a disorder characterized by deficits in inhibitory neurons, primarily due to haploinsufficiency of $Na_v1.1$.[48–50,102] Selective deletion of $Na_v1.1$ in PV interneurons leads to reduced PV interneuron excitability, decreased spontaneous inhibition of

excitatory neurons, and increased susceptibility to seizures.[141] Similar to impairments observed in mouse models of Dravet Syndrome and in *Scn8a*$^{D/+}$ mice, which express the N1768D *SCN8A* variant globally, we show here that selective expression of the GOF R1872W variant in PV interneurons is sufficient to induce spontaneous and audiogenic seizures and leads to seizure-induced death (SUDEP) in mice. Additionally, *Scn8a*$^{W/+}$-PV mice exhibited a reduced seizure frequency and increased survival compared to *Scn8a*$^{D/+}$ mice, and global expression of the R1872W variant or exclusive expression in excitatory neurons leads to a more severe SUDEP phenotype than *Scn8a*$^{W/+}$-PV mice.[89] This may indicate that although PV interneurons are an important contributor to the *SCN8A* DEE phenotype, dysfunction of excitatory neurons remains a critical aspect of the disease physiology, as previously published.[89,91,92] Overall, these findings not only support an important role for PV interneurons in the seizure phenotype of *SCN8A* DEE but also provide support for a major role for $Na_v1.6$ channels in controlling PV interneuron excitability in addition to $Na_v1.1$ channels.

Gain-of-function *SCN8A* mutations result in premature PV interneuron depolarization block

Proper function of *Scn8a* is critical in repetitive firing,[122] and as such, we reasoned that mutations affecting the function of *Scn8a* would impact the high-frequency, repetitive firing characteristic of PV interneurons. However, although at lower current injection magnitudes PV interneurons from both mutant mouse models were hyperexcitable, at higher magnitudes we observed PV interneuron action potential failure through depolarization block, resulting in overall PV interneuron hypoexcitability. Increased susceptibility to depolarization block due to a GOF sodium channel mutation

has been shown previously in both *SCN8A* DEE and *SCN1A* epileptic encephalopathy.[35,36] Additionally, depolarization block in PV interneurons leads to hyperactivity and subsequent epileptic discharges in excitatory cells, and rescue of depolarization block via optogenetic stimulation leads to a reduction in epileptiform activity.[116–118] Further, *in vivo* recording of PV interneurons shows evidence for PV depolarization block during seizure activity.[119]

Interestingly, the susceptibility to depolarization block and subsequent hypoexcitability in inhibitory interneurons reported here indicates that a mechanism for seizures in *SCN8A* DEE, a disorder characterized by primarily GOF sodium channel mutations, shares many similarities to that of Dravet Syndrome, a disorder primarily characterized by sodium channel haploinsufficiency in inhibitory neurons. A study using a model of Dravet Syndrome showed a similar pattern of initial hyperexcitability in PV interneurons followed by depolarization block.[142] However, impairment of PV interneuron excitability in Dravet Syndrome is specific to the P18-21 developmental time window,[49] whereas in *SCN8A* DEE, PV interneuron activity is more significantly impaired in adulthood. The initial hyperexcitability of inhibitory interneurons seen in both *SCN8A* DEE and Dravet Syndrome may play some role in the shared comorbidities between these two severe developmental disorders.

Notably, we observed a decrease in the upstroke and downstroke velocity of P18-21 *Scn8a* mutant PV interneurons, and consequently, an increase in their AP width. Although we did not observe any hypoexcitability in *Scn8a* mutant PV interneurons, this is strikingly similar to the physiology of PV interneurons in Dravet Syndrome in the same developmental time window.[49] This may underlie more

similarities between Dravet Syndrome and *SCN8A* DEE despite significant differences in LOF and GOF channel physiology.

Impaired synaptic transmission between mutant PV interneurons and pyramidal cells

Our study is the first to examine alterations in synaptic transmission between PV interneurons and excitatory neurons in *SCN8A* DEE, and we show a distinct impairment of inhibitory synaptic transmission onto excitatory pyramidal cells in two patient-derived mutation models. Synaptic transmission was impaired in both *Scn8a* mutant mouse models: *Scn8a*$^{W/+}$-PV connected pairs failed significantly more than WT at most frequencies, whereas *Scn8a*$^{D/+}$ pairs failed in an activity-dependent manner. Considering the fast-spiking nature of PV interneurons and the degree of inhibitory input they provide on neuronal excitatory networks, activity-dependent failure alone could have a significant impact on overall seizure susceptibility. A likely mechanism for this failure could be impaired AP propagation, as proper signaling from PV interneurons requires a specific density and function of sodium channels.[132] This is further supported by the observed increase in synaptic latency, indicating that propagation may be slowed in *Scn8a* mutant mice. Similarly, synaptic transmission between PV interneurons and pyramidal cells is also impaired in Dravet Syndrome, although unlike our findings in *SCN8A* DEE, intrinsic excitability deficits are restored in adult PV interneurons.[49,50] A limitation of the study is the number of synaptically-connected pairs recorded. It is possible that synaptic transmission is impaired in a non-activity dependent manner in both *Scn8a*$^{D/+}$ and *Scn8a*$^{W/+}$-PV mice, as a slight increasing trend in the failure rates of *Scn8a*$^{D/+}$ uIPSCs at low frequencies was observed.

Both depolarization block and synaptic transmission failure occurred at high PV interneuron firing frequencies, and as such, it is important to consider *in vivo* firing frequencies of PV interneurons. PV interneurons are a heterogeneous group made up of primarily basket cells and chandelier cells, which are named for their unique morphologies. These subtypes have slightly different firing patterns and synaptic targets.[94,97] Since our recordings are focused within cortical layers IV/V, it is likely that we recorded primarily from PV-positive basket cells rather than chandelier cells. *In vivo*, PV interneurons, particularly basket cells, are phase-locked to gamma oscillations, which typically occur between 40-100 Hz.[143] Events such as sharp wave ripples (SWRs) can lead to PV firing frequencies of >120Hz *in vivo*.[144] This demonstrates the relevance of both increased susceptibility of PV interneurons to depolarization block and of PV:PC synaptic transmission failure at high frequencies with expression of mutant *Scn8a*. These gamma oscillations and SWRs are most often associated with the hippocampus, however, there is evidence for oscillations in the cortex.[145,146] Recently, SWRs have been associated with epileptic discharges in Dravet Syndrome: an increase in SWR amplitude may lead to inhibitory depolarization block and a shift into seizure-like activity.[147] Considering the frequencies at which we observe PV interneuron failure in both *Scn8a* mutant mouse models, increased susceptibility to depolarization block and failure of inhibitory synaptic transmission could underlie a major mechanism of seizure generation in *SCN8A* developmental and epileptic encephalopathy.

Elevated sodium currents in *Scn8a* mutant PV interneurons

We observed an increase in I_{NaP} in both *Scn8a*$^{D/+}$ and *Scn8a*$^{W/+}$-PV interneurons with an increase in I_{NaR} in *Scn8a*$^{W/+}$-PV interneurons. However, we observed no

difference in the transient sodium current in *Scn8a*$^{D/+}$ and *Scn8a*$^{W/+}$-PV interneurons, although it is possible that excised somatic patches may not have recapitulated the high levels of $Na_v1.6$ in the axon. Previous studies suggest that *Scn8a* may have a much larger role in I_{NaR} than transient current.[122] Increases in I_{NaP} have been implicated in various epilepsies,[57,123,125,148] and prior computational modeling suggests that heightened I_{NaP} underlies the phenotype of increased susceptibility to depolarization block in inhibitory interneurons.[36] I_{NaP} also functions as an amplifier of synaptic currents,[149,150] although we did not observe differences in amplitude of uIPSCs in recordings of synaptically-connected pairs. Because I_{NaP} is a consistent, non-inactivating component of the sodium current,[125] we hypothesize that elevations in I_{NaP} contribute to premature failure of PV interneurons and subsequent entry into depolarization block. Additionally, I_{NaR} currents are crucial in facilitating repetitive, high-frequency firing as they impact fast inactivation through an open channel block,[121,151] and $Na_v1.6$ is a crucial contributor to I_{NaR}.[122] We only observed a significant increase in I_{NaR} in *Scn8a*$^{W/+}$-PV interneurons and not in *Scn8a*$^{D/+}$ PV interneurons, possibly due to mutation-specific effects: this has been observed previously in patient-derived neurons.[152] Increases in I_{NaR} likely provide excessive depolarizing current resulting in an increase in firing frequencies, which may be responsible for differences observed between *Scn8a*$^{D/+}$ and *Scn8a*$^{W/+}$-PV interneuron firing, as *Scn8a*$^{D/+}$ PV interneurons enter depolarization block at lower current injections.

It is also important to consider the potential consequences of a GOF $Na_v1.6$ mutation on the structural composition of the AIS. Although we observed no differences in the axonal expression of $Na_v1.6$, increased sodium channel function could lead to

compensatory changes in other channels. Sodium channels are expressed together with potassium channels at the AIS and both play crucial roles in controlling neuronal excitability.[12] Further, previous studies suggest interaction between sodium and potassium channels as a result of genetic mutations.[34,153,154] Potassium channels such as $K_v7.2$, which is encoded by *KNCQ2*, interacts with $Na_v1.6$, and is an important mediator of M-type potassium current,[155,156] or $K_v3.1$, which is important for repetitive, high-frequency firing,[157] could be impacted by these changes in sodium channel function and may underlie some physiological differences observed in *Scn8a* mutant PV interneurons. Interaction between *SCN8A* and *KCNQ2* has been shown previously in a DEE model: in DEE resulting from loss-of-function mutations in *KCNQ2,* an antisense oligonucleotide (ASO) to reduce the expression of *Scn8a* leads to a marked increase in survival.[153]

Implications for *SCN8A* developmental and epileptic encephalopathy

Patients with *SCN8A* variants are typically treated with sodium channel blockers and many are refractory to treatment, highlighting the need to further understand the basic mechanisms surrounding the *SCN8A* DEE phenotype. Hyperexcitability of excitatory neurons has often been suggested as the underlying cause behind seizures in *SCN8A* DEE, and, contradictory to our results here, a previous study suggests limited involvement of inhibitory interneurons due to the lack of seizures when the R1872W *SCN8A* variant is expressed in all inhibitory interneurons.[89] However, in the previous study, the SUDEP phenotype of mice expressing the R1872W variant globally (*Scn8a*$^{W/+}$; EIIa-Cre) is markedly more severe than that of mice expressing the R1872W variant exclusively in forebrain excitatory neurons (*Scn8a*$^{W/+}$; EMX1-Cre), with median

survival of 15 days and 46 days respectively, [89] suggesting the involvement of additional cell types. While we acknowledge the critical contributions of excitatory neuron dysfunction to the *SCN8A* DEE phenotype,[89,91,92] here we provide compelling support for a major involvement of PV inhibitory interneurons in the onset of spontaneous seizures and seizure-induced death in *SCN8A* DEE.

Gene therapies are in development for both *SCN8A* DEE and Dravet Syndrome, and downregulation of *Scn8a* has been shown to reduce seizures in both disorders.[53,55,85] Specifically, an antisense oligonucleotide (ASO) for *Scn8a* was able to significantly delay seizure onset and increase survival in mice that express the R1872W *SCN8A* variant globally.[85] This ASO treatment targeted both excitatory and inhibitory neurons. Our previous studies have shown that ASO-mediated rescue of PV interneuron firing reduces seizures and prevents SUDEP in a model of Dravet Syndrome[55]; a similar phenotype may be observed in *SCN8A* DEE where rescue of depolarization block prevents seizures and SUDEP. In a similar manner to Dravet Syndrome, specific targeting of inhibitory interneurons in *SCN8A* DEE may be a novel therapeutic strategy.

In conclusion, we show in this chapter that PV interneurons play a significant role in *SCN8A* developmental and epileptic encephalopathy. Elevations in I_{NaP} likely render PV interneurons more susceptible to action potential failure, and subsequent depolarization block leads to a decrease in network inhibition. PV interneurons also exhibit impaired synaptic transmission, and altogether, we observe that a gain-of-function *SCN8A* variant exclusively expressed in PV interneurons conveys susceptibility to spontaneous seizures and SUDEP. In the field of *SCN8A* DEE, prior research has

focused primarily on the impact of GOF *SCN8A* mutations on excitatory neurons.[89,91,92] These results, along with our previous work proposing that SST interneurons contribute to seizures,[36] shift the paradigm of the *SCN8A* DEE field from primarily considering excitatory neuron hyperexcitability as the main driver of the seizure phenotype and calls for future studies to further explore the importance of inhibitory neuron activity in *SCN8A* developmental and epileptic encephalopathy.

Chapter III: Vasoactive Intestinal Peptide Inhibitory Interneuron Dysfunction in *SCN8A* Developmental and Epileptic Encephalopathy

Rationale

In addition to seizures, patients with *SCN8A* DEE exhibit significant neurodevelopmental symptoms. Thus, there is a need to elucidate the physiological mechanisms behind the neurodevelopmental aspects of the disorder. Previous studies indicate that VIP interneurons, which provide disinhibition in cortical networks, may play a role both in seizure frequency in temporal lobe epilepsy and in the neurodevelopmental aspects of Dravet Syndrome. In this chapter, I examine VIP interneurons in the context of *SCN8A* DEE and find that a global gain-of-function *SCN8A* mutation leads to increased persistent sodium current and hyperexcitability in VIP interneurons. This, however, does not translate to seizure susceptibility with selective expression of a gain-of-function *SCN8A* mutation in VIP interneurons. Further, selective mutation expression in VIP interneurons does not convey hyperexcitability, indicating that changes in VIP interneuron physiology may be compensatory as a result of network dysfunction. From our results and previous literature, we believe that VIP interneuron dysfunction in a global *SCN8A* DEE model may be related to the behavioral comorbidities in *SCN8A* DEE and suggest that these disinhibitory interneurons likely do not drive the seizure phenotype.

Introduction

$Na_v1.6$ is prominent in various cell types throughout the central nervous system and is present at the AIS and nodes of Ranvier, where it is critical to action potential initiation and propagation.[11–13,62] Gain-of-function mutations in $Na_v1.6$ lead to hyperexcitability in excitatory neurons[91,92] and depolarization block in both PV and SST inhibitory interneurons.[36] Further, *Scn8a* mutations lead to deficits in synaptic transmission between cortical excitatory and inhibitory neurons. However, inhibitory interneurons are extremely heterogeneous[98], and there are many subpopulations unstudied in *SCN8A* DEE that play a major role in other epilepsies. The contributions of one major subclass, vasoactive intestinal peptide (VIP) interneurons, to *SCN8A* DEE remains unknown.

VIP interneurons are primarily disinhibitory and preferentially impair other inhibitory interneurons, with SST interneurons as their most frequent target.[158–160] VIP interneurons themselves are a diverse group, but in general they are largely located in cortical layer II/III. They are typically narrow and vertically oriented, exhibiting a bipolar morphology.[94,98,161] VIP interneurons in layer II/III have dendrites primarily in layer I-III of the cortex, whereas their axons extend throughout all layers.[162] Proper function of VIP interneurons is critical in cortical circuit development,[163] and they play an important role in attention, learning and memory, and sensory processing.[159,163–166] Consequently, VIP interneuron dysfunction may play a role in neurodevelopmental disorders, importantly, autism spectrum disorder (ASD), which is often linked with epileptic encephalopathy syndromes.[167–170] Additionally, VIP interneurons may play a role in seizures: in a model of temporal lobe epilepsy, modulation of VIP interneurons affects seizure frequency,

with inhibition of VIP interneurons leading to an increased seizure threshold, a decrease in seizure duration, and a decrease in seizure frequency overall.[171,172]

Notably, impairment of VIP interneurons has been shown in mouse models of Dravet Syndrome, a severe epilepsy syndrome typically resulting from mutations in *SCN1A*.[51,168] Dravet Syndrome often occurs due to a loss-of-function in $Na_v1.1$, yet it shows many similarities to *SCN8A* DEE, with severe seizures, intellectual and developmental comorbidities, and increased risk of SUDEP. Studies on VIP interneurons in Dravet Syndrome indicate that they likely contribute to neurodevelopmental comorbidities and an ASD-like behavioral phenotype.[51,168] Interestingly, single cell transcriptomics data suggests that VIP interneurons express *SCN8A*,[101] indicating that these cells may be affected by mutations in *SCN8A* and could play a role in *SCN8A* DEE.

Here, we examine the physiology of VIP interneurons first in a global knock-in mouse model of *SCN8A* DEE harboring the N1768D patient-derived *SCN8A* variant (*Scn8a*$^{D/+}$).[86] This mouse model exhibits spontaneous seizures and seizure-induced death, and previous studies have shown hyperexcitability in pyramidal neurons with significant deficits in both PV and SST interneurons.[36,87,91,92] Using whole-cell patch clamp electrophysiology, we observe a distinct increase in I_{NaP} in *Scn8a*$^{D/+}$ mice, a hallmark of the N1768D gain-of-function mutation. We identified two electrophysiologically distinct populations of VIP interneurons, as previously described[51,98]: irregular spiking (IS) and continuous adapting (CA). Interestingly, we found an increased proportion of CA VIP interneurons in *Scn8a*$^{D/+}$ mice. Both subtypes were intrinsically hyperexcitable, with increased spontaneous excitability and increased

input resistance in *Scn8a*$^{D/+}$ CA VIP interneurons. As a potential consequence of increased disinhibition, we observed a decrease in spontaneous inhibitory postsynaptic currents (sIPSCs) generated in PV interneurons, but not SST interneurons. Furthermore, we examined another mouse model with conditional expression of a *SCN8A* variant, using VIP-Cre to express the R1872W *SCN8A* mutation conditionally in VIP interneurons (*Scn8a*$^{W/+}$-VIP), similar to previous studies identifying the roles of pyramidal cells, SST interneurons, and PV interneurons.[36,89] These mice do not exhibit audiogenic seizures, and interestingly, unlike in *Scn8a*$^{D/+}$ mice, the excitability of VIP interneurons is not augmented, suggesting that changes in *Scn8a*$^{D/+}$ VIP interneurons may be compensatory. These results suggest that although VIP interneurons are impaired in a global mutation model of *SCN8A* DEE, they may play a limited role in seizure susceptibility and may instead be involved in another aspect of the *SCN8A* DEE phenotype.

Materials and Methods

Mouse Husbandry and Genotyping

Scn8a$^{D/+}$ mice were generated as previously described and maintained through crosses with C57BL/6J mice (Jax, #000664) to keep all experimental mice on a C57BL/6J genetic background.[87,89] Fluorescent labeling of VIP interneurons was achieved by first crossing homozygous VIP-IRES-Cre females (Jax #031628) with C57BL/6J males to generate VIP-Cre heterozygotes. Then, VIP-Cre heterozygote females were crossed with male *Scn8a*$^{D/+}$ or *Scn8a*$^{W/+}$ mice with a Cre-dependent tdTomato reporter (Jax, #007909). Fluorescent labeling of PV and SST interneurons was achieved similarly: by crossing PV- (Jax, #017320) or SST-Cre (Jax, #013044)

homozygous females with male *Scn8a*$^{D/+}$ mice with a Cre-dependent tdTomato reporter (Jax, #007909). Because certain transgenic mice entail the insertion of Cre directly into the coding sequence, for all experiments we used WT littermate controls that contained the same Cre allele but lacked the allele encoding the *Scn8a* variant. Experimental groups used ≥3 randomly-selected mice to achieve statistical power and roughly equal numbers of male and female mice to control for potential sex differences. No sex differences were observed. All genotyping was conducted through Transnetyx automated genotyping PCR services.

Immunohistochemistry

Brain tissue for immunohistochemistry was processed as previously described.[36,111] Mice were anesthetized and transcardially perfused with 10 mL Dulbecco's PBS (DPBS) followed by 10 mL 4% PFA. Brains were immersed in 4% PFA overnight at 4°C and stored in DPBS. 30 µm coronal brain sections were obtained using a cryostat. Sections were incubated with rabbit anti-$Na_V1.6$ (Alomone; 1:250) and mouse anti-AnkG (NeuroMab;1:100) diluted in 2% goat serum (Jackson ImmunoResearch Laboratories) with 0.1% Triton X (Sigma-Aldrich) in DPBS. The secondary antibodies, goat anti-mouse AlexaFluor-488 (Invitrogen) and goat anti-rabbit AlexaFluor 633 (Invitrogen), were diluted 1:500 in goat serum (2%) and Triton-X (0.1%) in DPBS. Sections were stained free-floating in primary antibody on a shaker at 4°C overnight and with secondary antibody for 1 h at room temperature the following day. Tissues were counterstained with NucBlue Fixed Cell ReadyProbes Reagent (DAPI) (ThermoFisher Scientific, catalog #R37606) included in the secondary antibody solution. Tissues were mounted on slides using AquaMount (Polysciences).

Brain Slice Preparation

Preparation of acute brain slices for patch-clamp electrophysiology experiments was modified from standard protocols previously described[36,89,91]. Mice (6-12 weeks old) were anesthetized with isoflurane and decapitated. The brains were rapidly removed and kept in chilled slicing solution, containing (in mM): 93 N-Methyl-D-glucamine (NMDG), 2.5 KCl, 1.25 NaH_2PO_4, 20 HEPES, 5 L-ascorbic acid (sodium salt), 2 thiourea, 3 sodium pyruvate, 0.5 $CaCl_2$, 10 $MgSO_4$, 25 D-glucose, 12 N-acetyl-L-cysteine, 30 $NaHCO_3$; pH adjusted to 7.2-7.4 using HCl (osmolarity 310 mOsm). 300 µm coronal brain sections were prepared using a Leica Microsystems VT1200 vibratome. Slices were collected and incubated in 37°C ACSF for 30 min, containing (in mM): 125 NaCl, 2.5 KCl, 1.25 NaH_2PO_4, 2 $CaCl_2$, 1 $MgCl_2$, 0.5 L-ascorbic acid, 10 glucose, 25 $NaHCO_3$, and 2 Na-pyruvate. Slices were continuously oxygenated with 95% O_2 and 5% CO_2 throughout the preparation. After slicing, brain slices were kept at room temperature for up to 6 h.

Electrophysiology Recordings

Brain slices were placed in a chamber superfused (~2 ml/min) with continuously oxygenated recording solution warmed to 32 ± 1°C. Cortical layer II/III VIP interneurons were identified as red fluorescent cells using a Carl Zeiss Axioscope microscope. Whole-cell recordings were performed using a Multiclamp 700B amplifier with signals digitized by a Digidata 1322A digitizer. Currents were amplified, lowpass filtered at 2 kHz, and sampled at 100 kHz. Borosilicate electrodes were fabricated using a Brown-Flaming puller (model P1000, Sutter Instruments) to have pipette resistances between 3

and 5 mΩ. All patch-clamp electrophysiology data were analyzed using custom MATLAB scripts and/or ClampFit 10.7.

Intrinsic Excitability Recordings

Current-clamp recordings of neuronal excitability were collected in ACSF solution identical to that used for preparation of brain slices. The internal solution contained the following (in mM): 120 K-gluconate, 10 NaCl, 2 $MgCl_2$, 0.5 K_2EGTA, 10 HEPES, 4 Na_2ATP, 0.3 NaGTP, pH 7.2 (osmolarity 290 mOsm). Intrinsic excitability was assessed using methods adapted from those previously described.[36,91] Briefly, resting membrane potential was manually recorded from the neuron at rest. Current ramps from 0 to 400 pA over 4 s were used to calculate passive membrane and AP properties, including threshold, upstroke and downstroke velocity, which are the maximum and minimum slopes on the AP, respectively; amplitude, which was defined as the voltage range between AP peak and threshold; APD_{50}, which is the duration of the AP at the midpoint between threshold and peak; input resistance, which was calculated using a −20 pA pulse in current-clamp recordings; and rheobase, which was defined as the maximum amount of depolarizing current that could be injected into neurons before eliciting an AP. AP frequency–current relationships were determined using 500ms or 1s current injections from −140 to 600 pA. To determine VIP interneuron subtype, we used an 8 s current injection at 2x rheobase, adjusted manually according to the protocol used to determine AP frequency-current relationship.

Persistent and Resurgent Sodium Current Recordings

The recording solution has been previously described[112,113] and contained (in mM): 100 NaCl, 40 TEACl, 10 HEPES, 3.5 KCl, 2 $CaCl_2$, 2 $MgCl_2$, 0.2 $CdCl_2$, 4 4-

aminopyridine (4-AP), 25 D-glucose. Steady-state I_{NaP} was elicited using a voltage ramp (20 mV/s) from −80 to −20 mV. To record I_{NaR}, VIP interneurons were held at −100 mV, depolarized to 30 mV for 20 ms, then stepped to voltages between −100 mV and 0 mV for 40 ms. After collecting recordings at baseline, protocols were repeated in the presence of 1μm tetrodotoxin (TTX; Alomone Labs) to completely isolate I_{NaP} and I_{NaR} currents. TTX-subtracted traces were analyzed by extracting the current at each mV. The half-maximal voltage for activation of I_{NaP} was calculated as previously described.[113]

Audiogenic seizure assessment

Audiogenic seizure susceptibility was determined using standard protocols, similar to those previously described.[107] To test for audiogenic seizures, mice were taken from their home cage and transferred to a clean test cage where they were allowed to acclimate for ~20 seconds before the onset of a 15 kHz acoustic stimulus. The stimulus duration lasted for 50 seconds or until the animal had a behavioral seizure. Audiogenic seizures were recorded using a laptop webcam.

Statistical Analysis

Analysis of electrophysiological data was performed blinded. All statistical comparisons were made using the appropriate test in GraphPad Prism 9. Categorical data were analyzed using the Chi-square or Fisher's exact test. Proportion data were analyzed using the Binomial test. For membrane and AP properties, spontaneous firing frequency, peak sodium currents, half-maximal voltages, and IPSC frequency and amplitude, mouse genotypes were compared by an unpaired t-test when the data were normally distributed with equal variances, by Welch’s t-test when the data were normally

distributed with unequal variances, and by the nonparametric Mann-Whitney test when the data were not normally distributed. Data were assessed for normality using the Shapiro-Wilk test. Bartlett's test with p=0.05 was used to assess equal variance. Data were tested for outliers using the ROUT method to identify outliers, and any outliers were removed. A two-way ANOVA followed by Tukey's test for multiple comparisons was used to compare groups in experiments in which repetitive measures were made from a single cell over various voltage commands or current injections. Data are presented as individual data points and/or mean ± SEM. Exact n and p-values are reported in figure legends.

Results

VIP interneurons express $Na_v1.6$

VIP interneurons are known to express the sodium channels $Na_v1.1$ and $Na_v1.2$, and recent transcriptomic studies suggest that they express *SCN8A* mRNA.[39,51,101] To confirm the presence of $Na_v1.6$ in VIP interneurons, we performed immunohistochemistry on WT and *Scn8a*$^{D/+}$ mice. We found that $Na_v1.6$ is expressed in the presumed axon of tdTomato-positive VIP interneurons in both WT and *Scn8a*$^{D/+}$ mice (Figure 3.1). We identified $Na_v1.6$ expression in 100% of VIP interneurons in 3 mice of each genotype. These data indicate that $Na_v1.6$ is present in the axon of VIP interneurons, suggesting that their physiology may be impacted by an *SCN8A* variant.

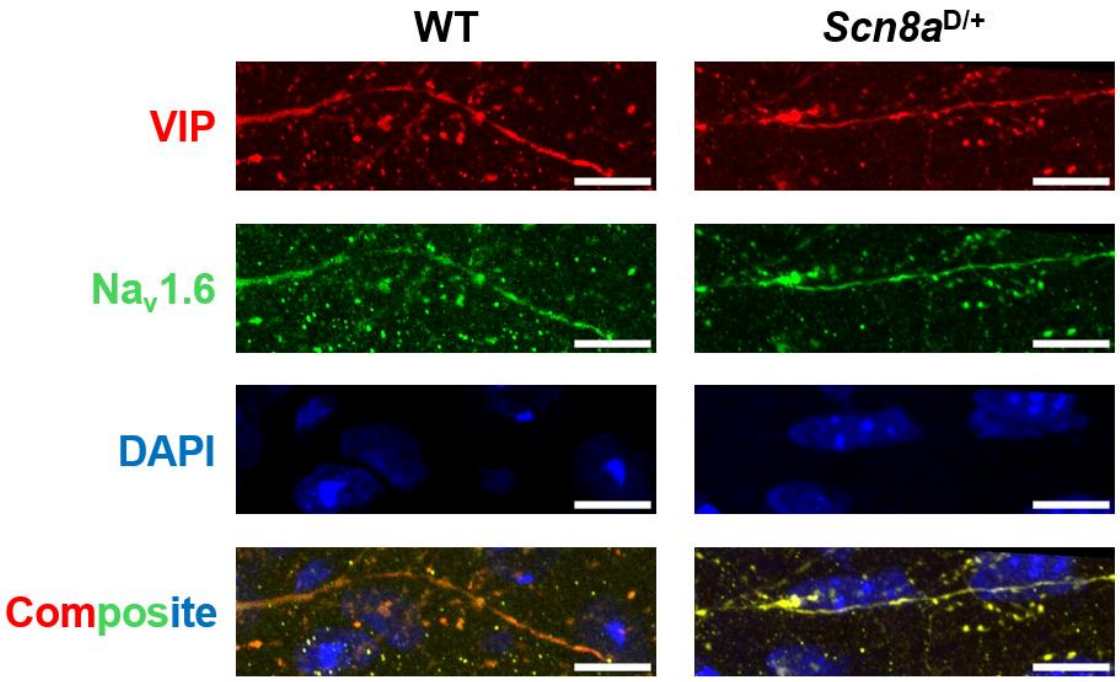

Figure 3.1: Expression of $Na_v1.6$ in VIP interneurons. Example immunohistochemistry images showing colocalization of VIP (red) and $Na_v1.6$ (green) immunofluorescence in adult WT and *Scn8a*$^{D/+}$ mice. Scale bar 10 µM. Images were collected from layer II/III of the somatosensory cortex in n=3 mice from each genotype.

N1768D *SCN8A* variant leads to an increased I_{NaP} in VIP interneurons

Gain-of-function mutations in $Na_v1.6$, specifically the N1768D *SCN8A* variant, lead to increases in I_{NaP} in pyramidal cells, SST interneurons, and PV interneurons. [36,91] I_{NaP} contributes to neuronal hyperexcitability in *SCN8A* DEE as well as other forms of epilepsy due to persistent membrane depolarization.[125,173] To assess I_{NaP} in VIP interneurons in WT and *Scn8a*$^{D/+}$ mice, we recorded I_{NaP} in fluorescently-labeled, layer II/III VIP interneurons in the somatosensory cortex in a whole-cell patch clamp configuration. We found that I_{NaP} was increased in *Scn8a*$^{D/+}$ VIP interneurons (-123.0 ± 14.2 pA) compared to WT (-57.4 ± 9.6 pA; Figure 3.2C). Half-maximal voltage of activation was not different between WT (-64.3 ± 2.1 mV) and *Scn8a*$^{D/+}$ VIP

interneurons (-60.9 ± 1.6 mV; Figure 3.2D). We also recorded the resurgent sodium current (I_{NaR}), a slow inactivating sodium current important for fast spiking that is increased in *Scn8a* mutant pyramidal cells and PV interneurons.[91,120–122] In VIP interneurons, we did not observe any significant differences in I_{NaR} between WT (-201.3 ± 32.0 pA) and *Scn8a*$^{D/+}$ (-249.1 ± 36.3 pA; Figure 3.2G). Although I_{NaR} did not differ in *Scn8a* mutant VIP interneurons, we were able to demonstrate an increase in I_{NaP}, a hallmark of gain-of-function *SCN8A* mutations that is indicative of potential hyperexcitability.

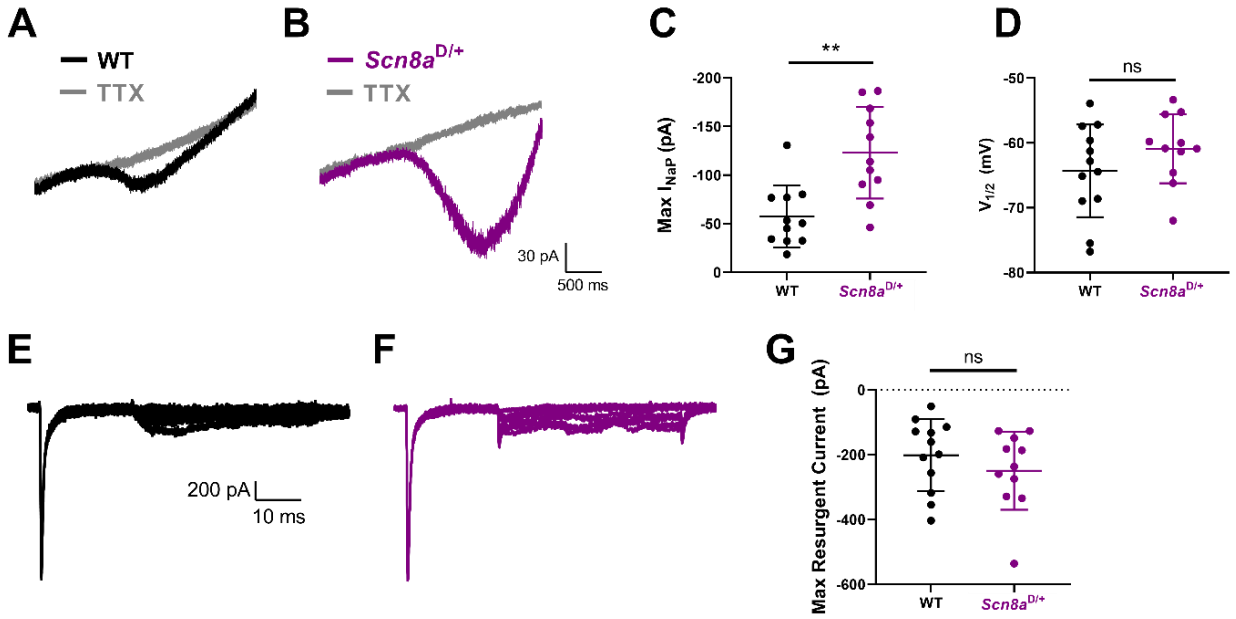

Figure 3.2: Voltage-gated sodium currents in WT and *Scn8a*$^{D/+}$ VIP interneurons. (**A,B**) Example traces of steady state I_{NaP} evoked by slow voltage ramps from WT (**A**, black) and *Scn8a*$^{D/+}$ (**B**, purple) VIP interneurons. Traces in gray show slow voltage ramp in the presence of 500 nM TTX. (**C**) Elevated maximum I_{NaP} in *Scn8a*$^{D/+}$ (*n*=11, 4 mice) VIP interneurons compared with WT (*n*=11, 4 mice) PV interneurons (**, p<0.01, unpaired t-test) (**D**) $V_{1/2}$ does not significantly differ between WT and *Scn8a*$^{D/+}$ mice (p>0.05, unpaired t-test). (**E,F**) Example traces of TTX-subtracted I_{NaR} for WT (**E**, black) and *Scn8a*$^{D/+}$ (**F**, purple) evoked by voltage commands in which the cell was stepped to membrane potentials of -100 to 0mV, increments of 10mV for 40 ms after first being stepped to 30mV for 20ms. (**G**) Maximum I_{NaR} magnitude was not different between WT (*n*=14, 5 mice) and *Scn8a*$^{D/+}$ (*n*=15, 5 mice) VIP interneurons (*p*>0.05, unpaired t-test).

VIP interneurons are hyperexcitable in a mouse model of *SCN8A* DEE

Considering the heightened I_{NaP} in *Scn8a*$^{D/+}$ VIP interneurons, we anticipated that VIP interneurons in *Scn8a*$^{D/+}$ mice would be hyperexcitable. To determine if intrinsic excitability of VIP interneurons is affected in WT and *Scn8a* mutant mice, we again performed whole-cell patch clamp on layer II/III somatosensory cortex VIP interneurons. This revealed two distinct firing patterns (Figure 3.3), as shown previously in studies classifying cortical interneurons as well as in studies of Dravet Syndrome.[51,98] An 8 second current injection showed continuous adapting (CA) VIP interneurons (Figure 3.3A), which fired continuously through the current injection, and irregular spiking (IS) VIP interneurons (Figure 3.3B), which fired an initial burst of APs followed by an intermittent firing pattern, in both WT and *Scn8a*$^{D/+}$ mice. To reliably and accurately separate the two groups, we used k-means clustering of the burst length and the coefficient of variation of the inter-spike interval (ISI CoV) on the 8 second current injection that revealed firing patterns (Figure 3.3 D,E). Interestingly, there was a higher proportion of CA VIP interneurons in *Scn8a*$^{D/+}$ mice (Figure 3.3C). Previous studies have demonstrated that the M-current, a slowly activating potassium current important for irregular firing,[174,175] can modulate the firing patterns of VIP interneurons, with inhibition of the M-current leading to more VIP interneurons firing continuously.[51] This

begins to suggest that compensation by potassium channels could play a role in VIP interneuron dysfunction in *SCN8A* DEE.

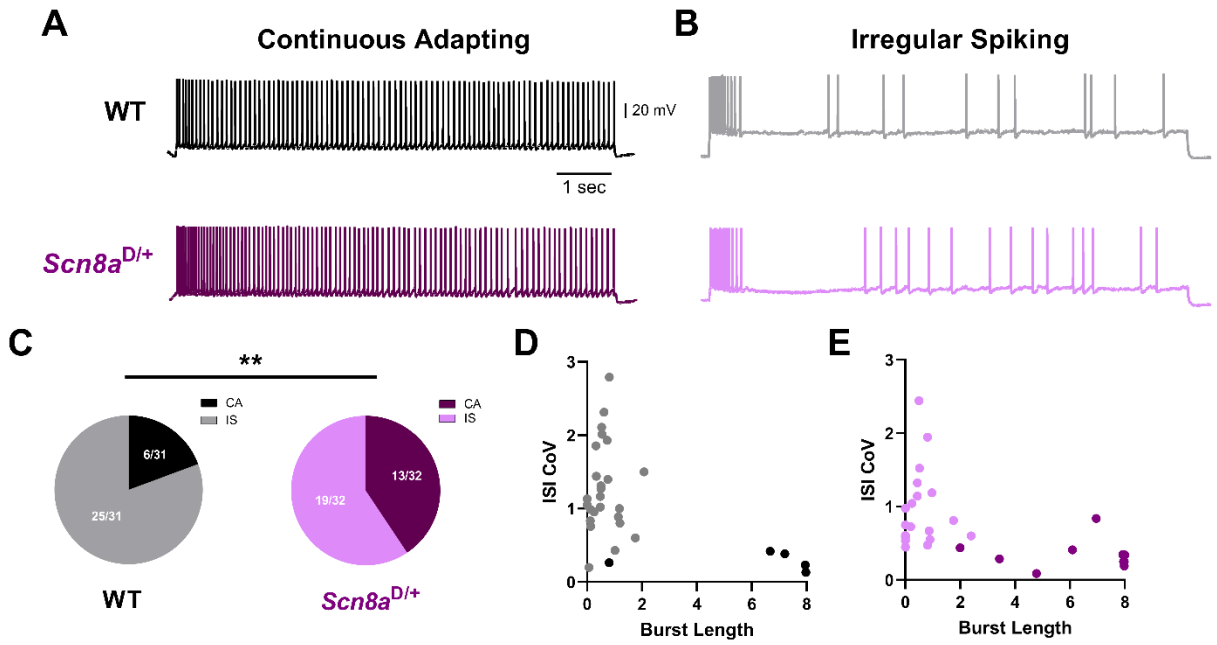

Figure 3.3: Electrophysiological characterization of WT and *Scn8a*$^{D/+}$ VIP interneurons. (**A, B**) Example traces of firing from continuous adapting (CA, **A**) and irregular spiking (IS, **B**) VIP interneurons in both WT and *Scn8a*$^{D/+}$ mice. Firing was elicited using an 8s current injection at 2x rheobase to ascertain firing pattern. (**C**) Proportions of CA and IS VIP interneurons. There is an increased proportion of CA VIP interneurons in *Scn8a*$^{D/+}$ mice compared to WT (**, p<0.01, Chi-square test). (**D, E**) K-means clustering for WT (**D**) and *Scn8a*$^{D/+}$ (**E**) VIP interneurons based on burst length and ISI coefficient of variation.

After dividing VIP interneurons into the CA and IS classifications, we showed that both CA and IS *Scn8a*$^{D/+}$ VIP interneurons are hyperexcitable compared to their WT counterparts. In response to varying current injection steps, the intrinsic excitability of CA and IS *Scn8a*$^{D/+}$ VIP interneurons was significantly increased (Figure 3.4B). Additionally, we observed an increase in input resistance specifically in *Scn8a*$^{D/+}$ CA VIP interneurons (380.5 ± 21.3 MΩ) when compared with WT (288.2 ± 22.2 MΩ; Figure 3.4C). There were no changes in other membrane and AP properties (Table 3.1).

Further, *Scn8a*$^{D/+}$ CA VIP interneurons displayed increased spontaneous excitability (4.76 ± 1.20 Hz) when compared to WT CA VIP interneurons (1.17 ± 0.63 Hz), with both an increase in spontaneous firing frequency (Figure 3.4E1) and an increase in proportion of spontaneously excitable cells (Figure 3.4F1). There were no significant differences in spontaneous excitability between WT and *Scn8a*$^{D/+}$ IS VIP interneurons (Figure 3.4 E2, F2). Generally, hyperexcitability in VIP interneurons may lead to increased inhibition of other inhibitory interneurons, which would in turn decrease overall inhibition in the cortex and could affect seizure generation.

	Vm (mV)	AP threshold (mV)	Rheobase (pA)	Upstroke Velocity (mV/ms)	Downstroke Velocity (mV/ms)	Amplitude (mV)	APD_{50} (ms)	Input Resistance (MΩ)	Spontaneous Firing Frequency (Hz)	Burst Duration (s)	ISI CoV
WT CA (*n*=6, 3)	-57.8 ± 4.4	-46.0 ± 2.0	23.3 ± 10.9	196.7 ± 28.8	-56.6 ± 5.8	69.2 ± 8.4	1.55 ± 0.23	288.2 ± 22.2	1.17 ± 0.63	N/A	0.26 ± 0.05
Scn8a$^{D/+}$ CA (*n*=13, 5)	-57.9 ± 1.1	-40.4 ± 3.6	4.62 ± 2.4	181.0 ± 15.9	-55.2 ± 3.4	72.1 ± 1.6	1.55 ± 0.14	380.5 ± 21.3 *	4.76 ± 1.2 *	N/A	0.28 ± 0.03
WT IS (*n*=25, 6)	-56.3 ± 1.9	-43.4 ± 1.2	27.2 ± 4.0	222.9 ± 15.1	-67.5 ± 3.4	72.7 ± 1.7	1.21 ± 0.06	359.6 ± 19.0	1.14 ± 0.4	0.63 ± 0.11	1.27 ± 0.12
Scn8a$^{D/+}$ IS (*n*=19, 5)	-54.4 ± 1.7	-45.3 ± 1.1	20.0 ± 5.1	205.7 ± 15.6	-66.4 ± 3.0	70.7 ± 2.5	1.22 ± 0.05	323.6 ± 17.2	2.55 ± 1.2	0.57 ± 0.15	0.88 ± 0.10 *

Table 3.1: Membrane, Action Potential, and Spontaneous Firing Properties of Adult Layer II/II WT and *Scn8a*$^{D/+}$ VIP Interneurons. Recordings were carried out in multiple cells from each animal (n=cells, animals). IS and CA cells were collected from the same animals and separated by k-means clustering. Data are presented as mean ± SEM.

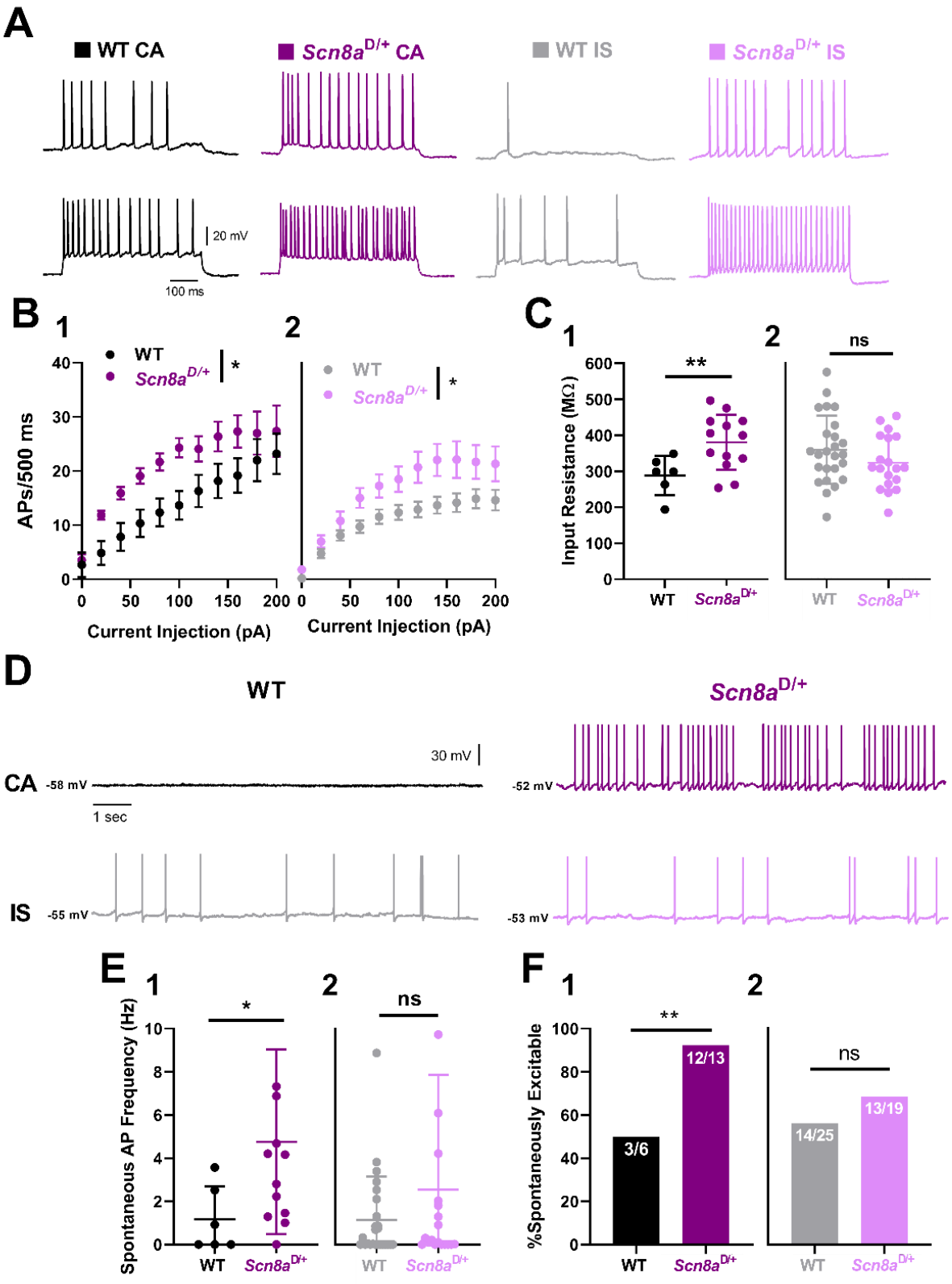
A
WT CA
Scn8aD/+ CA
WT IS
Scn8aD/+ IS
20 mV
100 ms
B
1
2
WT
Scn8aD/+
APs/500 ms
Current Injection (pA)
C
1
2
ns
Input Resistance (MΩ)
D
WT
Scn8aD/+
CA
IS
30 mV
1 sec
-58 mV
-52 mV
-55 mV
-53 mV
E
Spontaneous AP Frequency (Hz)
F
%Spontaneously Excitable
3/6
12/13
14/25
13/19

Figure 3.4: Differential impairment of intrinsic excitability in *Scn8a*$^{D/+}$ VIP interneurons. (**A**) Example traces of firing elicited from current injection steps at rheobase and 100 pA in WT CA (black), *Scn8a*$^{D/+}$ CA (purple), WT IS (grey), and *Scn8a*$^{D/+}$ IS (lavender) VIP interneurons. (**B**) In both CA (**B-1**) and IS (**B-2**) VIP interneurons, *Scn8a*$^{D/+}$ interneurons are hyperexcitable compared to WT (*, p<0.05, 2-way ANOVA with Tukey's multiple comparison test). (**C**) In CA VIP interneurons (**C-1**), input resistance is significantly increased in *Scn8a*$^{D/+}$ mice compared to WT (**, p<0.01, unpaired t-test), whereas there are no significant differences in input resistance between IS VIP interneurons (**C-2**) in WT and *Scn8a*$^{D/+}$ mice (p>0.05, unpaired t-test). (**D**) Example traces of spontaneous firing in WT and *Scn8a*$^{D/+}$ CA and IS VIP interneurons. (**E**) Spontaneous AP frequency in CA and IS VIP interneurons in WT and *Scn8a*$^{D/+}$ mice. *Scn8a*$^{D/+}$ CA VIP interneurons have an increased spontaneous AP frequency compared to their WT counterparts (**E-1**, *, p<0.05, unpaired t-test). There are no significant differences in spontaneous AP frequency between IS VIP interneurons in WT and *Scn8a*$^{D/+}$ mice (**E-2**, p>0.05, Welch's t-test). (**F**) Proportions of spontaneous excitability in CA and IS VIP interneurons in WT and *Scn8a*$^{D/+}$ mice. A higher proportion of *Scn8a*$^{D/+}$ CA VIP interneurons are spontaneously excitable compared to WT CA VIP interneurons (**F-1**, **, p<0.01, Binomial test). The proportion of spontaneously excitable cells is not different between WT and *Scn8a*$^{D/+}$ IS VIP interneurons (**F-2**, p>0.05, Binomial test).

Increased inhibitory input onto PV interneurons in *Scn8a*$^{D/+}$ mice

VIP interneurons preferentially target other inhibitory interneurons, namely SST and PV interneurons. To examine the impact of an increase in VIP interneuron excitability, we recorded spontaneous inhibitory postsynaptic currents (sIPSCs) from somatosensory cortex layer IV/V SST and PV interneurons in *Scn8a*$^{D/+}$ mice. To accurately identify SST and PV interneurons, we crossed *Scn8a*$^{D/+}$;tdT mice with either SST- or PV-Cre to fluorescently label SST or PV interneurons. Using whole-cell patch clamp, we found that frequency or amplitude of sIPSCs generated in *Scn8a*$^{D/+}$ SST interneurons were not significantly different from WT (Figure 3.5 C,D). Interestingly, SST interneurons are preferentially targeted by VIP interneurons.[158–160] However, we did observe that PV interneurons generated sIPSCs significantly more frequently in *Scn8a*$^{D/+}$ mice than in their WT counterparts (Figure 3.5 F,G), with no change in sIPSC

amplitude (Figure 3.5H). This data indicates an increase in inhibition of PV interneurons, which are impaired in *SCN8A* DEE, potentially leading to overall network disinhibition.

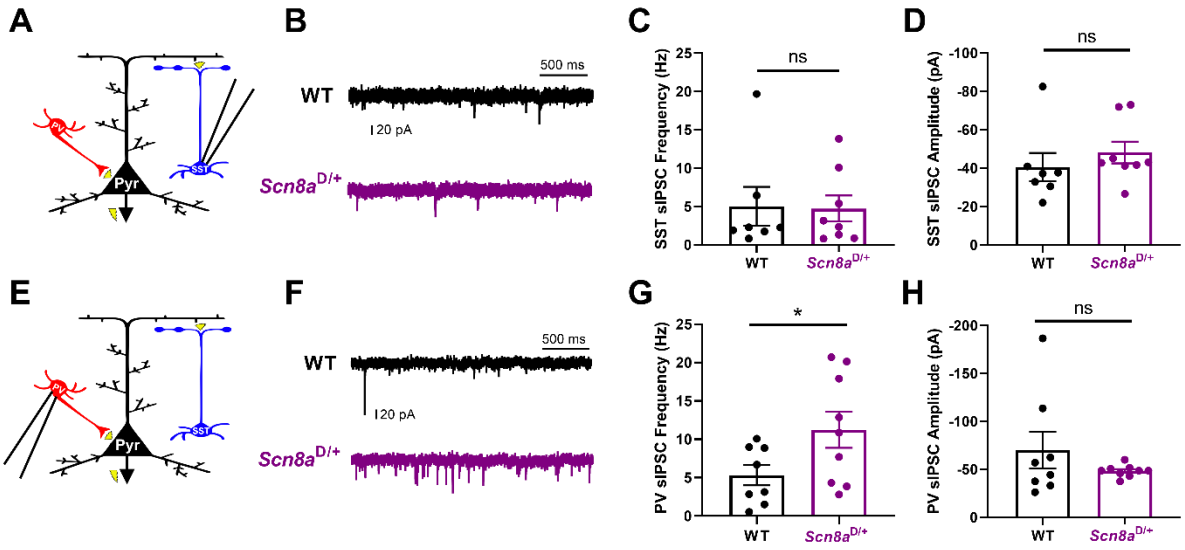

Figure 3.5: Spontaneous inhibition onto PV and SST interneurons. (**A**) Whole-cell recordings were collected from SST interneurons in layer IV/V somatosensory cortex of 6-8-week-old WT and *Scn8a*$^{D/+}$ mice. (**B**) Example traces of IPSCs generated in SST interneurons from WT (black) and *Scn8a*$^{D/+}$ (purple) mice. (**C**) Frequency of sIPSCs generated in SST interneurons is similar in *Scn8a*$^{D/+}$ (*n*=8, 3 mice) mice when compared to WT (*n*=7, 3 mice, Welch's t-test). (**D**) Amplitude of sIPSCs generated in SST interneurons is not significantly different between groups (*p*>0.05, unpaired t-test). (**E**) Whole-cell recordings were collected from PV interneurons in layer IV/V somatosensory cortex of 6-8-week-old mice. (**F**) Example traces of IPSCs generated in PV interneurons from WT and *Scn8a*$^{D/+}$ mice. (**G**) Frequency of sIPSCs generated in PV interneurons is increased in *Scn8a*$^{D/+}$ (*n*=9, 3 mice, *, *p*<0.05) mice when compared to WT (*n*=8, 3 mice, Welch's t-test). (**H**) Amplitude of sIPSCs generated in PV interneurons is not significantly different between groups (*p*>0.05, Mann-Whitney test).

Conditional expression of R1872W *SCN8A* variant in VIP interneurons

To identify whether VIP interneuron dysfunction is sufficient to convey seizure susceptibility in *SCN8A* DEE, we used the *Scn8a*$^{W/+}$ model of *SCN8A* DEE, which expresses the R1872W *SCN8A* variant in a Cre-dependent manner,[89] and crossed *Scn8a*$^{W/+}$;tdT mice with VIP-Cre to generate mice expressing the R1872W variant

exclusively in VIP interneurons. Our previous studies have demonstrated that mouse models of *SCN8A* DEE possessing either the N1768D or R1872W variant develop audiogenic seizures.[36,107] Here, we used a 15 kHz audiogenic stimulus to assess the susceptibility of *Scn8a*$^{W/+}$-VIP mice to audiogenic seizures (Figure 3.6). We found that 0/7 *Scn8a*$^{W/+}$-VIP mice were susceptible to audiogenic seizures at 6 weeks of age, an age at which other mouse models of *SCN8A* show seizure susceptibility.[36,87,89] Similarly, none of the WT controls were susceptible to audiogenic seizures. In contrast, we tested *Scn8a*$^{D/+}$ mice, which are known to have audiogenic seizures,[107] and 6/6 mice were susceptible to audiogenic seizures at 6 weeks. This indicates a lower seizure susceptibility for *Scn8a*$^{W/+}$-VIP mice and may suggest that VIP interneuron dysfunction may not be directly related to seizures in *SCN8A* DEE. Instead, the observed changes in VIP interneuron physiology may be related to other comorbidities seen in *SCN8A* DEE.

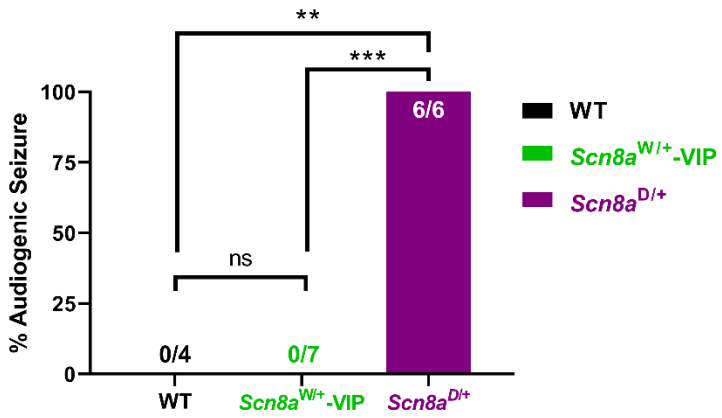

Figure 3.6: Susceptibility of *Scn8a*$^{W/+}$-VIP mice to audiogenic seizures. 0/7 *Scn8a*$^{W/+}$-VIP mice, which express the R1872W *SCN8A* mutation selectively in VIP interneurons, experience audiogenic seizures at 6 weeks. 0/4 control WT mice experience seizures. 6/6 *Scn8a*D/+ mice have an audiogenic seizure, significantly differing from both WT and *Scn8a*$^{W/+}$-VIP mice (**, p<0.01, ***, p<0.001, Fisher's exact test).

Further, we used whole-cell patch clamp electrophysiology to examine the physiology of *Scn8a*$^{W/+}$-VIP interneurons. We again used k-means clustering to divide VIP interneurons by firing patterns into the CA and IS classifications. Unlike in *Scn8a*$^{D/+}$ mice, we observed no difference in the proportion of CA and IS *Scn8a*$^{W/+}$-VIP interneurons when compared to WT (Figure 3.7A-C). Interestingly, we also found that there is no change in intrinsic excitability in *Scn8a*$^{W/+}$-VIP interneurons compared to WT (Figure 3.7 D, E). We also observed no differences between WT and *Scn8a*$^{W/+}$-VIP membrane/AP properties or spontaneous excitability (Table 3.2). This may suggest that

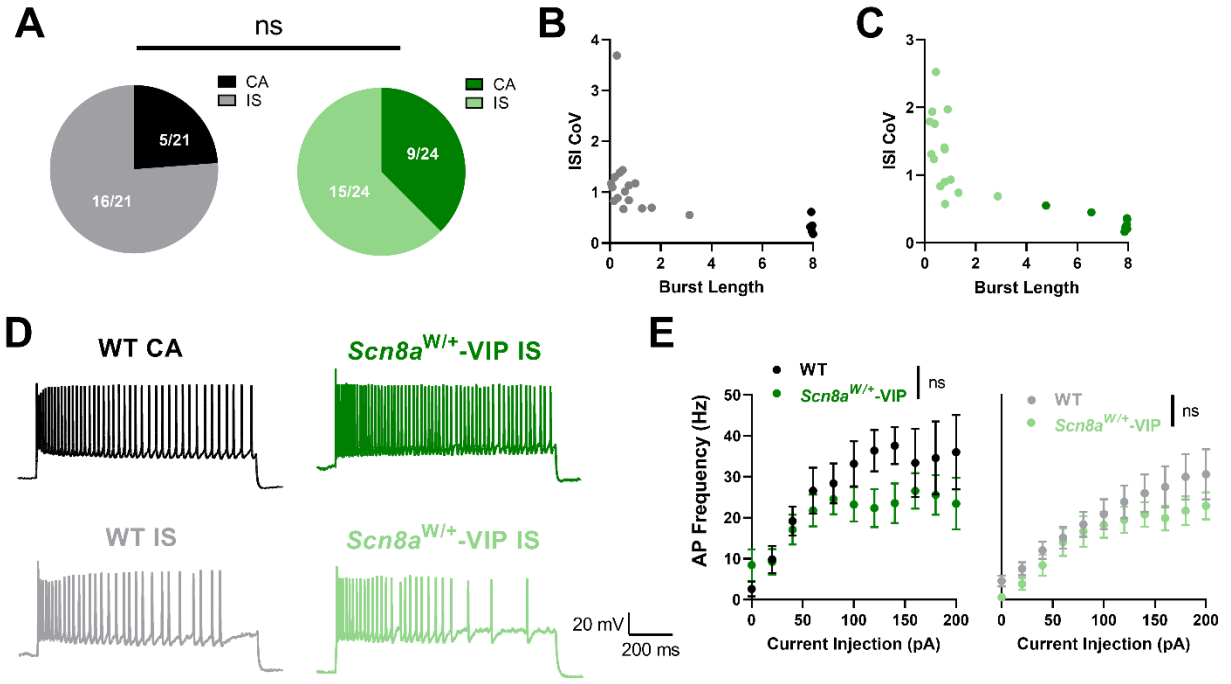

Figure 3.7: Intrinsic excitability in *Scn8a*$^{W/+}$-VIP interneurons. (**A**) Proportions of CA and IS VIP interneurons. There is no difference in the proportion of CA VIP interneurons in *Scn8a*$^{W/+}$-VIP mice compared to WT ($p>0.05$, Chi-square test). (**B, C**) K-means clustering for WT (**B**) and *Scn8a*$^{W/+}$-VIP (**C**) interneurons based on burst length and ISI coefficient of variation. (**D**) Example traces of firing elicited from current injection steps at 200 pA in WT IS (black), *Scn8a*$^{W/+}$-VIP IS (dark green), WT CA (grey), and *Scn8a*$^{W/+}$-VIP (light green) interneurons. (**E**) There is no difference in firing frequencies between CA WT and *Scn8a*$^{W/+}$-VIP interneurons and IS WT and *Scn8a*$^{W/+}$-VIP interneurons (2-way ANOVA with Sidak's multiple comparison test).

excitability changes observed in *Scn8a*$^{D/+}$ VIP interneurons are compensatory due to hyperactivity in other facets of the cortical network.

	Vm (mV)	AP threshold (mV)	Rheobase (pA)	Upstroke Velocity (mV/ms)	Downstroke Velocity (mV/ms)	Amplitude (mV)	APD_{50} (ms)	Input Resistance (MΩ)	Spontaneous Firing Frequency (Hz)	Burst Duration (s)	ISI CoV
WT CA (*n*=5, 3)	-54.0 ± 1.8	-43.9 ± 3.1	24.0 ± 4.0	237.8 ± 40.9	-60.8 ± 6.9	70.6 ± 4.3	1.29 ± 0.22	372.4 ± 46.9	0.60 ± 0.52		
Scn8a$^{W/+}$-VIP CA (*n*=9, 3)	-52.8 ± 1.6	-40.7 ± 1.2	24.4 ± 2.9	197.8 ± 23.7	-56.7 ± 3.4	67.7 ± 2.9	1.39 ± 0.12	383.2 ± 24.2	3.78 ± 1.7		
WT IS (*n*=16, 3)	-57.5 ± 2.3	-41.7 ± 1.4	33.8 ± 4.7	257.7 ± 22.9	-83.9 ± 9.0	72.3 ± 2.2	1.10 ± 0.15	317.9 ± 25.7	0.04 ± 0.3	0.72 ± 0.19	1.10 ± 0.19
Scn8a$^{W/+}$-VIP IS (*n*=15, 4)	-57.0 ± 1.4	-40.8 ± 1.2	41.3 ± 9.0	227.7 ± 19.8	-73.4 ± 6.0	66.1 ± 2.5	1.12 ± 0.12	270.0 ± 25.2	0.90 ± 0.55	0.79 ± 0.17	1.33 ± 0.15

Table 3.2: Membrane, Action Potential, and Spontaneous Firing Properties of Adult Layer II/II WT and *Scn8a*$^{W/+}$-VIP Interneurons. Recordings were carried out in multiple cells from each animal (n=cells, animals). IS and CA cells were collected from the same animals and separated by k-means clustering. Data are presented as mean ± SEM.

Discussion

In this study, we have examined VIP interneurons in *in vivo* models of *SCN8A* DEE and showed that: (1) VIP interneurons express $Na_V1.6$; (2) a global *SCN8A* mutation in VIP interneurons result in increased I_{NaP}; (3) *Scn8a*$^{D/+}$ VIP interneurons exhibit to an increased proportion of the continously adapting firing pattern; (4) VIP interneurons have heightened intrinsic excitability in a global expression model, *Scn8a*$^{D/+}$, but not in a conditional expression model, *Scn8a*$^{W/+}$-VIP; (5) selective expression of the R1872W *SCN8A* mutation in VIP interneurons does not convey susceptibility to audiogenic seizures. These results suggest that while VIP interneurons may be impaired in *SCN8A* DEE, this may be compensatory because of known network dysfunction, and they are likely not drivers of the seizure phenotype. However, our results do raise important questions both about interplay between sodium and potassium channels in *SCN8A* DEE and about the potential role of VIP interneurons in the behavioral and neurodevelopmental aspects of *SCN8A* DEE.

To our understanding, no previous study has found expression of $Na_v1.6$ in VIP interneurons. Currently, VIP interneurons are known to express sodium channels $Na_v1.1$ and $Na_v1.2$, with variants in $Na_v1.1$ leading to changes in VIP interneuron function in a mouse model of Dravet Syndrome.[39,51] Transcriptomics data suggests that *SCN8A* is expressed in VIP interneurons at a higher level than SST interneurons,[101] which we have previously shown are sufficient to generate audiogenic seizures in response to GOF *SCN8A* mutations.[36] We show here using immunostaining that $Na_v1.6$ is present at the AIS of VIP interneurons. This affects our understanding of VIP interneurons more generally, in the context of $Na_v1.6$ mutations and otherwise, and raises questions about sodium channel expression in the various VIP interneuron subtypes.

Our data shows that VIP interneurons exhibit I_{NaP}, and that this I_{NaP} is significantly increased in the presence of the N1768D *SCN8A* variant. We also observed a minimal I_{NaR} with no changes in *Scn8a*$^{D/+}$ mice, which is understandable considering that the function of I_{NaR} is to facilitate repetitive, high-frequency firing.[121,151] While they can fire consistently, VIP interneurons are not typically fast-spiking.[94,97] Nevertheless, increases in I_{NaP} lead to hyperexcitability in pyramidal cells, PV interneurons, and SST interneurons, and are implicated in various forms of epilepsy.[36,57,91,123,125,148] Concurrent with our previous results in other inhibitory interneuron subtypes, we believe that this increased I_{NaP} underlies the hyperexcitability shown in *Scn8a*$^{D/+}$ VIP interneurons. In concurrence with our hypothesis, we observed an increase in intrinsic excitability in both CA and IS *Scn8a*$^{D/+}$ VIP interneurons and an increase in spontaneous excitability only in CA *Scn8a*$^{D/+}$ VIP interneurons when compared to WT. We also noted an increase in

input resistance in CA *Scn8a*$^{D/+}$ VIP interneurons, implying that less stimulation is required for these neurons to reach threshold[176] and aligning with the observed spontaneous excitability phenotype. Interestingly, only IS VIP interneurons are hypoexcitable in a model of Dravet Syndrome,[51] providing an important distinction in VIP interneuron physiology of these phenotypically similar disorders.

Of note, we observed that there were more VIP interneurons with a CA firing pattern in *Scn8a*$^{D/+}$ mice. Previous literature suggested that an irregular spiking pattern in VIP interneurons was correlated with calretinin (CR) expression, and that continuously adapting cells were primarily found in cholecystokinin-positive (CCK) VIP interneurons.[177,178] However, more recent studies indicate that electrophysiological firing pattern does not correspond to these markers, with a large-scale study classifying them into 5 morpho-electric transcriptomic (MET) types in mice.[51,98] Within these MET-types, 4 of them have cell bodies primarily located in layers II/III, where we performed all of our recordings, and 3 of these have an irregular spiking pattern.[98] Notably, VIP interneuron electrophysiological firing pattern can be modulated through the M-type potassium current; an M-current inhibitor leads to IS VIP interneurons firing similarly to CA VIP interneurons.[51] The M-current is mediated by *KNCQ* channels, including *KCNQ2* and *KCNQ5*, which are expressed in VIP interneurons.[101,174,179,180] Sodium channel function has been shown to have an influence on potassium channel function in multiple genetic epilepsies.[34,153,154,181] Importantly, interaction between *SCN8A* and *KCNQ2* has been shown in a DEE model, and these ion channels are known to physically interact through an FGF bridging protein.[153,155] This suggests that *Scn8a*$^{D/+}$ VIP interneurons could have

augmented potassium channel function, likely due to an interplay between sodium and potassium channels as a result of the N1768D GOF mutation.

VIP interneurons primarily exert a disinhibitory influence on the cortical network, and as such, we hypothesized that hyperexcitability in VIP interneurons could lead to increased inhibition in other inhibitory interneuron subtypes and this could result in seizure susceptibility. We did observe an increase in inhibition onto PV interneurons, but not SST interneurons, in *Scn8a*$^{D/+}$ mice, however, mice expressing the R1872W GOF *SCN8A* mutation exclusively in VIP interneurons were not susceptible to audiogenic seizures. Mice conditionally expressing the R1872W GOF *SCN8A* mutation in all cells, forebrain excitatory cells, PV interneurons, and SST interneurons all experience audiogenic seizures,[36,110,114] which leads us to surmise that VIP interneurons may not be key to the seizure network of *SCN8A* DEE. Previous results indicate that optogenetic activation of VIP interneurons is insufficient to interrupt the firing patterns of fast-spiking PV interneurons,[182] suggesting that perhaps disinhibitory influence from VIP interneurons is not able to affect the fast spiking in PV interneurons leading up to a seizure event.[116,183] In a model of Dravet Syndrome, selective deletion of *Scn1a* in VIP interneurons also leads to the lack of a seizure phenotype, and impairment of VIP interneurons is instead related to neurodevelopmental comorbidities and autistic-like behaviors.[168] Generally, VIP interneurons are known to play a role in sensory processing along with learning and memory,[159,163–167] which could suggest that VIP interneurons are related to the cognitive dysfunction and developmental delay in *SCN8A* DEE.

Unexpectedly, VIP interneurons in the conditionally expressing *Scn8a*$^{W/+}$-VIP mice also showed no significant differences in AP properties or excitability, suggesting that their dysfunction in the global knock-in *Scn8a*$^{D/+}$ mice could be compensatory. Compensatory changes in inhibition have been shown previously in the kainic acid model of temporal lobe epilepsy,[184] and previous studies suggest potential compensation by pyramidal cells in Dravet Syndrome.[185] We have also observed some potential compensation by pyramidal cells in a model of *SCN8A* DEE with a mutation expressed exclusively in PV interneurons. It is possible that this compensation occurs due to an initial hyperexcitability of PV interneurons in *SCN8A* DEE, however, it is relatively unclear why the epilepsy network would generate a compensatory increase in disinhibition, as this seems antithetical to seizure prevention.

In conclusion, we demonstrate here that VIP interneurons express $Na_v1.6$ and exhibit I_{NaP} that is augmented by the N1768D GOF *SCN8A* variant, leading to hyperexcitability in two electrophysiological subtypes of VIP interneurons in a global mutation model. These two subtypes, whose firing patterns are modulated by M-type potassium current, are differentially represented in WT and *Scn8a*$^{D/+}$ mice. While these changes in *Scn8a*$^{D/+}$ VIP interneuron physiology do result in increased inhibition in PV interneurons, mice with VIP interneuron-specific expression of the R1872W GOF *SCN8A* variant are not susceptible to audiogenic seizures and VIP interneurons in these mice are not hyperexcitable. Our findings in this study suggest that VIP interneurons are impacted by globally expressed variants in *SCN8A* and raise questions about potential interactions between a GOF sodium channel variant and potassium channel function, as

well as the possible implications of increased VIP interneuron function on the neurodevelopmental comorbidities of *SCN8A* DEE.

Chapter IV: Conclusions and Future Directions

SCN8A DEE is a severe, treatment-resistant epilepsy syndrome in which patients suffer seizures, developmental delay, cognitive and motor impairment, and an increased risk of SUDEP. Previous understanding of *SCN8A* DEE centered around excitatory neuron dysfunction due to *de novo* gain-of-function mutations in $Na_v1.6$. Our previous study showed that SST interneurons, while not sufficient to elicit spontaneous seizures in response to *SCN8A* mutations, contribute to seizure activity *in vitro* and *in vivo*. However, SST interneurons are one of many inhibitory interneuron subtypes that express $Na_v1.6$ and therefore would be impacted by *SCN8A* mutations. In this thesis, my results have provided compelling evidence that inhibitory interneurons are critical contributors to the *SCN8A* DEE phenotype by elucidating the physiology of parvalbumin-positive and vasoactive intestinal peptide-positive interneurons, which together make up the majority of inhibitory interneurons in the brain. There is still much work to be done surrounding *SCN8A* DEE pathophysiology in order to develop effective and accessible treatments, but I am confident that the body of work described in this thesis will contribute to a better understanding of *SCN8A* DEE and of the impact of gain-of-function sodium channel mutations on inhibition overall.

In Chapter II, I demonstrated that a gain-of-function VGSC mutation selectively expressed in PV interneurons, a prominent inhibitory interneuron subtype, leads to spontaneous seizures and seizure-induced death in mice. Despite initial hyperexcitability, *Scn8a* mutant PV interneurons experience action potential failure via

depolarization block, which may be mediated by an increase in the persistent sodium current. Subsequently, inhibition onto excitatory pyramidal cells is decreased. Additionally, synaptic connections between *Scn8a* mutant PV interneurons and pyramidal cells are impaired, with both an increased failure rate and an increased synaptic latency. In this chapter, I also showed key comparisons between *SCN8A* DEE and Dravet Syndrome, indicating that the physiology of a gain-of-function disorder and a loss-of-function disorder may be more similar than they were previously considered. I also recognize the importance of excitatory neurons in this chapter, as a global *SCN8A* mutation model is significantly more severe than a model selectively expressing an *SCN8A* mutation selectively in PV interneurons. In Figure 4.1, I show our overarching hypothesis for the WT and *Scn8a* mutant networks with reference to the sufficiency of inhibitory dysfunction for seizure generation and the important contribution of excitation in *SCN8A* DEE.

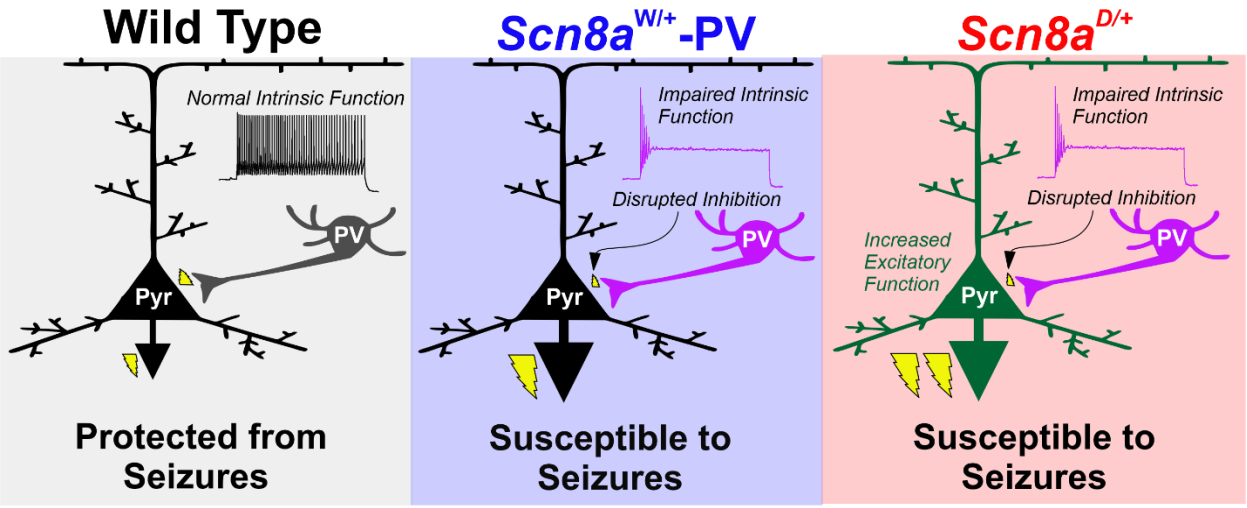

Figure 4.1: Overarching hypothesis from Chapter II. In WT mice, both pyramidal cells and PV interneurons have normal intrinsic function, and mice do not experience seizures. In conditional *Scn8a*$^{W/+}$-PV mice, pyramidal neurons are relatively normal, yet PV interneurons express a GOF *SCN8A* mutation, experience depolarization block, and exhibit impaired inhibitory synaptic transmission, making the mice susceptible to spontaneous seizures. In global *Scn8a*$^{D/+}$ mice, both excitatory pyramidal neurons and inhibitory PV interneurons express a GOF *SCN8A* mutation, leading to both excitatory cell hyperexcitability and disrupted inhibition from PV interneurons, resulting in increased seizure burden.

In Chapter III, I show that VIP interneurons express $Na_v1.6$ and that they are impacted by GOF *SCN8A* mutations. Similar to other cell types, the N1768D GOF *SCN8A* mutation results in increased persistent sodium current in VIP interneurons and facilitates cell hyperexcitability. In accordance with previous literature, VIP interneurons have distinct firing patterns: CA and IS, but interestingly, there is a higher proportion of CA VIP interneurons in *SCN8A* mutant mice. This suggests an interplay with voltage-gated potassium channels, as these are thought to be the determinants of VIP interneuron firing pattern. The demonstrated changes in VIP interneurons likely impact the other inhibitory subtypes that they target — PV interneurons experience increased inhibition in a global *SCN8A* mutation model. However, *SCN8A* mutations selectively in VIP interneurons do not convey hyperexcitability or seizure susceptibility, suggesting that changes in VIP interneurons in a global model may be compensatory, and that VIP interneurons instead may be involved in the non-seizure aspects of the *SCN8A* DEE phenotype.

My results in chapters II and III seem somewhat contradictory: impaired inhibition of PV interneurons due to depolarization block and activity-dependent synaptic failure is sufficient to cause seizures, yet, in a global model, PV interneurons experience increased inhibition from hyperexcitable disinhibitory VIP interneurons. However, I

believe these results work in tandem with what we currently know about inhibitory cells in seizure generation generally and in the case of *SCN8A* DEE. As a personal hypothesis, I believe that initial PV interneuron hyperexcitability may lead to compensation and become subject to increased inhibitory drive from disinhibitory interneurons. However, leading up to a seizure event, there is an increased activation of GABAergic neurons,[186–188] and this likely causes *Scn8a* mutant PV interneurons to enter depolarization block, which can precede epileptic discharges *in vitro* and *in vivo*.[115–118] With regards to VIP interneuron activity, VIP interneuron activation is insufficient to interrupt PV interneuron firing patterns[182] and may not affect the increased firing of PV interneurons leading up to a seizure. Likely, the observed changes in PV, VIP, and SST interneurons due to GOF *SCN8A* mutations work in tandem with increased excitatory neuron excitability to generate seizures, as indicated in Figure 4.1.

Currently, most patients with *SCN8A* DEE are refractory. Sodium channel blockers are primarily used to treat GOF *SCN8A* DEE, with the first line treatments being oxcarbazepine or carbamazepine. Interestingly, levetiracetam seems to be poorly tolerated in most patients with a GOF *SCN8A* variant.[189] The mechanism of action of levetiracetam is through interaction with the synaptic vesicle protein 2A (SV2A), which affects synaptic transmission and is particularly relevant for GABAergic transmission at high (≥80 Hz) frequencies.[190–192] In Chapter II of this thesis, I demonstrated an activity-dependent deficit in inhibitory synaptic transmission in mouse models of *SCN8A* DEE, which may indicate why levetiracetam is poorly tolerated in GOF *SCN8A* DEE. Future treatment for *SCN8A* DEE will likely trend towards gene therapies, with two different mechanisms: 1) reducing the expression of *Scn8a* to combat the effects of the GOF

mutation or 2) correcting the underlying mutation leading to *SCN8A* DEE. Currently, there is an ASO for *Scn8a* that reduces the expression of the *SCN8A* transcript and is effective at treating *SCN8A* DEE in mice even after the onset of spontaneous seizures.[85,193] The *Scn8a* ASO is also effective at treating epilepsies caused by mutations in *SCN1A, KCNA1,* and *KCNQ2*.[85,153] However, ASO treatment requires continuous doses of ASO, whereas patients may find more relief with a one-time correction via gene editing. Editing of the N1768D *SCN8A* mutation via CRISPR/Cas9 has recently been shown to rescue seizures, SUDEP, and neuronal hyperexcitability in the *Scn8a*$^{D/+}$ mouse model of *SCN8A* DEE.[194] This, along with unpublished data from our lab showing the efficacy of an adenine base editor for correcting an *SCN8A* mutation, bring substantial promise for more effective treatment of *SCN8A* DEE.

$Na_v1.6$ is a crucial sodium channel subtype for proper nervous system function, and this is made clear by the multitudes of symptoms shown in *SCN8A* DEE patients. Understanding the cell-type specific expression and physiological consequences of $Na_v1.6$ variants is important for not only *SCN8A* DEE, but also for the many other disorders that show aberrant $Na_v1.6$ including multiple sclerosis and dystonia.[195–198] Further, physiological understanding of network dysfunction in *SCN8A* DEE will yield insight into seizure generation both in epilepsy-related channelopathies and in epilepsy more generally. To gain a better physiological understanding of *Scn8a* mutations on network function, the mechanism behind *SCN8A* DEE resulting from loss-of-function mutations must be better understood. LOF *Scn8a* mutations are often associated with intellectual disability without seizures or with absence epilepsy.[80,199] This may result from a decreased excitability in excitatory cells, as indicated by mice deficient for

Nav1.6.[112] However, some reports have shown severe DEE with LOF *Scn8a* mutations.[77,79,82,200] While there are many physiological characterizations of LOF $Na_v1.6$ channels and a likely resulting hypo excitability of pyramidal cells,[77,80,82,83,201] there is work to be done characterizing the impacts of these mutations on the many pieces of neuronal networks.

A key facet of seizures is the balance between excitation and inhibition. The work in this dissertation demonstrates the sufficiency of impaired inhibition alone to generate seizures in a gain-of-function sodium channelopathy. The findings here raise many questions, including the specific role of parvalbumin interneurons in seizure generation, effects of a gain-of-function $Na_v1.6$ mutation on action potential propagation, the role of potassium channels in *SCN8A* DEE, and the underlying physiology behind neurodevelopmental comorbidities in *SCN8A* DEE. Further, models of *SCN8A* DEE serve as excellent models for spontaneous seizures and SUDEP, allowing for the broad application of these results in the epilepsy field. In total, this thesis serves to further unravel the complex mechanisms of gain-of-function *SCN8A* DEE by nearly completing the characterization of inhibitory interneurons, shifting our mechanistic understanding of this devastating disorder and providing novel insights for future therapeutic intervention.

References

1. Stafstrom, C. E. & Carmant, L. Seizures and Epilepsy: An Overview for Neuroscientists. *Cold Spring Harb Perspect Med* **5**, a022426 (2015).
2. Fiest, K. M. *et al.* Prevalence and incidence of epilepsy. *Neurology* **88**, 296–303 (2017).
3. Genetic determinants of common epilepsies: a meta-analysis of genome-wide association studies. *Lancet Neurol* **13**, 893–903 (2014).
4. Rastin, C., Schenkel, L. C. & Sadikovic, B. Complexity in Genetic Epilepsies: A Comprehensive Review. *Int J Mol Sci* **24**, 14606 (2023).
5. Veeramah, K. R. *et al.* De novo pathogenic SCN8A mutation identified by whole-genome sequencing of a family quartet affected by infantile epileptic encephalopathy and SUDEP. *Am J Hum Genet* **90**, 502–510 (2012).
6. Burgess, D. L. *et al.* Mutation of a new sodium channel gene, Scn8a, in the mouse mutant ‘motor endplate disease’. *Nat Genet* **10**, 461–465 (1995).
7. Meisler, M. SCN8A encephalopathy: Mechanisms and Models. *Epilepsia* **60**, S86–S91 (2019).
8. Talwar, D. & Hammer, M. F. SCN8A Epilepsy, Developmental Encephalopathy, and Related Disorders. *Pediatric Neurology* **122**, 76–83 (2021).
9. Larsen, J. *et al.* The phenotypic spectrum of SCN8A encephalopathy. *Neurology* **84**, 480–489 (2015).
10. Gardella, E. & Møller, R. S. Phenotypic and genetic spectrum of SCN8A-related disorders, treatment options, and outcomes. *Epilepsia* **60 Suppl 3**, S77–S85 (2019).

11. Caldwell, J. H., Schaller, K. L., Lasher, R. S., Peles, E. & Levinson, S. R. Sodium channel Nav1.6 is localized at nodes of Ranvier, dendrites, and synapses. *Proceedings of the National Academy of Sciences* **97**, 5616–5620 (2000).
12. Lorincz, A. & Nusser, Z. Cell-type-dependent molecular composition of the axon initial segment. *J Neurosci* **28**, 14329–14340 (2008).
13. Li, T. *et al.* Action potential initiation in neocortical inhibitory interneurons. *PLoS Biol* **12**, e1001944 (2014).
14. Hodgkin, A. L. & Huxley, A. F. A quantitative description of membrane current and its application to conduction and excitation in nerve. *J Physiol* **117**, 500–544 (1952).
15. Hodgkin, A. L. & Huxley, A. F. Currents carried by sodium and potassium ions through the membrane of the giant axon of Loligo. *J Physiol* **116**, 449–472 (1952).
16. Hodgkin, A. L. & Huxley, A. F. The components of membrane conductance in the giant axon of Loligo. *J Physiol* **116**, 473–496 (1952).
17. Hodgkin, A. L. & Huxley, A. F. The dual effect of membrane potential on sodium conductance in the giant axon of Loligo. *J Physiol* **116**, 497–506 (1952).
18. Hartshorne, R. P., Messner, D. J., Coppersmith, J. C. & Catterall, W. A. The saxitoxin receptor of the sodium channel from rat brain. Evidence for two nonidentical beta subunits. *J Biol Chem* **257**, 13888–13891 (1982).
19. Noda, M. *et al.* Primary structure of Electrophorus electricus sodium channel deduced from cDNA sequence. *Nature* **312**, 121–127 (1984).
20. Guy, H. R. & Seetharamulu, P. Molecular model of the action potential sodium channel. *Proc Natl Acad Sci U S A* **83**, 508–512 (1986).

21. Isom, L. L. *et al.* Primary structure and functional expression of the beta 1 subunit of the rat brain sodium channel. *Science* **256**, 839–842 (1992).
22. Isom, L. L. *et al.* Structure and function of the β2 subunit of brain sodium channels, a transmembrane glycoprotein with a CAM motif. *Cell* **83**, 433–442 (1995).
23. Morgan, K. *et al.* β3: An additional auxiliary subunit of the voltage-sensitive sodium channel that modulates channel gating with distinct kinetics. *Proc Natl Acad Sci U S A* **97**, 2308–2313 (2000).
24. Yu, F. H. *et al.* Sodium channel beta4, a new disulfide-linked auxiliary subunit with similarity to beta2. *J Neurosci* **23**, 7577–7585 (2003).
25. Goldin, A. L. *et al.* Messenger RNA coding for only the alpha subunit of the rat brain Na channel is sufficient for expression of functional channels in Xenopus oocytes. *Proc Natl Acad Sci U S A* **83**, 7503–7507 (1986).
26. Clatot, J. *et al.* Voltage-gated sodium channels assemble and gate as dimers. *Nat Commun* **8**, 2077 (2017).
27. Payandeh, J., Scheuer, T., Zheng, N. & Catterall, W. A. The crystal structure of a voltage-gated sodium channel. *Nature* **475**, 353–358 (2011).
28. Catterall, W. A. Voltage-gated sodium channels at 60: structure, function and pathophysiology. *J Physiol* **590**, 2577–2589 (2012).
29. Kontis, K. J., Rounaghi, A. & Goldin, A. L. Sodium Channel Activation Gating Is Affected by Substitutions of Voltage Sensor Positive Charges in All Four Domains. *J Gen Physiol* **110**, 391–401 (1997).
30. Yang, N., George, A. L. & Horn, R. Molecular basis of charge movement in voltage-gated sodium channels. *Neuron* **16**, 113–122 (1996).

31. Catterall, W. A. Ion Channel Voltage Sensors: Structure, Function, and Pathophysiology. *Neuron* **67**, 915–928 (2010).
32. Vassilev, P. M., Scheuer, T. & Catterall, W. A. Identification of an intracellular peptide segment involved in sodium channel inactivation. *Science* **241**, 1658–1661 (1988).
33. West, J. W. *et al.* A cluster of hydrophobic amino acid residues required for fast Na(+)-channel inactivation. *Proc Natl Acad Sci U S A* **89**, 10910–10914 (1992).
34. Spratt, P. W. E. *et al.* Paradoxical hyperexcitability from NaV1.2 sodium channel loss in neocortical pyramidal cells. *Cell Rep* **36**, 109483 (2021).
35. Berecki, G. *et al.* SCN1A gain of function in early infantile encephalopathy. *Ann Neurol* **85**, 514–525 (2019).
36. Wengert, E. R. *et al.* Somatostatin-Positive Interneurons Contribute to Seizures in SCN8A Epileptic Encephalopathy. *J Neurosci* **41**, 9257–9273 (2021).
37. Beckh, S., Noda, M., Lübbert, H. & Numa, S. Differential regulation of three sodium channel messenger RNAs in the rat central nervous system during development. *EMBO J* **8**, 3611–3616 (1989).
38. Ogiwara, I. *et al.* Nav1.1 Localizes to Axons of Parvalbumin-Positive Inhibitory Interneurons: A Circuit Basis for Epileptic Seizures in Mice Carrying an Scn1a Gene Mutation. *J. Neurosci.* **27**, 5903–5914 (2007).
39. Yamagata, T., Ogiwara, I., Mazaki, E., Yanagawa, Y. & Yamakawa, K. Nav1.2 is expressed in caudal ganglionic eminence-derived disinhibitory interneurons: Mutually exclusive distributions of Nav1.1 and Nav1.2. *Biochem Biophys Res Commun* **491**, 1070–1076 (2017).

40. Van Wart, A., Trimmer, J. S. & Matthews, G. Polarized distribution of ion channels within microdomains of the axon initial segment. *J Comp Neurol* **500**, 339–352 (2007).
41. Claes, L. *et al.* De novo mutations in the sodium-channel gene SCN1A cause severe myoclonic epilepsy of infancy. *Am J Hum Genet* **68**, 1327–1332 (2001).
42. Shmuely, S., Sisodiya, S. M., Gunning, W. B., Sander, J. W. & Thijs, R. D. Mortality in Dravet syndrome: A review. *Epilepsy Behav* **64**, 69–74 (2016).
43. de Lange, I. M. *et al.* Outcomes and comorbidities of SCN1A-related seizure disorders. *Epilepsy Behav* **90**, 252–259 (2019).
44. Strzelczyk, A. & Schubert-Bast, S. A Practical Guide to the Treatment of Dravet Syndrome with Anti-Seizure Medication. *CNS Drugs* **36**, 217–237 (2022).
45. Buck, M. L. & Goodkin, H. P. Stiripentol: A Novel Antiseizure Medication for the Management of Dravet Syndrome. *Ann Pharmacother* **53**, 1136–1144 (2019).
46. Strzelczyk, A. *et al.* Efficacy, tolerability, and retention of fenfluramine for the treatment of seizures in patients with Dravet syndrome: Compassionate use program in Germany. *Epilepsia* **62**, 2518–2527 (2021).
47. Heger, K. *et al.* A retrospective review of changes and challenges in the use of antiseizure medicines in Dravet syndrome in Norway. *Epilepsia Open* **5**, 432–441 (2020).
48. Tai, C., Abe, Y., Westenbroek, R. E., Scheuer, T. & Catterall, W. A. Impaired excitability of somatostatin- and parvalbumin-expressing cortical interneurons in a mouse model of Dravet syndrome. *Proc Natl Acad Sci U S A* **111**, E3139-3148 (2014).

49. Favero, M., Sotuyo, N. P., Lopez, E., Kearney, J. A. & Goldberg, E. M. A Transient Developmental Window of Fast-Spiking Interneuron Dysfunction in a Mouse Model of Dravet Syndrome. *J Neurosci* **38**, 7912–7927 (2018).
50. Kaneko, K. *et al.* Developmentally regulated impairment of parvalbumin interneuron synaptic transmission in an experimental model of Dravet syndrome. *Cell Rep* **38**, 110580 (2022).
51. Goff, K. M. & Goldberg, E. M. Vasoactive intestinal peptide-expressing interneurons are impaired in a mouse model of Dravet syndrome. *eLife* **8**, e46846 (2019).
52. Colasante, G. *et al.* dCas9-Based Scn1a Gene Activation Restores Inhibitory Interneuron Excitability and Attenuates Seizures in Dravet Syndrome Mice. *Mol Ther* **28**, 235–253 (2020).
53. Han, Z. *et al.* Antisense oligonucleotides increase Scn1a expression and reduce seizures and SUDEP incidence in a mouse model of Dravet syndrome. *Sci Transl Med* **12**, eaaz6100 (2020).
54. Lim, K. *et al.* Antisense oligonucleotide modulation of non-productive alternative splicing upregulates gene expression. *Nature Communications* **11**, (2020).
55. Wengert, E. R. *et al.* Targeted Augmentation of Nuclear Gene Output (TANGO) of Scn1a rescues parvalbumin interneuron excitability and reduces seizures in a mouse model of Dravet Syndrome. *Brain Research* **1775**, 147743 (2022).
56. Lossin, C., Wang, D. W., Rhodes, T. H., Vanoye, C. G. & George, A. L. Molecular basis of an inherited epilepsy. *Neuron* **34**, 877–884 (2002).

57. Rhodes, T. H., Lossin, C., Vanoye, C. G., Wang, D. W. & George, A. L. Noninactivating voltage-gated sodium channels in severe myoclonic epilepsy of infancy. *Proc Natl Acad Sci U S A* **101**, 11147–11152 (2004).
58. Spampanato, J., Aradi, I., Soltesz, I. & Goldin, A. L. Increased neuronal firing in computer simulations of sodium channel mutations that cause generalized epilepsy with febrile seizures plus. *J Neurophysiol* **91**, 2040–2050 (2004).
59. Kahlig, K. M., Misra, S. N. & George, A. L. Impaired Inactivation Gate Stabilization Predicts Increased Persistent Current for an Epilepsy-Associated SCN1A Mutation. *J. Neurosci.* **26**, 10958–10966 (2006).
60. Bikson, M., Hahn, P. J., Fox, J. E. & Jefferys, J. G. R. Depolarization Block of Neurons During Maintenance of Electrographic Seizures. *Journal of Neurophysiology* **90**, 2402–2408 (2003).
61. Bianchi, D. *et al.* On the mechanisms underlying the depolarization block in the spiking dynamics of CA1 pyramidal neurons. *J Comput Neurosci* **33**, 207–225 (2012).
62. Hu, W. *et al.* Distinct contributions of Na(v)1.6 and Na(v)1.2 in action potential initiation and backpropagation. *Nat Neurosci* **12**, 996–1002 (2009).
63. Tian, C., Wang, K., Ke, W., Guo, H. & Shu, Y. Molecular identity of axonal sodium channels in human cortical pyramidal cells. *Front. Cell. Neurosci.* **8**, (2014).
64. Boiko, T. *et al.* Functional specialization of the axon initial segment by isoform-specific sodium channel targeting. *J Neurosci* **23**, 2306–2313 (2003).
65. Sanders, S. J. *et al.* De novo mutations revealed by whole-exome sequencing are strongly associated with autism. *Nature* **485**, 237–241 (2012).

66. Berkovic, S. F. *et al.* Benign familial neonatal-infantile seizures: characterization of a new sodium channelopathy. *Ann Neurol* **55**, 550–557 (2004).
67. Kamiya, K. *et al.* A nonsense mutation of the sodium channel gene SCN2A in a patient with intractable epilepsy and mental decline. *J Neurosci* **24**, 2690–2698 (2004).
68. Allen, N. M. *et al.* Unexplained early onset epileptic encephalopathy: Exome screening and phenotype expansion. *Epilepsia* **57**, e12-17 (2016).
69. Wolff, M. *et al.* Genetic and phenotypic heterogeneity suggest therapeutic implications in SCN2A-related disorders. *Brain* **140**, 1316–1336 (2017).
70. Ben-Shalom, R. *et al.* Opposing Effects on NaV1.2 Function Underlie Differences Between SCN2A Variants Observed in Individuals With Autism Spectrum Disorder or Infantile Seizures. *Biol Psychiatry* **82**, 224–232 (2017).
71. Kearney, J. A. *et al.* A gain-of-function mutation in the sodium channel gene Scn2a results in seizures and behavioral abnormalities. *Neuroscience* **102**, 307–317 (2001).
72. Liao, Y. *et al.* SCN2A mutation associated with neonatal epilepsy, late-onset episodic ataxia, myoclonus, and pain. *Neurology* **75**, 1454–1458 (2010).
73. Lauxmann, S. *et al.* Relationship of electrophysiological dysfunction and clinical severity in SCN2A-related epilepsies. *Hum Mutat* **39**, 1942–1956 (2018).
74. Smith, R. S. *et al.* Sodium Channel SCN3A (NaV1.3) Regulation of Human Cerebral Cortical Folding and Oral Motor Development. *Neuron* **99**, 905-913.e7 (2018).

75. Zaman, T. *et al.* Mutations in SCN3A cause early infantile epileptic encephalopathy. *Ann Neurol* **83**, 703–717 (2018).
76. Zaman, T. *et al.* SCN3A-related neurodevelopmental disorder: A spectrum of epilepsy and brain malformation. *Ann Neurol* **88**, 348–362 (2020).
77. Johannesen, K. M. *et al.* Genotype-phenotype correlations in SCN8A-related disorders reveal prognostic and therapeutic implications. *Brain* **145**, 2991–3009 (2022).
78. Gardella, E. *et al.* The phenotype of SCN8A developmental and epileptic encephalopathy. *Neurology* **91**, e1112–e1124 (2018).
79. Hack, J. B. *et al.* Distinguishing Loss-of-Function and Gain-of-Function SCN8A Variants Using a Random Forest Classification Model Trained on Clinical Features. *Neurology Genetics* **9**, e200060 (2023).
80. Wagnon, J. L. *et al.* Loss-of-function variants of SCN8A in intellectual disability without seizures. *Neurol Genet* **3**, e170 (2017).
81. Wagnon, J. L. *et al.* Partial loss-of-function of sodium channel SCN8A in familial isolated myoclonus. *Hum Mutat* **39**, 965–969 (2018).
82. de Kovel, C. G. F. *et al.* Characterization of a de novo SCN8A mutation in a patient with epileptic encephalopathy. *Epilepsy Research* **108**, 1511–1518 (2014).
83. Liu, Y., Koko, M. & Lerche, H. A *SCN8A* variant associated with severe early onset epilepsy and developmental delay: Loss- or gain-of-function? *Epilepsy Research* **178**, 106824 (2021).

84. Johnson, J. P. *et al.* NBI-921352, a first-in-class, NaV1.6 selective, sodium channel inhibitor that prevents seizures in Scn8a gain-of-function mice, and wild-type mice and rats. *eLife* **11**, (2022).
85. Lenk, G. M. *et al.* Scn8a Antisense Oligonucleotide Is Protective in Mouse Models of SCN8A Encephalopathy and Dravet Syndrome. *Ann Neurol* **87**, 339–346 (2020).
86. Jones, J. M. & Meisler, M. H. Modeling human epilepsy by TALEN targeting of mouse sodium channel Scn8a. *Genesis* **52**, 141–148 (2014).
87. Wagnon, J. L. *et al.* Convulsive seizures and SUDEP in a mouse model of SCN8A epileptic encephalopathy. *Hum Mol Genet* **24**, 506–515 (2015).
88. Hammer, M. F. *et al.* Sex differences in physiological response to increased neuronal excitability in a knockin mouse model of pediatric epilepsy. *Clin Sci (Lond)* **138**, 205–223 (2024).
89. Bunton-Stasyshyn, R. K. A. *et al.* Prominent role of forebrain excitatory neurons in SCN8A encephalopathy. *Brain* **142**, 362–375 (2019).
90. Wong, J. C. *et al.* Autistic-like behavior, spontaneous seizures, and increased neuronal excitability in a Scn8a mouse model. *Neuropsychopharmacology* **46**, 2011–2020 (2021).
91. Ottolini, M., Barker, B. S., Gaykema, R. P., Meisler, M. H. & Patel, M. K. Aberrant Sodium Channel Currents and Hyperexcitability of Medial Entorhinal Cortex Neurons in a Mouse Model of SCN8A Encephalopathy. *J Neurosci* **37**, 7643–7655 (2017).
92. Lopez-Santiago, L. F. *et al.* Neuronal hyperexcitability in a mouse model of SCN8A epileptic encephalopathy. *Proc Natl Acad Sci U S A* **114**, 2383–2388 (2017).

93. Makinson, C. D. *et al.* Regulation of Thalamic and Cortical Network Synchrony by Scn8a. *Neuron* **93**, 1165-1179.e6 (2017).
94. Tremblay, R., Lee, S. & Rudy, B. GABAergic Interneurons in the Neocortex: From Cellular Properties to Circuits. *Neuron* **91**, 260–292 (2016).
95. Bernard, C., Cossart, R., Hirsch, J. C., Esclapez, M. & Ben-Ari, Y. What is GABAergic Inhibition? How Is it Modified in Epilepsy? *Epilepsia* **41**, S90–S95 (2000).
96. Kumar, S. S. & Buckmaster, P. S. Hyperexcitability, Interneurons, and Loss of GABAergic Synapses in Entorhinal Cortex in a Model of Temporal Lobe Epilepsy. *J. Neurosci.* **26**, 4613–4623 (2006).
97. Rudy, B., Fishell, G., Lee, S. & Hjerling-Leffler, J. Three groups of interneurons account for nearly 100% of neocortical GABAergic neurons. *Dev Neurobiol* **71**, 45–61 (2011).
98. Gouwens, N. W. *et al.* Integrated Morphoelectric and Transcriptomic Classification of Cortical GABAergic Cells. *Cell* **183**, 935-953.e19 (2020).
99. Tasic, B. *et al.* Shared and distinct transcriptomic cell types across neocortical areas. *Nature* **563**, 72–78 (2018).
100. Bhattacherjee, A. *et al.* Spatial transcriptomics reveals the distinct organization of mouse prefrontal cortex and neuronal subtypes regulating chronic pain. *Nat Neurosci* **26**, 1880–1893 (2023).
101. Paul, A. *et al.* Transcriptional Architecture of Synaptic Communication Delineates GABAergic Neuron Identity. *Cell* **171**, 522-539.e20 (2017).

102. Tran, C. H. *et al.* Interneuron Desynchronization Precedes Seizures in a Mouse Model of Dravet Syndrome. *J. Neurosci.* **40**, 2764–2775 (2020).
103. Bouilleret, V., Loup, F., Kiener, T., Marescaux, C. & Fritschy, J.-M. Early loss of interneurons and delayed subunit-specific changes in GABAA-receptor expression in a mouse model of mesial temporal lobe epilepsy. *Hippocampus* **10**, 305–324 (2000).
104. van Vliet, E. A., Aronica, E., Tolner, E. A., Lopes da Silva, F. H. & Gorter, J. A. Progression of temporal lobe epilepsy in the rat is associated with immunocytochemical changes in inhibitory interneurons in specific regions of the hippocampal formation. *Experimental Neurology* **187**, 367–379 (2004).
105. Bausch, S. B. Axonal sprouting of GABAergic interneurons in temporal lobe epilepsy. *Epilepsy Behav* **7**, 390–400 (2005).
106. Wittner, L. & Maglóczky, Z. Synaptic Reorganization of the Perisomatic Inhibitory Network in Hippocampi of Temporal Lobe Epileptic Patients. *Biomed Res Int* **2017**, 7154295 (2017).
107. Wengert, E. R. *et al.* Adrenergic Mechanisms of Audiogenic Seizure-Induced Death in a Mouse Model of SCN8A Encephalopathy. *Front. Neurosci.* **15**, (2021).
108. Kobayashi, Y. & Hensch, T. Germline recombination by conditional gene targeting with Parvalbumin-Cre lines. *Frontiers in Neural Circuits* **7**, (2013).
109. Luo, L. *et al.* Optimizing Nervous System-Specific Gene Targeting with Cre Driver Lines: Prevalence of Germline Recombination and Influencing Factors. *Neuron* **106**, 37-65.e5 (2020).

110. Wenker, I. C. *et al.* Forebrain epileptiform activity is not required for seizure-induced apnea in a mouse model of Scn8a epilepsy. *Frontiers in Neural Circuits* **16**, (2022).
111. Thompson, J. A. *et al.* Astrocyte reactivity in a mouse model of SCN8A epileptic encephalopathy. *Epilepsia Open* **7**, 280–292 (2022).
112. Royeck, M. *et al.* Role of Axonal NaV1.6 Sodium Channels in Action Potential Initiation of CA1 Pyramidal Neurons. *Journal of neurophysiology* **100**, 2361–80 (2008).
113. Wengert, E., Saga, A., Panchal, P., Barker, B. & Patel, M. Prax330 reduces persistent and resurgent sodium channel currents and neuronal hyperexcitability of subiculum neurons in a mouse model of SCN8A epileptic encephalopathy. *Neuropharmacology* **158**, 107699 (2019).
114. Wenker, I. C. *et al.* Postictal Death Is Associated with Tonic Phase Apnea in a Mouse Model of Sudden Unexpected Death in Epilepsy. *Ann Neurol* **89**, 1023–1035 (2021).
115. Ziburkus, J., Cressman, J. R., Barreto, E. & Schiff, S. J. Interneuron and pyramidal cell interplay during in vitro seizure-like events. *J Neurophysiol* **95**, 3948–3954 (2006).
116. Cammarota, M., Losi, G., Chiavegato, A., Zonta, M. & Carmignoto, G. Fast spiking interneuron control of seizure propagation in a cortical slice model of focal epilepsy. *J Physiol* **591**, 807–822 (2013).

117. Kim, C. M. & Nykamp, D. Q. The influence of depolarization block on seizure-like activity in networks of excitatory and inhibitory neurons. *J Comput Neurosci* **43**, 65–79 (2017).
118. Călin, A., Ilie, A. S. & Akerman, C. J. Disrupting Epileptiform Activity by Preventing Parvalbumin Interneuron Depolarization Block. *J Neurosci* **41**, 9452–9465 (2021).
119. Jayant, K. *et al.* Flexible Nanopipettes for Minimally Invasive Intracellular Electrophysiology In Vivo. *Cell Reports* **26**, 266-278.e5 (2019).
120. Raman, I. M. & Bean, B. P. Resurgent Sodium Current and Action Potential Formation in Dissociated Cerebellar Purkinje Neurons. *J. Neurosci.* **17**, 4517–4526 (1997).
121. Khaliq, Z. M., Gouwens, N. W. & Raman, I. M. The Contribution of Resurgent Sodium Current to High-Frequency Firing in Purkinje Neurons: An Experimental and Modeling Study. *J. Neurosci.* **23**, 4899–4912 (2003).
122. Raman, I. M., Sprunger, L. K., Meisler, M. H. & Bean, B. P. Altered Subthreshold Sodium Currents and Disrupted Firing Patterns in Purkinje Neurons of Scn8a Mutant Mice. *Neuron* **19**, 881–891 (1997).
123. Hargus, N. J., Nigam, A., Bertram, E. H. & Patel, M. K. Evidence for a role of Nav1.6 in facilitating increases in neuronal hyperexcitability during epileptogenesis. *J Neurophysiol* **110**, 1144–1157 (2013).
124. Jarecki, B. W., Piekarz, A. D., Jackson, J. O. & Cummins, T. R. Human voltage-gated sodium channel mutations that cause inherited neuronal and muscle channelopathies increase resurgent sodium currents. *J Clin Invest* **120**, 369–378 (2010).

125. Wengert, E. R. & Patel, M. K. The Role of the Persistent Sodium Current in Epilepsy. *Epilepsy Curr* **21**, 40–47 (2020).
126. Estacion, M. *et al.* A novel de novo mutation of SCN8A (Nav1.6) with enhanced channel activation in a child with epileptic encephalopathy. *Neurobiology of Disease* **69**, 117–123 (2014).
127. Wagnon, J. L. *et al.* Pathogenic mechanism of recurrent mutations of SCN8A in epileptic encephalopathy. *Ann Clin Transl Neurol* **3**, 114–123 (2016).
128. Fatt, P. & Katz, B. Spontaneous subthreshold activity at motor nerve endings. *J Physiol* **117**, 109–128 (1952).
129. Ropert, N., Miles, R. & Korn, H. Characteristics of miniature inhibitory postsynaptic currents in CA1 pyramidal neurones of rat hippocampus. *The Journal of Physiology* **428**, 707–722 (1990).
130. Ma, Y. & Prince, D. A. Functional alterations in GABAergic fast-spiking interneurons in chronically injured epileptogenic neocortex. *Neurobiology of Disease* **47**, 102–113 (2012).
131. Rossignol, E., Kruglikov, I., van den Maagdenberg, A. M. J. M., Rudy, B. & Fishell, G. CaV2.1 ablation in cortical interneurons selectively impairs fast-spiking basket cells and causes generalized seizures. *Ann Neurol* **74**, 209–222 (2013).
132. Hu, H. & Jonas, P. A supercritical density of Na+ channels ensures fast signaling in GABAergic interneuron axons. *Nat Neurosci* **17**, 686–693 (2014).
133. Kraushaar, U. & Jonas, P. Efficacy and Stability of Quantal GABA Release at a Hippocampal Interneuron–Principal Neuron Synapse. *J. Neurosci.* **20**, 5594–5607 (2000).

134. Caillard, O. *et al.* Role of the calcium-binding protein parvalbumin in short-term synaptic plasticity. *Proceedings of the National Academy of Sciences* **97**, 13372–13377 (2000).
135. Xiang, Z., Huguenard, J. R. & Prince, D. A. Synaptic Inhibition of Pyramidal Cells Evoked by Different Interneuronal Subtypes in Layer V of Rat Visual Cortex. *Journal of Neurophysiology* **88**, 740–750 (2002).
136. Katz, B. & Miledi, R. THE MEASUREMENT OF SYNAPTIC DELAY, AND THE TIME COURSE OF ACETYLCHOLINE RELEASE AT THE NEUROMUSCULAR JUNCTION. *Proc R Soc Lond B Biol Sci* **161**, 483–495 (1965).
137. Sabatini, B. L. & Regehr, W. G. Timing of Synaptic Transmission. *Annual Review of Physiology* **61**, 521–542 (1999).
138. Boudkkazi, S. *et al.* Release-dependent variations in synaptic latency: a putative code for short- and long-term synaptic dynamics. *Neuron* **56**, 1048–1060 (2007).
139. Boudkkazi, S., Fronzaroli-Molinieres, L. & Debanne, D. Presynaptic action potential waveform determines cortical synaptic latency. *The Journal of Physiology* **589**, 1117–1131 (2011).
140. Pouille, F. & Scanziani, M. Enforcement of Temporal Fidelity in Pyramidal Cells by Somatic Feed-Forward Inhibition. *Science* **293**, 1159–1163 (2001).
141. Rubinstein, M. *et al.* Dissecting the phenotypes of Dravet syndrome by gene deletion. *Brain* **138**, 2219–2233 (2015).
142. Yuan, Y. *et al.* Antisense oligonucleotides restore excitability, GABA signalling and sodium current density in a Dravet syndrome model. *Brain* **147**, 1231–1246 (2024).

143. Bartos, M., Vida, I. & Jonas, P. Synaptic mechanisms of synchronized gamma oscillations in inhibitory interneuron networks. *Nat Rev Neurosci* **8**, 45–56 (2007).
144. Lapray, D. *et al.* Behavior-dependent specialization of identified hippocampal interneurons. *Nat Neurosci* **15**, 1265–1271 (2012).
145. Buzsáki, G. & Draguhn, A. Neuronal Oscillations in Cortical Networks. *Science* **304**, 1926–1929 (2004).
146. Baker, S. N. Oscillatory interactions between sensorimotor cortex and the periphery. *Current Opinion in Neurobiology* **17**, 649–655 (2007).
147. Cheah, C. S., Beckman, M. A., Catterall, W. A. & Oakley, J. C. Sharp-Wave Ripple Frequency and Interictal Epileptic Discharges Increase in Tandem During Thermal Induction of Seizures in a Mouse Model of Genetic Epilepsy. *Frontiers in Cellular Neuroscience* **15**, (2021).
148. Hargus, N. J. *et al.* Temporal Lobe Epilepsy Induces Intrinsic Alterations in Na Channel Gating in Layer II Medial Entorhinal Cortex Neurons. *Neurobiol Dis* **41**, 361–376 (2011).
149. Schwindt, P. C. & Crill, W. E. Amplification of synaptic current by persistent sodium conductance in apical dendrite of neocortical neurons. *Journal of Neurophysiology* **74**, 2220–2224 (1995).
150. Stuart, G. Voltage–activated sodium channels amplify inhibition in neocortical pyramidal neurons. *Nat Neurosci* **2**, 144–150 (1999).
151. Raman, I. M. & Bean, B. P. Inactivation and Recovery of Sodium Currents in Cerebellar Purkinje Neurons: Evidence for Two Mechanisms. *Biophysical Journal* **80**, 729–737 (2001).

152. Tidball, A. M. *et al.* Variant-specific changes in persistent or resurgent sodium current in SCN8A-related epilepsy patient-derived neurons. *Brain* **143**, 3025–3040 (2020).
153. Hill, S. F., Ziobro, J. M., Jafar-Nejad, P., Rigo, F. & Meisler, M. H. Genetic interaction between Scn8a and potassium channel genes Kcna1 and Kcnq2. *Epilepsia* **63**, e125–e131 (2022).
154. Zhang, J. *et al.* Severe deficiency of the voltage-gated sodium channel NaV1.2 elevates neuronal excitability in adult mice. *Cell Reports* **36**, 109495 (2021).
155. Pablo, J. L. & Pitt, G. S. FGF14 is a regulator of KCNQ2/3 channels. *Proc Natl Acad Sci U S A* **114**, 154–159 (2017).
156. Jentsch, T. J. Neuronal KCNQ potassium channels:physislogy and role in disease. *Nat Rev Neurosci* **1**, 21–30 (2000).
157. Rudy, B. & McBain, C. J. Kv3 channels: voltage-gated K+ channels designed for high-frequency repetitive firing. *Trends in Neurosciences* **24**, 517–526 (2001).
158. Lee, S., Kruglikov, I., Huang, Z. J., Fishell, G. & Rudy, B. A disinhibitory circuit mediates motor integration in the somatosensory cortex. *Nat Neurosci* **16**, 1662–1670 (2013).
159. Pfeffer, C. K., Xue, M., He, M., Huang, Z. J. & Scanziani, M. Inhibition of Inhibition in Visual Cortex: The Logic of Connections Between Molecularly Distinct Interneurons. *Nat Neurosci* **16**, 1068–1076 (2013).
160. Jiang, X. *et al.* Principles of connectivity among morphologically defined cell types in adult neocortex. *Science* **350**, aac9462 (2015).

161. Lee, B. R. *et al.* Signature morphoelectric properties of diverse GABAergic interneurons in the human neocortex. *Science* **382**, eadf6484 (2023).
162. Prönneke, A. *et al.* Characterizing VIP Neurons in the Barrel Cortex of VIPcre/tdTomato Mice Reveals Layer-Specific Differences. *Cerebral Cortex* **25**, 4854–4868 (2015).
163. Batista-Brito, R. *et al.* Developmental Dysfunction of VIP Interneurons Impairs Cortical Circuits. *Neuron* **95**, 884-895.e9 (2017).
164. Turi, G. F. *et al.* Vasoactive intestinal polypeptide-expressing interneurons in the hippocampus support goal-oriented spatial learning. *Neuron* **101**, 1150-1165.e8 (2019).
165. Letzkus, J. J., Wolff, S. B. E. & Lüthi, A. Disinhibition, a Circuit Mechanism for Associative Learning and Memory. *Neuron* **88**, 264–276 (2015).
166. Fu, Y. *et al.* A Cortical Circuit for Gain Control by Behavioral State. *Cell* **156**, 1139–1152 (2014).
167. Ramos-Prats, A. *et al.* VIP-expressing interneurons in the anterior insular cortex contribute to sensory processing to regulate adaptive behavior. *Cell Reports* **39**, (2022).
168. Goff, K. M., Liebergall, S. R., Jiang, E., Somarowthu, A. & Goldberg, E. M. VIP interneuron impairment promotes in vivo circuit dysfunction and autism-related behaviors in Dravet syndrome. *Cell Reports* **42**, 112628 (2023).
169. Goff, K. M. & Goldberg, E. M. A Role for VIP Interneurons in Neurodevelopmental Disorders. *Dev Neurosci* **43**, 168–180 (2021).

170. Srivastava, S. & Sahin, M. Autism spectrum disorder and epileptic encephalopathy: common causes, many questions. *J Neurodev Disord* **9**, 23 (2017).
171. Khoshkhoo, S., Vogt, D. & Sohal, V. S. Dynamic, Cell-Type-Specific Roles for GABAergic Interneurons in a Mouse Model of Optogenetically Inducible Seizures. *Neuron* **93**, 291–298 (2017).
172. Rahimi, S. *et al.* The role of subicular VIP-expressing interneurons on seizure dynamics in the intrahippocampal kainic acid model of temporal lobe epilepsy. *Experimental Neurology* **370**, 114580 (2023).
173. Stafstrom, C. E. Persistent Sodium Current and Its Role in Epilepsy. *Epilepsy Curr* **7**, 15–22 (2007).
174. Brown, D. A. & Adams, P. R. Muscarinic suppression of a novel voltage-sensitive K+ current in a vertebrate neurone. *Nature* **283**, 673–676 (1980).
175. Stiefel, K. M., Englitz, B. & Sejnowski, T. J. Origin of intrinsic irregular firing in cortical interneurons. *Proceedings of the National Academy of Sciences* **110**, 7886–7891 (2013).
176. Kernell, D. Input resistance, electrical excitability, and size of ventral horn cells in cat spinal cord. *Science* **152**, 1637–1640 (1966).
177. Porter, J. T. *et al.* Properties of bipolar VIPergic interneurons and their excitation by pyramidal neurons in the rat neocortex. *European Journal of Neuroscience* **10**, 3617–3628 (1998).
178. He, M. *et al.* Strategies and Tools for Combinatorial Targeting of GABAergic Neurons in Mouse Cerebral Cortex. *Neuron* **91**, 1228–1243 (2016).

179. Lee, I.-C., Yang, J.-J., Liou, Y.-M. & Wong, S.-H. KCNQ2 Selectivity Filter Mutations Cause Kv7.2 M-Current Dysfunction and Configuration Changes Manifesting as Epileptic Encephalopathies and Autistic Spectrum Disorders. *Cells* **11**, 894 (2022).
180. Pattnaik, B. R. & Hughes, B. A. Effects of KCNQ channel modulators on the M-type potassium current in primate retinal pigment epithelium. *Am J Physiol Cell Physiol* **302**, C821–C833 (2012).
181. Shore, A. N. *et al.* Heterozygous expression of a Kcnt1 gain-of-function variant has differential effects on SST- and PV-expressing cortical GABAergic neurons. *eLife* **13**, (2024).
182. Chamberland, S. *et al.* Brief synaptic inhibition persistently interrupts firing of fast-spiking interneurons. *Neuron* **111**, 1264-1281.e5 (2023).
183. Trevelyan, A. J., Sussillo, D., Watson, B. O. & Yuste, R. Modular Propagation of Epileptiform Activity: Evidence for an Inhibitory Veto in Neocortex. *J Neurosci* **26**, 12447–12455 (2006).
184. Pan, G. *et al.* Compensatory Mechanisms Modulate the Neuronal Excitability in a Kainic Acid-Induced Epilepsy Mouse Model. *Front Neural Circuits* **12**, 48 (2018).
185. Liu, Y. *et al.* Dravet syndrome patient-derived neurons suggest a novel epilepsy mechanism. *Annals of Neurology* **74**, 128–139 (2013).
186. Lillis, K. P., Kramer, M. A., Mertz, J., Staley, K. J. & White, J. A. Pyramidal cells accumulate chloride at seizure onset. *Neurobiology of Disease* **47**, 358–366 (2012).

187. Muldoon, S. F. *et al.* GABAergic inhibition shapes interictal dynamics in awake epileptic mice. *Brain* **138**, 2875–2890 (2015).

188. Elahian, B. *et al.* Low-Voltage Fast Seizures in Humans Begin with Increased Interneuron Firing. *Ann Neurol* **84**, 588–600 (2018).

189. Conecker, G. *et al.* Global modified Delphi consensus on diagnosis, phenotypes, and treatment of -related epilepsy and/or neurodevelopmental disorders. *Epilepsia* **65**, 2322–2338 (2024).

190. Contreras-García, I. J. *et al.* Levetiracetam Mechanisms of Action: From Molecules to Systems. *Pharmaceuticals (Basel)* **15**, 475 (2022).

191. Meehan, A. L., Yang, X., McAdams, B. D., Yuan, L. & Rothman, S. M. A new mechanism for antiepileptic drug action: vesicular entry may mediate the effects of levetiracetam. *J Neurophysiol* **106**, 1227–1239 (2011).

192. Meehan, A. L., Yang, X., Yuan, L.-L. & Rothman, S. M. Levetiracetam has an activity-dependent effect on inhibitory transmission. *Epilepsia* **53**, 469–476 (2012).

193. Hill*, S. F. *et al.* Long-Term Downregulation of the Sodium Channel Gene Scn8a Is Therapeutic in Mouse Models of Epilepsy. *Annals of Neurology* **95**, 754–759 (2024).

194. Yu, W. *et al.* Allele-Specific Editing of a Dominant Epilepsy Variant Protects against Seizures and Lethality in a Murine Model. *Annals of Neurology* **n/a**,.

195. Craner, M. J. *et al.* Molecular changes in neurons in multiple sclerosis: Altered axonal expression of Nav1.2 and Nav1.6 sodium channels and Na+/Ca2+ exchanger. *Proc Natl Acad Sci U S A* **101**, 8168–8173 (2004).

196. Alrashdi, B. *et al.* Nav1.6 promotes inflammation and neuronal degeneration in a mouse model of multiple sclerosis. *J Neuroinflammation* **16**, 215 (2019).
197. Sprunger, L. K., Escayg, A., Tallaksen-Greene, S., Albin, R. L. & Meisler, M. H. Dystonia Associated With Mutation of the Neuronal Sodium Channel Scn8a and Identification of the Modifier Locus Scnm1 on Mouse Chromosome 3. *Human Molecular Genetics* **8**, 471–479 (1999).
198. Hamann, M., Meisler, M. H. & Richter, A. Motor disturbances in mice with deficiency of the sodium channel gene *Scn8a* show features of human dystonia. *Experimental Neurology* **184**, 830–838 (2003).
199. Papale, L. A. *et al.* Heterozygous mutations of the voltage-gated sodium channel SCN8A are associated with spike-wave discharges and absence epilepsy in mice. *Human Molecular Genetics* **18**, 1633–1641 (2009).
200. Blanchard, M. G. *et al.* De novo gain-of-function and loss-of-function mutations of SCN8A in patients with intellectual disabilities and epilepsy. *J Med Genet* **52**, 330–337 (2015).
201. Liu, Y. *et al.* Neuronal mechanisms of mutations in SCN8A causing epilepsy or intellectual disability. *Brain* **142**, 376–390 (2019).
202. Wengert, E. R., Miralles, R. M. & Patel, M. K. Voltage-Gated Sodium Channels as Drug Targets in Epilepsy-Related Sodium Channelopathies. in *Ion Channels as Targets in Drug Discovery* (eds. Stephens, G. & Stevens, E.) 91–114 (Springer International Publishing, Cham, 2024). doi:10.1007/978-3-031-52197-3_4.

Appendix: Notes on Figures/Tables

Chapter I: Figure 1.1 and Table 1.1 were adapted from [28]. Figures 1.2, 1.3, 1.4, and 1.5 were created by me in for publication in a textbook chapter.[202] Figure 1.6 was adapted from [87] and [89].

Chapter II: All figures and tables were adapted from (Miralles et al., 2024, *JCI Insight*), a manuscript of which I am sole lead author that has been accepted for publication, with the exception of Figure 2.3 and Figure 2.7, which were created by me from data collected by me and my co-authors.

Chapter III: All figures and tables are currently unpublished data compiled by me and collected primarily by me and my undergraduate student, Shrinidhi Kittur. This data will be compiled into a manuscript on which my undergraduate student and I will be co-lead authors.

Chapter IV: Figure 4.1 was adapted by me from similar figures (i.e. Figure 1.2).